Comparison of Capacitance-Resistance Model and Tracer Flooding to Estimate Interwell Connectivity

by

Adilet Aliyev

THESIS SUPERVISOR

Peyman Pourafshary

Thesis submitted to the School of Mining and Geosciences of Nazarbayev University in Partial Fulfillment of the Requirements for the Degree of

Master of Science in Petroleum Engineering

Nazarbayev University

2022

ORIGINALITY STATEMENT

I, Adilet Aliyev, hereby declare that this submission is my own work and to the best of my knowledge it contains no materials previously published or written by another person, or substantial proportions of material which have been accepted for the award of any other degree or diploma at Nazarbayev University or any other educational institution, except where due acknowledgement is made in the thesis.

Any contribution made to the research by others, with whom I have worked at NU or elsewhere is explicitly acknowledged in the thesis.

I also declare that the intellectual content of this thesis is the product of my own work, except to the extent that assistance from others in the project's design and conception or in style, presentation and linguistic expression is acknowledged.

Signed on 28.03.2022

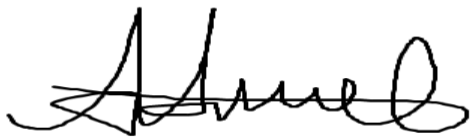

ABSTRACT

When it comes to managing waterflooding activities in a field, interwell connection is a critical factor to consider. This parameter is important to be analyzed to determine the distribution of injected fluids in a reservoir and toward the producing wells. The Capacitance-Resistance Model (CRM), which was first developed in the early 2000s, is an analytical technique for waterflooding modeling and optimization. Producing and injecting data are utilized as input in order to calculate the material balance and estimate factors such as the interwell connectivity of the wells. This study was focused on the accuracy of applying the Capacitance-Resistance Model to estimate the interwell connectivity and compare it with results obtained by tracer flooding tests. A technique like this allows for a more accurate assessment of the link between the wells as well as a more cost-effective and timely choice on the next field development stages. Data from tracer tests and CRM were used to determine connectivity values for synthetic and actual fields, which were then examined and compared. CRM was capable of modeling floods and estimating production in these areas with a level of accuracy that was acceptable. In order to increase the accuracy of the CRM technique used to compute the interwell connection between injector/producer pairs, other parameters such as well spacing and fluid loss during the injection were taken into consideration. CRM, according to our findings, may be used to provide a rapid approximation of interwell connection under specific assumptions, and it is suggested as a substitute for tracer flooding analysis in situations when the tracer test is either not feasible or too costly to do.

ACKNOWLEDGMENT

I would like to acknowledge and give my warmest thanks to my supervisor, Dr. Peyman Pourafshary, who guided me throughout this project. His guidance and patience carried me through the writing of this project. I would also like to thank Davood Zivar who helped me and explained unfamiliar parts of this project. His assistance was greatly appreciated. I wish to extend my special thanks to RSS Pro Company for offering valuable data which I used in my project.

TABLE OF CONTENTS

LIST OF FIGURES

LIST OF TABLES

CHAPTER 1. INTRODUCTION

Reservoir characterization is the study of reservoir attributes through the lenses of geology, geophysical, petrophysical, and engineering disciplines, including the uncertainty analysis of geologic and engineering data and spatial variations. Two critical factors are:

1) characterization of the reservoir's physical characteristics, including its porosity and permeability;

2) characterization of its depositional facies.

From a causal viewpoint, sedimentation, diagenesis, fracture, faulting, and diapirism are the primary mechanisms influencing geological and petrophysical properties and spatial distributions. To model the subsurface region, development of a range of models is a way to avoid future uncertainty. The disparity among the models displays our confusion. One or few models are typically used in a given project due to the cost of running several models via a flow simulator. The choosing of a model should be achieved with different parameters or new knowledge such that it is more precise and reliable. Streamline simulation helps analyze the effects of geologic instability on fluid movement and storage parameters, making it possible to use a more computationally expensive but more practical simulation. One of the primary goals of reservoir characterization is to develop a prediction model of a reservoir using a combination of descriptive and quantitative methodologies.

Reservoir characterization has developed into a broader field, combining many divisions of geoscience and engineering. The method involves geological or geophysical analyses and petrophysical characterization of the reservoir. Petrophysical research is essential for knowing the properties of a reservoir in an oilfield.

Another subfield of petroleum engineering is reservoir simulation, which helps characterize the reservoir. Reservoir simulation is one of the essential components of field development, and it is crucial for understanding reservoir behavior. The primary purpose of a reservoir analysis is to anticipate the performance of a reservoir and suggest strategies and procedures for optimizing eventual recovery. Computer simulations are utilized to divide the reservoir into a number of blocks and solve the fundamental equations of fluid flow in porous media at each block, allowing for a more comprehensive examination of the reservoir (Aziz & Settari, 1979). Finite-difference techniques are the most often used simulation methodologies;

however, recent simulation models include finite-volume and finite-element methods to discretize governing equations.

Some simulators represent fluid flow using mathematical methodologies, such as material balance, while others employ graphical approaches. Although this kind of reservoir simulation may not always accurately represent the full spectrum of characteristics or processes under the surface, it is a relatively rapid and affordable technique for reservoir engineers to manage reservoirs better. Some examples of these fast analytical reservoir simulation techniques include the Havlena–Odeh and Tarner methods, fractional flow curve methods (such as the Buckley–Leverett one-dimensional displacement method and the Deitz method for inclined structures), sweep efficiency estimation techniques for waterfloods, and decline curve analysis, among other things.

Figure 1 depicts the many reservoir models that may be examined in this process, ranging from primary analogs and decline curves to comprehensive physics models. As a result, model complexity and resolution may be adjusted depending on the particular aims of the study, data availability, and reservoir and production system type. Full physics models include connected flow and geomechanical models, coupled surface and subsurface flow models, as well as compositional and temperature simulators. While understanding the underlying physics of these complex systems is beneficial, these models need extra high-quality data, computational resources, time, and processes to be incorporated into a decision-making process effectively. Simple analytical models, on the other hand, can capture the key driving mechanisms with fewer data, computer resources, and development time. However, their simple assumptions may be incorrect in certain instances, and the anomalous behaviors seen in the field may go unaccounted for by these models. As a result, effective implementation of these models requires familiarity with a wide range of analytical solutions and their underlying assumptions and the ability to make appropriate revisions to individual circumstances. Even when a more complicated grid-based reservoir model is justified, analytical models may accelerate learning and minimize uncertainty in early evaluations.

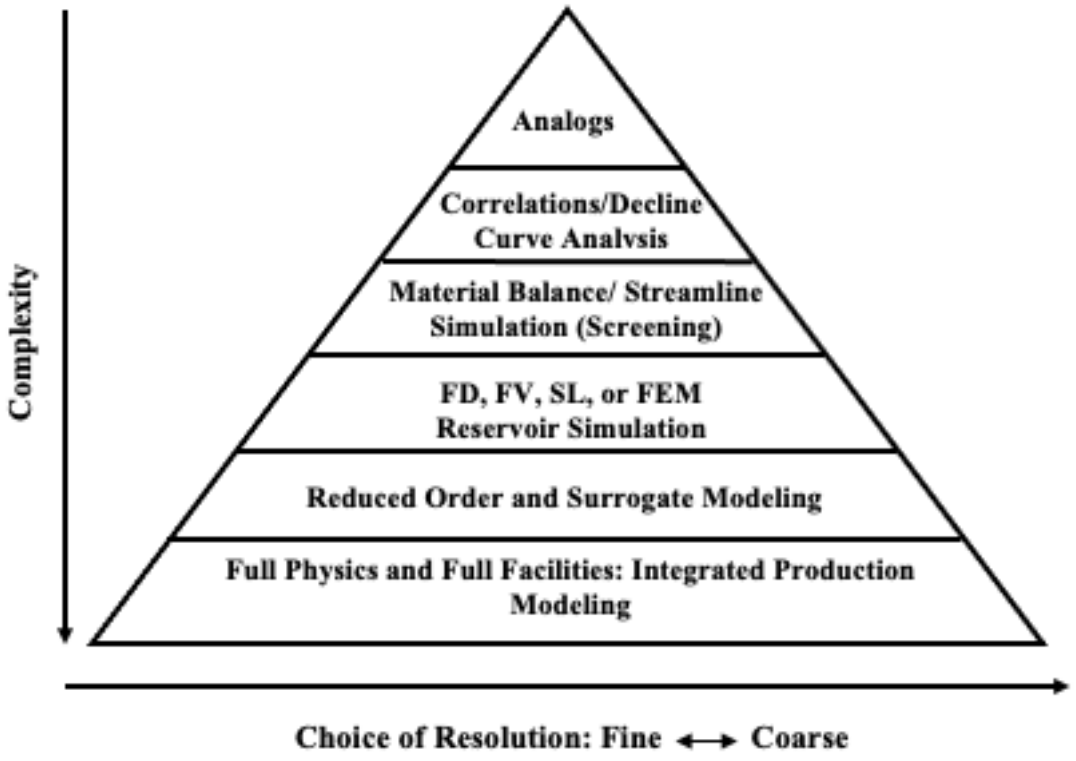

Figure 1. Types of reservoir models (adapted from Gildin & King (2013)).

Such computational tools are helpful during the whole lifetime of the field. Several tools and numerical techniques are practical during the enhanced oil recovery process. These approaches include pumping fluids into reservoirs to increase production. Due to the heterogeneity and complexity of the majority of reservoirs, having a comprehensive understanding of reservoir property distributions, especially communication across wells, is one of the essential factors in ensuring that fluid injection programs are effective. The history-matching process is one example of numerical reservoir simulation. This simulation requires building a geological model and the entry of several input parameters about reservoir and well properties. Because only a few pieces of the required information are accessible and typically known with a high degree of uncertainty, the model calibration produces non-unique results. Furthermore, the history matching procedure is time-consuming and labor-intensive. Consequently, numerical modeling may not always be a viable option, especially in a highly dynamic situation when immediate reservoir management decisions are necessary.

1.1 Capacitance – Resistance Model

Another way of doing quick simulations is analogous to the governing equations of fluid flow in porous media and electrical current in electrical circuits. A potential difference

drives the movement of fluids and the flow of electrons (current). Due to the compressibility of fluids, they are retained in the reservoir, while electrons are kept in capacitors in circuits. Initially introduced by Yousef et al. (2007), capacitance resistance models (CRMs) are a collection of straightforward material-balance models based on this analogy and simulating the capacity and resistivity of porous media. These models can account for well interference and forecast reservoir performance based on historical data by using just production and injection rates and, if available, the producer's bottom-hole pressure (BHP).

Sayarpour (2009) extended CRM by providing analytical solutions to the model's fundamental differential equation. Sayarpour (2009) proposed three reservoir-control volume solutions: field drainage volume, producer drainage volume, and drainage volume between injector/producer pairs. CRM may be used for a single well, a group of wells, or an entire field study using these analytical tools. The approach used is determined by the user's objectives and desired level of precision. In general, it treats the reservoir as if it were a system, with the injection rates serving as the inputs and the production rates serving as outputs (Figure 2). It is possible to determine the injection performance over a period of time by examining the CRM parameters, which are connectivities and time constants. Capacitance (compressibility) and resistive (transmissibility) effects are included in the CRM equations.

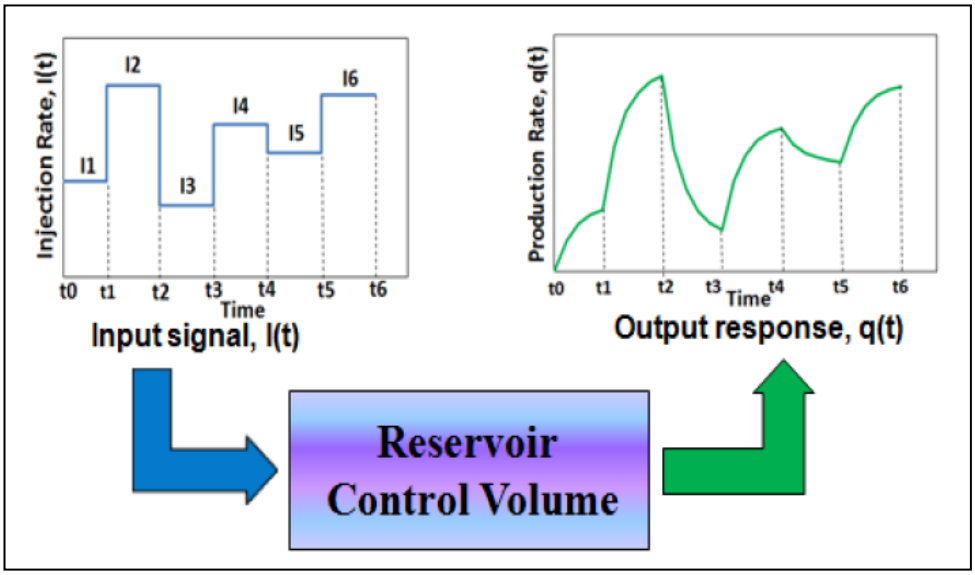

Figure 2. Schematic representation of the impact of an injection rate signal on total production response for an arbitrary reservoir control volume in the CRM (Sayarpour, (2009))

CRM calculates model parameters primarily based on historical data matching and matching of data. The quantity of oil produced is forecasted based on CRM data to optimize the amount of oil produced. The reallocation of water injection optimizes future oil. It is

recommended over other tools because of its simplicity, low computing time, and the use of readily accessible field data. However, it has several severe limitations, such as the sensitivity to reservoir events and the number of data inaccuracies.

1.1.1 CRM Development

Capacitance – Resistance Model is a fast and straightforward approach and a powerful tool for reservoir engineering, which couples' material balance and inflow equations. This material balance model was reached out to a few reservoir control volumes by utilizing superposition in time and space (Yousef et al. (2006); Liang et al. (2007); Sayarpour et al. (2009)). The main material balance equation for all representation is:

$$c_t V_p \frac{d\bar{P}}{dt} = \omega(t) - q(t) \quad \text{Eq. 1}$$

where c_t – total compressibility, V_p – pore volume, P – volume averaged pressure, w(t) – injection rate, q(t) – total production rate (oil+water). The deliverability equation is defined as:

$$q(t) = J(\tilde{P}(t) - P_{wf}(t)) \quad \text{Eq. 2}$$

where P_{wf} is the producer's BHP, and J is the productivity index. Thus, $\tilde{P}$ can be expressed in terms of q, $P_{wf,}$ and J and substituted in Equation (1) to obtain the following Equation:

$$\tau \frac{dq}{dt} + q(t) = w(t) - \tau J \frac{dP_{wf}}{dt} \quad \text{Eq. 3}$$

where the volumes must be at reservoir conditions and τ is the time constant given by:

$$\tau = \frac{c_t V_p}{J} \quad \text{Eq. 4}$$

Different reservoir control volumes are applied to portray the reservoir models. As the CRM investigation is generally centered around the interwell scale, it can unveil the diverse potential for recuperation measures. Such CVs as CRMT: single tank, CRMP: producer based, CRMIP: injector-producer pair based. Certain assumptions included a comprehensive derivation of Equation (3) based on an immiscible two-phase material balance.:

1. constant temperature;
2. slightly compressible fluids;
3. negligible capillary pressure effects;
4. constant volume with instantaneous pressure equilibrium;
5. constant J.

These assumptions also apply to the multiple CRM representations. The general analytical solution of Equation (3) can be discretized as follows:

$$q(t_n) = q(t_0)e^{-\frac{-t_n-t_0}{\tau}} + \sum_{k=1}^{n}((1-e^{-\frac{\Delta t_k}{\tau}})\left(w(t_k) - J\tau\frac{\Delta P_{wf}(t_k)}{\Delta t_k}\right)e^{-\frac{-t_n-t_k}{\tau}} \quad \text{Eq. 5}$$

CRMT: Single Tank

CRMT is defined as the drainage volume of the whole reservoir (Figure 3) or a specific portion of the reservoir containing various injectors and producers. When the field size is small, the CRMT enables quick history matching and prediction. Due to the inexpensive cost and utility of its estimated parameters as a starting point for more rigorous representations, they may give insight into effective injection rates in reservoir sites. To examine flow patterns and optimize reservoir hydrocarbon recovery, it is required to employ models that allow for the calculation of individual well flow rates rather than a single pseudo-well. The material balance is calculated using a single pseudo-producer and a single pseudo-injector by summing all of the relevant rates (Sayarpour et al. (2009)), which are assumed to be constant. Adding the parameter f (sometimes referred to as interwell connection, gain, or injection allocation factor) to Equation (3) allows it to account for the impacts of leakage (f <1), aquifer pressure support (f >1), and communication across reservoirs (Fox et al. (1988); Weber (2009)). In turn, this leads to the existence of the following ordinary differential equation (ODE):

$$\tau\frac{dq(t)}{dt} + q(t) = fw(t) - \tau J\frac{dP_{wf}(t)}{dt} \quad \text{Eq. 6}$$

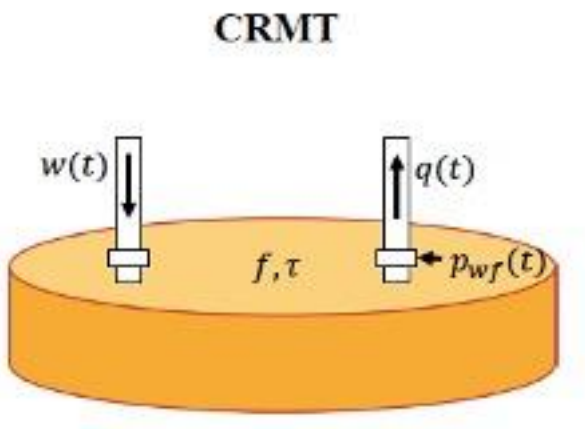

Figure 3. CRMT representation (adapted from Holanda et al. (2018))

CRMP: Producer-based

In the producer-based representation (CRMP), reservoir control volumes are specified as the drainage volume of each producer, including any injectors that impact their production

rates, as illustrated in Figure 4. All injectors can affect a producer unless a spatial window is set. Liang et al. (2007) were the first to introduce the CRMP. The CRMP allocates a one-time constant (t_j) to each producer's drainage volume and one connectivity (f_{ij}) to each well pair, resulting in the following continuity equation for producer j:

$$\tau_j \frac{dq_j}{dt} + q_j(t) = \sum_{i=1}^{N_{inj}} f_{ij} w_i(t) - \tau_j J_j \frac{dP_{wf,j}}{dt} \quad \text{Eq. 7}$$

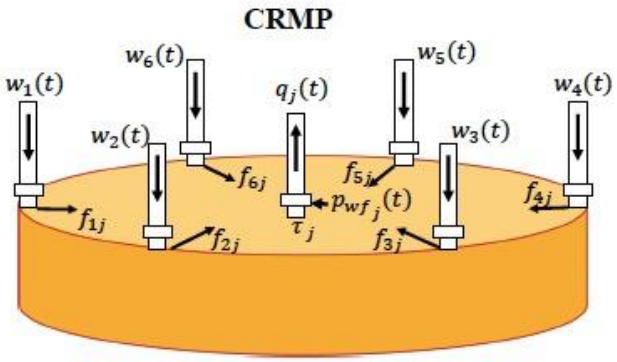

Figure 4. CRMP representation (adapted from Holanda et al. (2018))

CRMIP: injector-producer pair based

Using the injector–producer pair-based representation (CRMIP), where each injector–producer pair is assigned one time constant (t_{ij}) and one connectivity (f_{ij}), as seen in Figure 5. As a result of using this strategy, the number of parameters is increased. The material balance equation is similar to Equation 6 for CRMT:

$$\tau_{ij} \frac{dq_{ij}(t)}{dt} + q_{ij}(t) = f_{ij} w_i(t) - \tau_{ij} J_{ij} \frac{dP_{wf,j}(t)}{dt} \quad \text{Eq. 8}$$

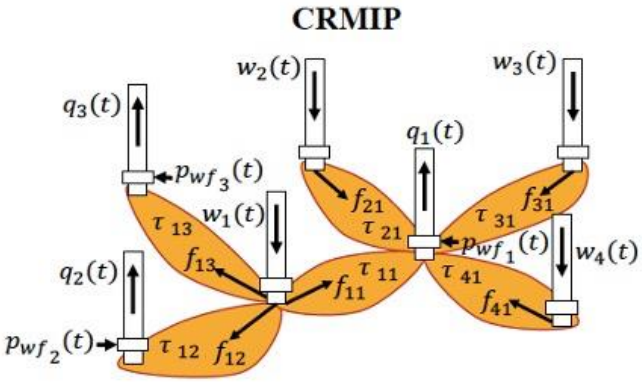

Figure 5. CRMP representation (adapted from Holanda et al. (2018))

1.1.2 Connectivity

The interwell connectivity, f_{ij}, also known as gain or allocation factor, is a critical component in the CRM. It is defined as the volume percentage of injected fluid from injector I that can be ascribed to the output at well j. At stable injection conditions, a defined rise in the injection rate by Δw_i is followed by an equal increase in the output rate by Δq_j, the rate at which the reservoir volumes are being filled. The knowledge presented produces an interpretation of the reservoir behavior and reaction to the control variables in the secondary and tertiary recovery processes. Knowledge of interwell connectivity is more critical in more complicated reservoirs such as heavy oil and heterogeneous formations. Simulation of fluid flow in porous media can also evaluate connectivity between wells.

As such, one must keep in mind that gains (fij) are only applicable to mature waterfloods when injection rates and the BHP of producers remain roughly constant. This is a relatively limiting situation since there are no substantial variations in the flow pattern.

Interwell connectivity may be an effective method to assess the influence of geologic characteristics on the productivity of floods. The development of CRM-based studies illustrates the increasing sophistication and realism of the basic geologic models. The knowledge gathered through reservoir connectivity may often be traced back to the geological factors that influence hydrocarbon recovery and recovery rates. For example, the dynamic behavior of fractures that fell behind water breakthroughs, such as flipping the location of the injection wells or causing a big difference in the amount of fluid injected into the formation and the amount created from the well, their fracture velocity will shift unexpectedly. Fractures, for example, may generate rapid water breakthrough in a producer (high f_{ij}) or water leakage to a thief zone (low f_{ij}), both of which are linked with poor sweep-efficiency, necessitating a redesign of the flooding process.

1.1.3 Applications of CRM

Capacitance – Resistance Model can be considered as a newly developed tool. However, this tool has many applications in the petroleum industry, even though CRM was initially designed for the waterflooding process.

For the case of primary recovery, Equation 3 was simplified to mitigate the influence of injection (w(t) = 0) (Nguyen et al. (2011); Izgec et al. (2012)). Drainage pore volumes (V_{pj}) and productivity indices (J_j) for each producer, together with average compartment pressure

(P(t), from Equation (2)), can only be calculated using the formulae in these works if c_t and BHP variations are known. They may be used to multiwell systems without knowing reservoir parameters (such as porosity, permeability, and thickness) and are an alternative to the classic build-up test since no shut-in period is necessary. Pseudopressure functions developed by Izgec et al. (2012) allowed this technology to be used in gas wells.

The CRM has been used to enhance oil recovery (EOR) processes, despite the models given so far being primarily built for waterflooding applications. In some papers, the models that were used in waterflooding are used in the same way. In others, unique changes have been made to account for the unique features of the EOR process. Even though these simple models don't take into account the complexity of the physical and chemical interactions between fluids and rocks, the examples that are most commonly used show that they have a good history of matching and forecasting with grid-based reservoir simulations and field results. CRM, on the other hand, can be very useful in many EOR processes because it can help to figure out what drives pressure support, how different the reservoir is, and how quickly the flood front moves before building more detailed and time-consuming simulation models.

Several factors may be optimized during field development to conform with safety requirements, environmental laws, contractual obligations, or improve net present value (NPV). Examples of these variables include the bottom-hole pressure or injection speeds (with substantial control); location and direction of new wells (well positioning problem), the injected EOR fluids (e.g., fluid type, concentration, duration, and rate of each injected slug): (e.g., propped volume and number of stages for hydraulic fractures; concentration, injection rates and duration of acidizing treatment).

During the existence of a single oil field, the consistency of the oil grew and dropped due to improvements in the recovery phase. After primary recovery, the rate of crude oil output falls and is approximately equivalent to the rate of crude oil flow. Oil saturation reduces with time when a secondary recovery process, such as waterflooding, is done. Only oil is generated when the flooding agent is missing and the oil fractional flow is at its peak. However, until the flooding agent can breakthrough at the producers, the oil cut decreases monotonically, and the reservoir oil saturation may eventually reduce to the residual oil saturation of secondary recovery. If non-recovery and recovery mechanisms are not pursued, oil cuts would ultimately go zero. During tertiary recovery, the residual oil saturation is partly or entirely mobilized, and the amount will rise before a plateau is hit. By that point, the cut will extend beyond zero. The

cumulative oil production (N_P) can match the initial oil in place if the field has no residual oil at the end of tertiary recovery.

Oil extraction values are readily obtained during secondary and tertiary oil recovery. Then, integrating overall output estimations with oil recovery models allows one to provide reliable estimates of oil production rates for secondary and tertiary recoveries for a single producer, a group of producers, or a whole region. The historical oil output rate is used to find oil fractional flow model parameters and then uses these models to forecast potential oil production.

$$f_w = \frac{1+\frac{kk_{ro}A}{q\mu_o}\left(\frac{\partial P_c}{\partial x}-\Delta\rho g sin\alpha\right)}{1+\frac{k_{ro}\mu_w}{k_{rw}\mu_o}} = \frac{1+\frac{kk_{ro(S)}A}{q\mu_o}\left(\frac{\partial P_c}{\partial x}-\Delta\rho g sin\alpha\right)}{1+\frac{k_{ro(S)}\mu_w}{k_{rw(S)}\mu_o}} \quad \text{Eq. 9}$$

Equation 9 indirectly includes time as a variable that accounts for changes in permeability. Considering various forms of relative permeability curves and the influence of capillary pressures, we may evaluate oil fractions as a result of normalized water saturation. Normalized water saturation is represented by:

$$S(t) = \frac{S_w(t)-S_{wr}}{1-S_{or}-S_{wr}} \quad \text{Eq. 10}$$

where *Sw(t)* is the reservoir water saturation and is a function of time. By determining values of the initial and residual water and oil saturations, we can use water injection and oil/water production data to determine the normalized average water saturation in the reservoir over time. The average water saturation in the reservoir changes by the rate of water accumulation in the reservoir for each production interval:

$$\bar{S}_w(t_n) = \bar{S}_w(t_{n-1}) + \frac{(i(t_n)-q_w(t_n))}{V_p}\Delta t_n \quad \text{Eq. 11}$$

The last step to assess the oil/water fractional flow is to compare the oil and water permeability to saturation. Several statistical relationships are observed for total permeability versus the critical variable.

Due to find the oil/water fractional flow, it is essential to know the following:

1. Residual water saturation, *Swr*,
2. Residual oil saturation, *Sor*,
3. Pore volume, *VP*,
4. Relative permeability parameters.

These criteria may be calculated by history-matching.

Ignoring capillary strain for horizontal planes and utilizing specific gravity to approximate relative permeability curves. Equation 3 can be adjusted to yield a fractional flow as:

$$f_o(S) = 1 - \left[1 + \frac{(1-S)^m}{M_o S^n}\right]^{-1} \quad \text{Eq. 12}$$

where *m* and *n* are relative-permeability exponents, and *Mo* is the end-point mobility ratio:

$$M_o = \frac{k_{rw}^o \mu_o}{k_{ro}^o \mu_w} \quad \text{Eq. 13}$$

The Buckley-Leverett dependent fractional-flow model (BLBFFM) has unknown end-point mobility ratio (Mo), relative-permeability curve exponents (m and n), and BLBFFM (BLBFFM). Equation 9, BLBFFM. All three parameters uniforms. It also models parameters, which are unknowns in the BLBFFM, which may be assessed during history-matching. There are two basic BLBFFM variants: linear (m = n = 1) and nonlinear (m 1, n = 1). The BLBFFMs have structural characteristics that are restricted in certain circumstances.

As a tertiary recovery process, additional oil recovery is achieved by mobilizing the oil in the previously contained reservoir. The larger the interaction of the flood with the gasoline, the better the recovery. A front breakthrough of all oil should occur before production, and the residual oil saturation should be low. The oil output volume rises with time as the sum of trapped/residual oil increases and the oil front bursts beyond its reserve boundary. Finally, the oil production hits its limit and steadily decreases, and finally exceeds zero when either miscibility is lost, or the trapped residual oil vanishes.

Immiscible floods require a fractional-flow model for CO2-oil miscible flood as a function of time to break the share of oil production rate from the CRM's overall production rate calculation. The K-factor model or Koval process can be used in this case.

The K-factor or Koval model is one of the early methods to modeling oil/solvent flow focused on the Buckley and Leverett system for flow in a flood scenario. In his approach, Koval (1963) updated the (Leverett & Buckley, 1942) fractional-flow equation by the effective viscosity, E, which is based on data utilizing the following Equation 14:

$$E = \left[0.78 + 0.22 * \left(\frac{\mu_o}{\mu_s}\right)^{0.25}\right]^4 \quad \text{Eq. 14}$$

Through neglecting the effects of gravity in the Leverett fractional-flow model, Equation 15, Koval's alternate solvent extraction process:

$$f_s = \frac{1}{1+\frac{1-S_s}{S_s}\frac{1}{K}} \quad \text{Eq. 15}$$

where S_s is the solubility exponent, and K =(E/H). The H component quantifies the variability of the media. If the medium is homogeneous, then H=1, If heterogeneous, then H>1. A solvent fractional-flow model was presented/developed after the breakthrough.

VP_i as a function of pore volume injected (K) for K=1.5 to K=10.

$$f_s = \frac{K-\left(\frac{K}{V_{Pi}}\right)^{0.5}}{K-1} \quad \text{Eq. 16}$$

The pore volume injected at the time of solvent breakthrough is 1/K, and solvent fractional-flow will be one when the pore volume injected is equal to K. Based on the Koval Model, the cumulative oil production, as a function of injected pore volume and Koval factor is

$$N_p(t) = N_p(V_{Pi}) = \frac{2\left(\frac{K}{V_{Pi}}\right)^{0.5} - 1 - V_{Pi}}{K-1} \quad \text{Eq. 17}$$

Kaviani (2014) provided a sensitivity analysis on various parameters in order to figure out their impact on the reservoir model. Due to this analysis, Kaviani defined a dimensionless number, the CM number (C), which helps specify the range of applications of the CRM. Such parameters as diffusivity constant, the number of producers, the number of data, and noise were used on synthetic fields created on Eclipse 100™. The reservoir conditions must satisfy the main CM assumptions to estimate representative parameter values within the analysis time window (time span t_0 – t where the flow rates are used):

1. Constant number of producers;
2. Constant producer productivity indices;
3. Known or constant producer BHP;
4. Sufficient and accurate data;
5. Slightly compressible fluid;
6. Near-unit mobility ratio.

However, not all of these assumptions may be satisfied in real fields.

To enhance the efficacy of any EOR process, it is critical to understand displacement efficiency at the interwell scale (e.g., pore, interwell, basin). Yousef et al. (2009) sought to

establish a diagnostic tool for the injection sweep efficiency on an interwell scale when they created a flow capacity map. Izgec (2012) also provided an example of how this idea may be used. To show them on this figure, the cumulative flow capacity (Fmj) and cumulative storage capacity (mj) must be derived using the CRMIP parameters. These measures are defined as follows:

$$F_{mj} = \frac{\sum_{i=1}^{m} f_{ij}}{\sum_{i=1}^{N_{inj}} f_{ij}} \quad \text{Eq. 18}$$

$$\Phi_{mj} = \frac{\sum_{i=1}^{m} f_{ij}\tau_{ij}}{\sum_{i=1}^{N_{inj}} \tau_{ij}} \quad \text{Eq. 19}$$

There are four producers in a channelized reservoir shown in Figure 6. This map shows how the flow is spread over the pore volume associated with each producer, i.e., the proportion of flow originating from a particular percentage of the pore volume. – All of the pore volumes are swept equally in an ideal displacement. The unit slope line would suit the curve in this scenario. Consequently, the differences between the 45° lines of each curve in the porous media may be linked to various forms of heterogeneity in the porous media (e.g., fractures, high-permeability layers) and serve as an indicator of the sweep efficiency of a producer. The more efficient it is, the closer it gets to the 45° line. In order to adequately mobilize the oil left behind the recent flood front, the flow capacity map permits the identification of problematic wells that may need an EOR operation.

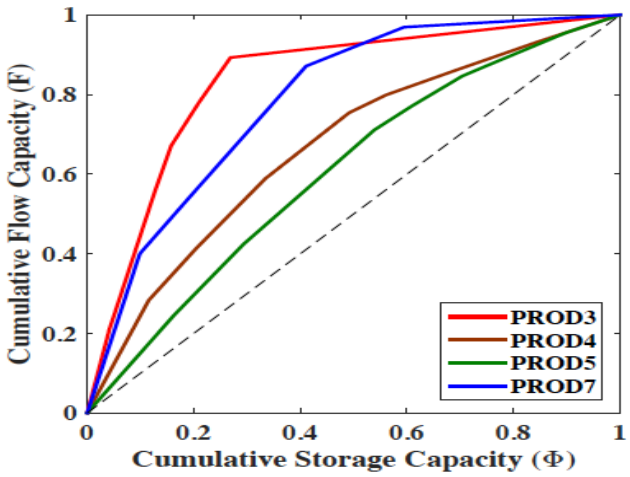

Figure 6. Flow capacity plot for four producers

Several authors implemented CRM to model and evaluate Enhanced Oil Recovery (EOR) processes such as:

- CO_2 flooding (Sayarpour (2008); Eshraghi et al. (2016));
- Water alternating gas flooding (Sayarpour (2008); Laochamroonvorapongse (2013); Laochamroonvorapongse et al. (2014));
- Simultaneous water and gas flooding (Nguyen, 2012);
- Hydrocarbon gas and nitrogen injection (Salazar et al. (2012));
- Isothermal EOR (solvent flooding, surfactant-polymer flooding, polymer flooding, alkaline surfactant polymer flooding) (Mollaei and Delshad (2011));
- Hot waterflooding (Duribe (2016));
- Low salinity water flooding (Zivar et al. (2022)).

Additionally, CRM was modified to be applied in CO_2 Sequestration modeling (Tao (2012); Tao et al. (2013); Tao et al. (2015)) and geothermal reservoirs simulation (Akin (2014) and Li et al. (2017)).

1.2 Tracer Flow Testing

Tracer testing is just a method of determining the subsurface characteristics. Tracer testing may be described as the injection of one or more tracers (often chemical compounds) into the subsurface to estimate the subsurface's flow and storage characteristics in its most basic form. Using a tracer test to characterize groundwater characteristics is an indirect means of doing so. In this case, the accuracy of the model used to do the analysis is directly related to the quality of the study.

Tracer testing provides a number of benefits as well as disadvantages. Due to the indirect nature of the approach, test analysis cannot be considered unique for all reservoirs. Various reservoir descriptions may provide varied tracer test results for the same tracer test. This is because test analysis produces volume-averaged features independent of spatial order to a certain degree. In comparison to other direct characterization methods (e.g., coring), tracer testing has the benefit that the volume tested may be tailored to be at the proper size for the application in question.

An important point to remember when discussing tracer tests is that they are nothing more than a way to estimate the flow parameters of a porous medium; they have no intrinsic value on their own. Tracer tests are used to answer questions about a specific medium's flow and storage characteristics. There are maybe the following questions:

- What properties of a given medium need to be estimated? At what volume?

- Can a tracer test obtain an estimate of this property at that scale?
- Is a tracer test the best method for estimating the property?

A tracer test may evaluate medium properties. Tracer residence times are used to compute swept pore volume (the volume of the medium immediately contacted by tracers) and phase volumes (or saturations). With the correct tracers and data, one can determine total pore volume, phase volumes, and saturations. When using several extraction wells, the geographical distribution of these properties may be estimated from the changes in residence durations for each injection/extraction well combination. Similar tracer studies done at different times may assess cleaning efficiency (for example, before and after a remediation procedure). In certain cases, the surface area may be determined by comparing the residence times of conservative and adsorbing tracers. Using tracers of different molecule sizes and diffusivity rates, one may estimate the fracture-matrix surface area for mass exchange. The reactivity of a medium may be determined via reactive tracer injections and in situ decay rates.

Tracer test analysis may also provide information on more particular medium characteristics. It is possible, for example, to extract streamline geometries (flow and storage capacity) from a cumulative tracer recovery history graphic and use them in other applications. The proportion of rapid or slow flow routes is immediately visible from that figure, allowing for identifying flow conditions at the extremes. It is possible to get estimates of dispersivities and other constitutive relations by using a numerical model in conjunction with flow geometry obtained from tracer experiments (relative permeability and capillary pressure versus saturation). Generally speaking, tracer testing characterizes subsurface properties. These properties are summarized in Table 1:

Table 1. Summary of properties available from the tracer test

1	Fluid velocities
2	Swept pore volume
3	Phase volumes or saturations
4	Surface areas for heat or mass transfer

5	Biological activity (decay constants)
6	Flow and pore geometry distributions
7	Clean-up efficiency
8	Hydraulic conductivity
9	Phase dispersivities

1.2.1 Conductivity

The hydraulic conductivity of a system changes as fluid flows through rock. The frictional resistance is governed by the fracture network geometry, fracture surface geometry (including fracture coating, fault gauge, and other properties), and fluid viscosity.

Hydraulic conductivity is spread unevenly across a flow channel, which is obvious once you recognize what you're looking at. The hydraulic gradient and its direction cause flow to be unevenly distributed along a fracture plane. This phenomenon is known as flow channeling. In fracture planes, channeling can occur due to a variety of factors, including

1) the variable aperture of the flow porosity between adjacent fracture surfaces,
2) intersecting fractures where the fracture intersection itself acts as a flow tube or "wormhole" of enhanced transmissivity, and
3) joint intersections with offset displacements.

It should be observed that both offset displacements at joint intersections and lateral displacements of mated fracture surfaces may result in significantly anisotropic flow channeling effects when they are combined. It is also possible that the presence of loose fracture filling materials and secondary mineralizations will significantly impact the degree of channeling.

In-fracture dissolution and precipitation processes, as well as large-scale tectonic events, all cause changes in hydrodynamic characteristics. Dissolution-precipitation feedback effects may occur when reactive materials are transferred in a strongly channeled flow. However, it may also occur at present temperatures if there are major changes in the groundwater chemistry or other situations. In essence, it may respond unfavorably when fast-moving water contacts slower-moving water or rock in channels or stagnant places parallel to the main flow

path. Changes in chemistry and temperature may trigger the reaction. Spheroidal weathering processes may enhance the effective hydraulic aperture, resulting in an increase in the effective hydraulic aperture.

Because channeling affects not only the hydraulic features of the fracture but also its retention capacity, it is important to understand how channeling affects fractures. In example, channeling minimizes the contact area between running groundwater and the rock matrix when compared to when groundwater runs over the full fracture surface. This is especially true for retention via matrix diffusion.

When studying a three-dimensional fracture network, the geometry of the individual fractures in conjunction with the degree of connectedness of the fracture network has a significant impact on the hydraulic conductivity of the rock volume as a whole, according to the literature. As a result, when scaling up from a tracer test, the flow scenario gets progressively complicated as the length scale of the tracer test increases. In actuality, the flow channel geometry is significantly more complicated than the geometry of the hydraulically conducting components.

1.3 CRM and Tracer Flow Testing

Since the CRM gives an assessment of total fluid production and is restricted to immiscible displacement, an extra process is needed for computing tracer concentration to couple into the CRM. In such a manner, tracer models are then evolved dependent on miscible displacement theory.

Two prominent effects have an effect on the distribution of the tracer flow: small-scale dispersion and large-scale channeling (a combination of heterogeneity and viscous fingering). It begins by developing the tracer models independently of these two influences. The dispersion model was constructed using solutions to the convection-diffusion equation, which describes mixing on a fundamental scale. The Koval model was developed from the Koval theory, which predicts that miscible displacement would be shown using a single component to demonstrate heterogeneity. At this phase, both the dispersion effect (dispersion-only model) and the channeling effect (Koval model) are numerically consolidated and combined into a single model (Lake L. W., 2017).

Dispersion happens in a miscible displacement and causes a local mixing between two miscible liquids. The convection-dispersion Equation (CDE) in one-dimension, expecting homogeneous porous medium, isothermal conditions, incompressible liquid and rock, ideal mixing, and single-phase flow can be communicated in dimensionless structure as (Lake L. , 2014):

$$\frac{\partial c_D}{\partial t_D} + \frac{\partial c_D}{\partial x_D} - \frac{1}{N_{Pe}} \frac{\partial^2 c_D}{\partial x_D^2} = 0 \quad \text{Eq. 20}$$

where c_D is the dimensionless concentration, x_D is the dimensionless distance, t_D is the dimensionless time; the cumulative fluid injection per unit pore volume, N_{Pe} is the Peclet number; the ratio of convective and dispersive transport. The smaller the Peclet number, the more significant dispersion occurs.

The effluent concentration can be determined from the solution for CDE. Superposition in time is applied to the solution to incorporate both the front and back edge of the tracer slug injection. At that point, composing this arrangement condition utilizing the term of injected tracer concentration (c_o), delivered tracer concentration (c) and accepting zero initial concentration yields:

$$c = \frac{c_o}{2}\left[erfc\left(\frac{1-t_D}{2\sqrt{\frac{t_D}{N_{Pe}}}}\right) + e^{N_{Pe}} erfc\left(\frac{1-t_D}{2\sqrt{\frac{t_D}{N_{Pe}}}}\right)\right] - \frac{c_o}{2}\left[erfc\left(\frac{1-t_{Dx}}{2\sqrt{\frac{t_{Dx}}{N_{Pe}}}}\right) + e^{N_{Pe}} erfc\left(\frac{1-t_{Dx}}{2\sqrt{\frac{t_{Dx}}{N_{Pe}}}}\right)\right]$$

Eq. 21

and $$t_D = \frac{\sum_{t=0}^{t} i(t)}{V_p} \quad \text{Eq. 22} \qquad t_{Dx} = \frac{\sum_{t=t_x}^{t} i(t)}{V_p} \quad \text{Eq. 23}$$

Koval (1963) built up a model to anticipate the performance of unstable miscible displacement brought about by fingering a miscible solvent into the oil. The impacts that cause fingering are joined into one parameter, the Koval factor (Kv). The Koval model is analogous to (Leverett & Buckley, 1942) by applying straight-line permeability into fractional flow equation. With the front-facing advance formula, the fractional effluent flow can be determined from Equation 20 (Lake et al., 2014).

$$F_S|_{x_D=1} = \begin{cases} 0; \ t_D < \frac{1}{K_v} \\ \frac{K_v - \left(\frac{K_v}{t_D}\right)^{\frac{1}{2}}}{K_v - 1}; \ \frac{1}{K_v} < t_D < K_v \\ 1; \ t_D > K_v \end{cases} \quad \text{Eq. 24}$$

Applying this Equation to the tracer flow, $F_S|xD$=1 in this setting just methods the small part of tracer answer for all-out fluid at a producer. Since injected tracer solution is not 100% v/v tracer, F_S should be standardized by an injected tracer concentration (c_o) to acquire the delivered tracer concentration (c):

$$c = \frac{Tracer\ Volume}{Total\ Produced\ Volume} = c_o * F_S \quad \text{Eq. 25}$$

Tracer flow in the reservoir has a unity mobility ratio, so the Koval factor is equivalent to the heterogeneity factor addressing the channeling. The more influential the Koval factor, the more diverting in a tracer flow; the more unfavorable sweep would be in a displacement.

The Koval fractional flow was created under consistent displacing liquid injection with no neighborhood mixing. Combining the equations, a tracer breakthrough curve for consistent tracer injection can be developed, and the curve characteristic is characterized by the Koval factor, reflecting the large-scale heterogeneity.

In the case of multiple injectors and producers, where injected fluid can be distributed to several production wells because of interwell connectivity (f_{ij}), dimensionless time in the produced tracer concentration equations can be used for considering the effect of partial injection fluid volume:

$$t_D = \frac{f_{ij} \sum_{t=0}^{t} i(t)}{V_p} \quad \text{Eq. 26}$$

From another hand, each producer can gain the fluid from many injectors. Therefore, the concentration of tracer flowing in the reservoir is diluted at the wellbore by the tracers from other injection wells. Hence, the concentration has to be corrected:

$$c_{out_{ij}} = \frac{c_{ij} * q_{ij}}{q_j} \quad \text{Eq. 27}$$

where c_{outij} is the tracer concentration of tracer i at producer j accounting for total produced volume, c_{ij} is the tracer concentration calculated from the equations, which is based on fluid from injector i only. q_{ij} is the fluid from injector i to producer j. q_j is the total produced fluid at producer j.

A history matching of production data is performed by nonlinear regression, which minimizes the difference between the calculated and measured rates. If the system is at equilibrium, the history matching can be done simultaneously for all production wells. This means an absolute error of the production calculation is minimized over the entire field production. The least-square objective function for production matching is

$$\min z = \sum_{k=1}^{n} \sum_{j=1}^{N_p} \left(\left(q_j^k\right)_{obs} - \left(q_j^k\right)_{cal} \right)^2 \quad \text{Eq. 28}$$

where $(q_{jk})_{obs}$ is the observed production rate data of producer j at time step k and $(q_{jk})_{cal}$ is the model-calculated production rate of producer j at time step k. The constraints are:

$$\tau_j > 0 \; and \; f_{ij} \geq 0 \qquad \text{Eq. 29} \sum_{j=1}^{N_p} f_{ij} \leq 1 \; for \; any \; i \quad \text{Eq. 30}$$

While the CRM calculates total fluid production, the tracer model computes produced tracer concentration. Injection and production rates, along with the outcomes acquired from the CRM, are needed to contribute to the tracer model. Produced tracer concentration for every injector-producer pair (c_{outij}) is then determined by utilizing the tracer model equations introduced previously. This parameter is utilized to match with the produced tracer concentration estimated in the field. Like the CRM, produced tracer matching is basically a nonlinear regression technique to get best-fit model parameters. Since the tracer models are applied to an individual injector-producer pair, tracer concentration estimation error is limited for each well pair autonomously. The target work for tracer history matching is:

For any injector-producer pair, ij:

$$\min z = \sum_{k=1}^{n} \sum_{j=1}^{N_p} \left(\left(c_{out_{ij}}^k\right)_{obs} - \left(c_{out_{ij}}^k\right)_{cal} \right)^2 \quad \text{Eq. 31}$$

where $c^k{}_{outij}$ is the produced tracer concentration from injector i at producer j at time step k. The constraint is:

$$V_{p_{ij}}, N_{Pe_{ij}} > 0 \; and \; K_{v_{ij}} \geq 1 \qquad \text{Eq. 32}$$

The following methods were tested to integrate the CRM and tracer models: serial fitting and simultaneous fitting.

Allowing each model to run separately, one at a time is a simple way to integrate the tracer model into the CRM. The CRM is used to approximate the gains and time constant in this process by comparing output data. The calculated gains from the CRM are then input into the tracer model, which is used to measure and match produced tracer concentration, calculating the tracer model parameters. Figure 7 depicts a workflow that can be seen in this situation.

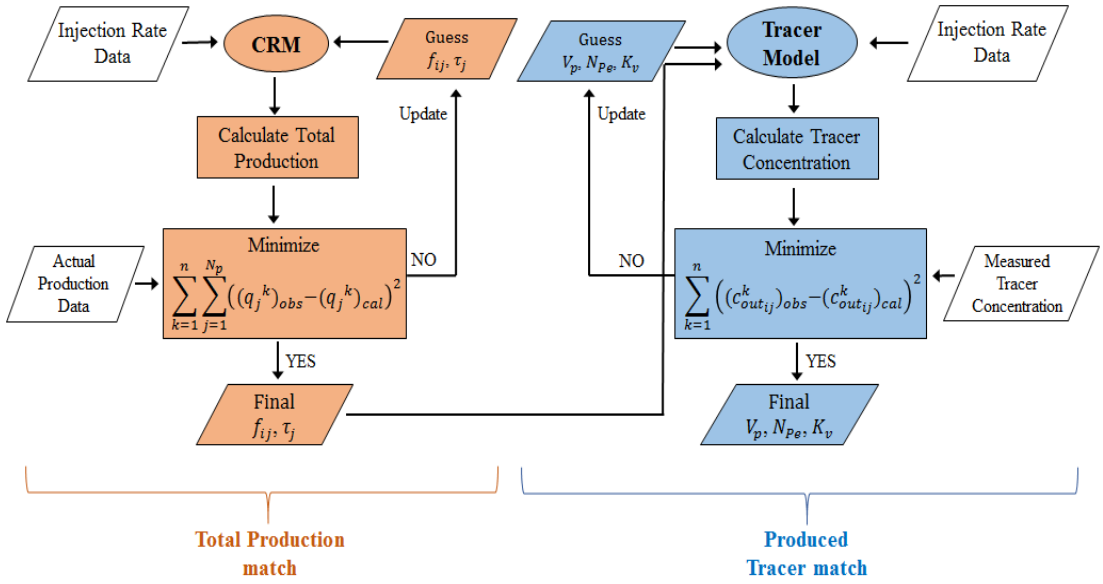

Figure 7. Workflow for integrating the CRM and tracer models by serial fitting (Lake L. W., 2017)

Simultaneous fitting requires data to be fitted for both the CRM and the tracer models simultaneously. Figure 8 shows the workflow for the simultaneous fitting process. Simultaneous fitting considers the gains as fitting parameters in both the CRM and the tracer model, unlike serial fitting, which fixes the gains inputting into the tracer model.

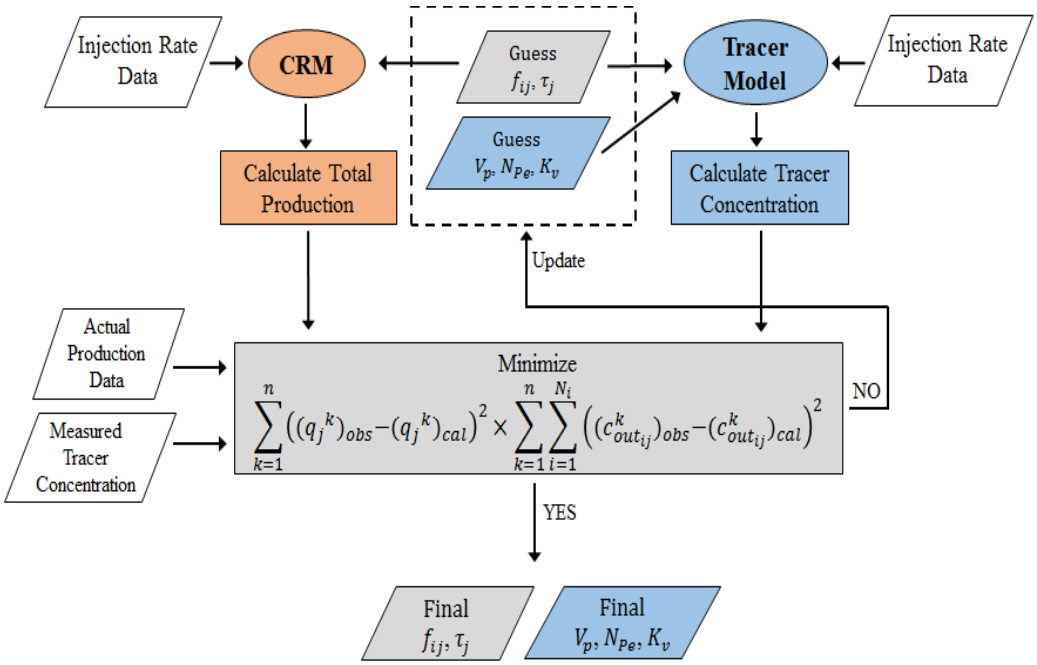

Figure 8. Workflow for integrating the CRM and tracer models by simultaneous fitting (Lake L. W., 2017)

1.4 Problem statement

Any field operations are costly and require some time to take place. Some operations require the stoppage of production, some of them not. Tracing flow testing does not require injection or production interruption because tracer agents (chemicals) are mixed with injection water. However, many considerations have to be made in order to fit the cost and ecological requirements when preparing the chemicals.

Capacitance – Resistance Model (CRM) is a rapid, simple, and powerful analytic tool that can forecast and optimize future oil production by modeling the waterflooding process. CRM does not need any geological knowledge and instead relies only on injection and production data for its inputs. It treats the reservoir as if it were a system, with the injection rates serving as the inputs and the production rates serving as the outputs. When evaluating the percentages of injected fluid and the time it takes for the fluid to reach a producer over a period of time, the injection performance may be determined. This approach has found application also for tracers testing. However, available works show a need for tracer concentration for CRM calculation.

Considering all of this information, the following questions can be raised:

1. How beneficial will be the conventional workflow of CRM to mimic the tracer flow testing?
2. What effect will be shown in the case of introducing additional restrictions or their changes on the interwell connectivity?
3. How effective will CRM be if it replaces tracer flow testing?

1.5 Objective

Specifically, the objective of this study is to determine if the typical CRM methodology can be used to simulate tracer flow testing in advance without combining the CRM with tracer concentrations. The interwell connectivities may act as "tracer concentrations" and, as a result, may be used to determine the flow path. Due to this reason, there is no need to go further for production optimization. In addition, two parameters are introduced: well spacing and fluid loss. These settings are required in order to get findings that are more similar to those obtained from the tracer test. The various cases have been carried out on two fields: a synthetic field and a real field, in order to determine if CRM may be used to replace the tracer flow test. Only acceptable scenarios are included in this study, which better describe the CRM as a tool for replacing the tracer test than any other.

1.6 Outline

This thesis consists of 4 chapters:

- Chapter 1 is an introduction that describes the background of CRM and tracer flow test, and consists of problem statement and objective;
- Chapter 2 is a methodology which was used in order to implement CRM;
- Chapter 3 is the results obtained from CRM for 4 cases based on synthetic field, and 1 case for real field;
- Chapter 4 is a conclusion of this work with some recommendation for future research.

CHAPTER 2. METHODOLOGY

When comparing CRM and tracer tests, the depth of investigation should be taken into consideration. The tracer chemical agent is often injected into an injector and monitored in the surrounding area during a tracer test. Hence, the injector/producer connectivity is determined for selected producers. A similar strategy is used in our CRM methodology. To evaluate the CRM and tracer techniques, this research used a synthetic field as well as a real field to collect data from both. The commercial simulator CMG was used to create the synthetic field, and the program was also used to model the injection/production history of the field. A field in Kazakhstan was also evaluated, and data on production/injection history, tracer test results, and tracer test assessment were gathered from that location. In order to remove well shut-in times and workover events from the production data, a pre-processing procedure has to be conducted first.

The following steps were applied to both fields:

1. Data gathering;
2. Data preprocessing;
3. Application of the CRM.

Data gathering

In all simulation procedures, gathering relevant data is the very first step that must be completed. Only injection/production data, as well as BHP (if available), are required by the CRM. As a result of this feature, the CRM is far less computationally intensive than competing commercial simulators. But it is still required to understand other components of the reservoir that are not taken into consideration during the modeling process, such as well location, petrophysical and fluid properties, geological parameters, and so on.

For the purposes of this investigation, two fields were introduced: synthetic field and real field. Each field has a unique data collection method that must be followed. In the case of the synthetic field that was created in the commercial simulator CMG, the process of getting the required data is simplified, and the reservoir may have either idealistic or near-realistic features depending on the data that is collected. There is nothing that can be modified

considerably in the actual world, and the data is set in stone. The real field data can have some gaps in production/injection history. Due to this reason, the next step is required.

Data Pre-processing

This step is necessary to smooth the fluctuations in production/injection data. The synthetic field requires no pre-processing technique because all information from such fields is available in full. During the real field's lifetime, different events can happen, for example, wells shut-in periods, workover jobs, emergencies, etc. Due to these reasons, there is a definite need to use such approaches. The CRM is sensitive to the available data and it is not recommended to have gaps in the data because misinterpretation can happen. To overcome this issue, the averaging of the available data was used to fill in the blanks when wells are temporarily shut for some periods due to numerous reasons.

Tracer injection analysis

The response seen in Figure 9 is typical of a tracer test. Using fluid samples obtained from production wells, it is possible to determine whether or not there is communication between injector and producer wells. To capture the tracer flow throughout a short and long time period, the sampling frequency was increased during the early phases of the inquiry; however, the frequency of samples collected decreased as time progressed in the analysis. Because of the tracer response curves, it is easy to determine the tracer retrieval percentages as well as the amount of fluid that is moved between each injector-producer pair using a single tracer response curve. Because of the existence of high permeability sections, greater conductivity between injector-producer pairs may be detected when tracer breakthrough occurs early in the time; however, when tracer breakthrough occurs late in the time, connection is weaker.

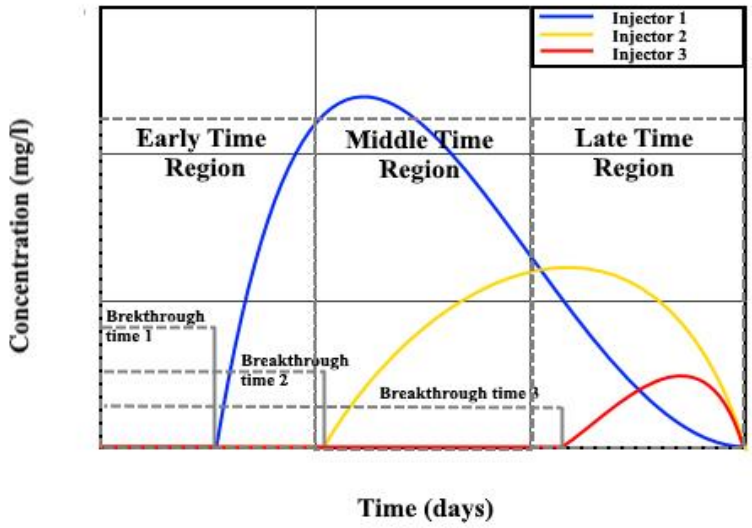

Figure 9. Schematical representation of tracer breakthrough curve response

Application of the CRM model

This is the core step which includes several sub-steps: selecting of appropriate CRM model, setting the constraints, using the appropriate solver tool. For this study, conventional Capacitance-Resistance Model – Producer-based (CRMP) workflow is used, which is shown in Equation 32. Due to the specificity of this work, different constraints were tested.

$$q_j(t_n) = q_j(t_0) * \left(e^{-\left(\frac{t_n - t_0}{\tau_j}\right)} \right) + \sum_{k=1}^{n} \left\{ e^{-\left(\frac{t_n - t_k}{\tau_j}\right)} * \left(1 - e^{-\frac{\Delta t_k}{\tau_j}} \right) \right\} \left[\sum_{i=1}^{N_i} f_{ij} I_i^{(k)} \right] \qquad \text{Eq. 32}$$

As an initialization, the MS Excel build-in solver is used. For this purpose, Generalized Reduced Gradient (GRG) Nonlinear was chosen as an optimization technique. The generalized reduced gradient is an iterative numerical method for solving optimization problems, which allows determining the "conditional" extremum of the objective function (minimum or maximum value). First, it was developed by Frank et al. (1956), and further expanded by Abadie and Carpentier (1969). The following algorithm is implemented in MS Excel Solver:

1. Divide the column vector of unknowns into a column vector of dependent (Y) and independent (X) variables. As a result, the problem of finding the extremum of a function is rewritten as follows:

   $$f(X, Y) \rightarrow min \qquad \text{Eq. 33}$$

   System of equations with restrictions:

$$g(X,Y) = \begin{cases} g_1(X,Y) = 0 \\ \dots \\ g_m(X,Y) = 0 \end{cases} \quad \text{Eq. 34}$$

2. Define analytical relations (in symbolic form) for calculating the reduced function gradient:
    - Determine the derivative of the objective function with respect to independent variables, taking into account the explicit dependence of the function on independent (X) and dependent (Y) variables:

$$\frac{\partial f(X,Y)}{\partial X}; \frac{\partial f(X,Y)}{\partial Y} \quad \text{Eq. 35}$$

    - Determine the derivative of the system of equations written for constraints with respect to independent variables, taking into account the explicit dependence of the function on independent (X) and dependent (Y) variables:

$$\frac{\partial g(X,Y)}{\partial X}; \frac{\partial g(X,Y)}{\partial Y} \quad \text{Eq. 36}$$

3. Set the initial approximation for the column vector of independent (X) variables:

$$X = \{x_1, \dots \dots, x_{n-m}\} \quad \text{Eq. 37}$$

At this step, the iteration process begins.

4. Determine the column vector of dependent (Y) variables at the current calculation step using a system of equations with restrictions:

$$g(X,Y) = \begin{cases} g_1(X,Y) = 0 \\ \dots \\ g_m(X,Y) = 0 \end{cases} \quad \text{Eq. 38}$$

5. Determine the value of the reduced gradient for the current step:

$$\nabla F_p = \left(\frac{\partial f(X,Y)}{\partial X}\right) - \left(\frac{\partial f(X,Y)}{\partial Y}\right) * \left(\frac{\partial g(X,Y)}{\partial Y}\right)^{-1} * \left(\frac{\partial g(X,Y)}{\partial X}\right) \quad \text{Eq. 39}$$

6. Determine the calculation step from the search condition for the extremum for the following function:

$$F(x_k \pm \lambda_k * \nabla F_p(x_k)) \quad \text{Eq. 40}$$

7. Determine the column vector of independent (X) variables at the next calculation step:

$$X_{k+1} = X_k \pm \nabla F_{p_k} * \lambda_k \quad \text{Eq. 41}$$

8. Check the criteria for stopping the iterative process:
    - the search trajectory remains in a small neighborhood of the current search point;
    - the increment of the objective function does not change;

- the gradient of the objective function at the local minimum point vanishes.

Otherwise, return to "step 4" and continue the iterative calculation.

Thus, in accordance with the presented method, there is a movement from any admissible point along the line (area) of the restriction until the extremum of the objective function f(x) (maximum or minimum of the function) is reached.

After all steps are done, obtained values of interwell connectivity can be compared with the values obtained from tracer test.

Fields description

Synthetic field

A sector with dimensions 50 (i) ×50 (j) ×5 (k) is developed by the CMG simulator in the black oil model (Figure 10). 9 production and 4 injection wells are added to the model. The average porosity for the entire field is 19.27% (min = 0% and max = 44.7%), the average permeability is 68 mD (min = 0.003 mD and max = 4020 mD). The initial pressure of the reservoir is 3000 psi, with a production bottomhole pressure of 500 psi.

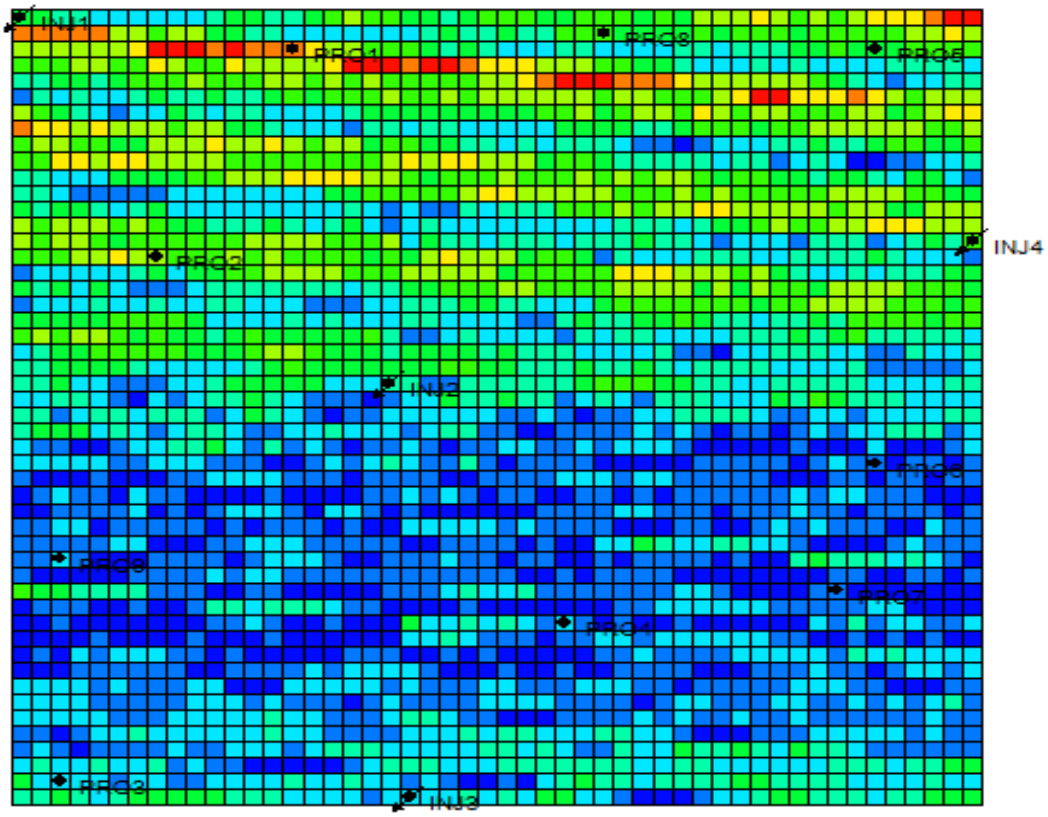

Figure 10. Synthetic field well's location

A parameter named well spacing was introduced. The well spacing is the maximum distance between an injector and a producer which is affected by that injector. Hence, the connectivity for an injector/producer pair, in which the distance between them is more than the well spacing is assumed to be zero. This parameter is schematically shown in Figure 11-a. Another parameter that was added to the CRM calculations was a fluid loss. Some part of the injected fluid from each injector may flow out of the reservoir and does not reach a producer. Hence, the summation of interwell connectivity for an injector may be less than one, which means that we need to tune the Σf_{ij} for the injector i to consider the fluid migration. Also, it is possible that water is reached to the producer not from the injectors but from other sources such as an aquifer, hence Σf_{ij} for a producer j may be higher than 1. This effect was also considered by the adjustment of the model. This parameter is also schematically shown in Figure 11-b.

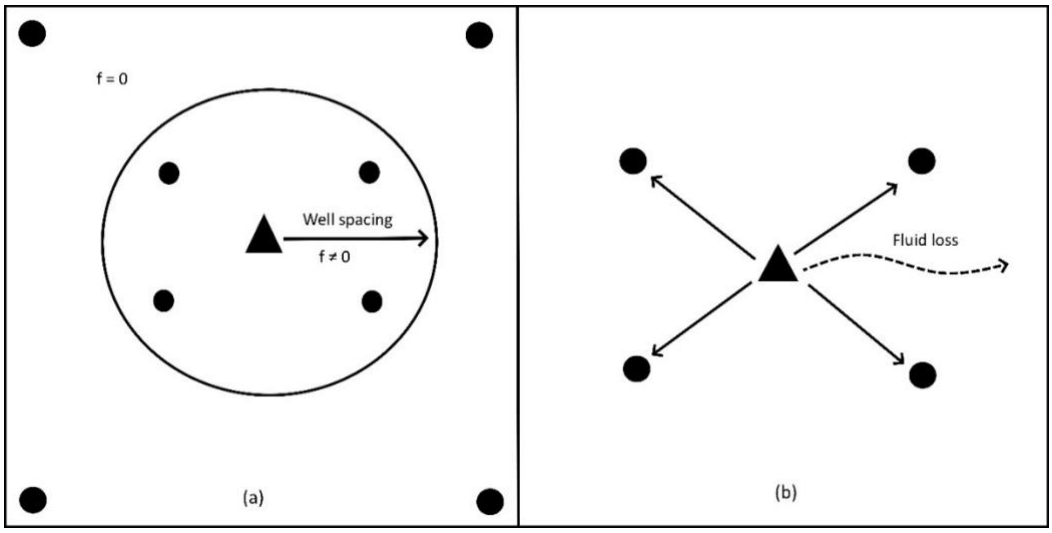

Figure 11. Schematic representation of (a) well spacing and (b) fluid loss

Real field

On the Y field (Figure 12) located in the West Kazakhstan region, there is a well stock in the amount of 70 wells that operate with high water cut (more than 80%). To understand the source of the produced water and the connectivity between injectors and producers, the tracer test was carried out in some injectors.

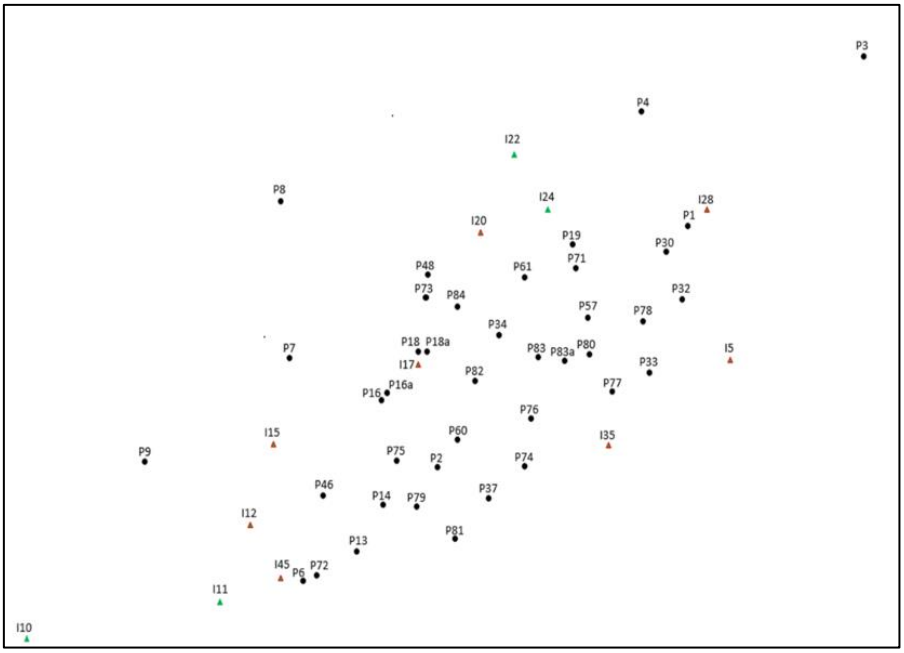

Figure 12. Well's location at Field Y

In this field, a given volume of a labeled liquid was injected and pushed back to the production wells by a continuous displacing waterflooding. Simultaneously, sampling is started from the production wellhead. Selected samples are analyzed under laboratory conditions to determine the tracer's presence and concentration. The observed tracer concentration versus time at each producer was analyzed to evaluate the influence of the waterflooding on the producing wells. Environmentally friendly water-soluble sodium fluorescein and ammonium nitrate chemical agents were selected for each injection well. These agents do not affect the properties of the flow and do not chemically interact with oil. The distance from injection wells to production wells ranges from 550 m to 1300 m. By the time of testing, tracer studies were carried out within 9 days. The tracer agent was injected through two injection wells (11 and 22). 18 wells were selected as control wells (wells 13, 14, 19, 30, 32, 34, 37, 46, 48, 57, 61, 71, 72, 73, 75, 79, 81, 84) as shown in Figure 13.

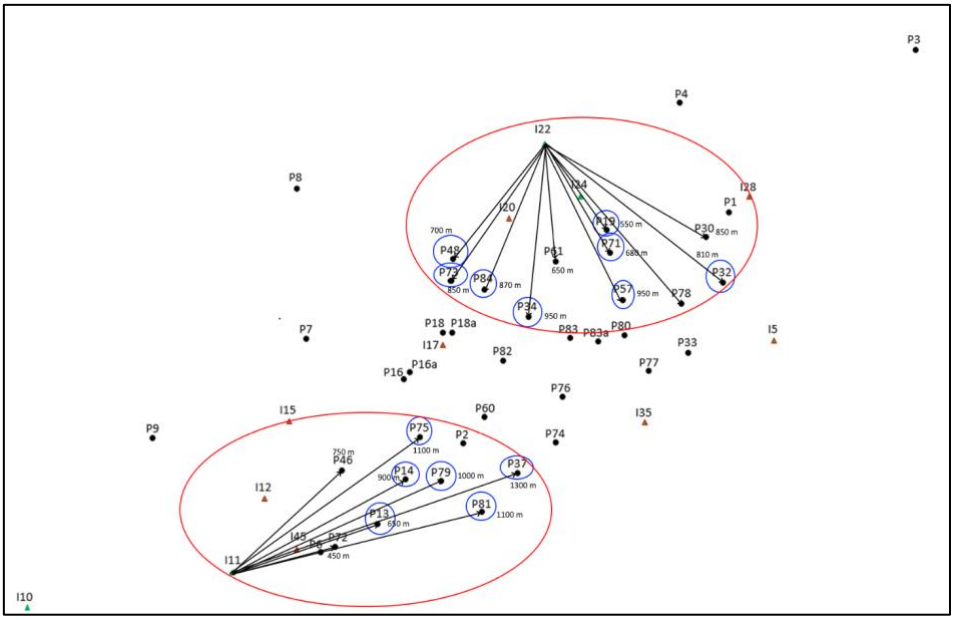

Figure 13. Observations wells for tracer test. Red circles represent the depth of investigation

CHAPTER 3. RESULTS AND DISCUSSIONS

The tracer flow test was carried out on the synthetic field. A slug of tracer chemical agent was injected into each injector and the response was observed in each producer and analyzed. The absorption of the tracers in the reservoir was ignored.

Figure 14 – 37 show the graphs of the tracer rates injection. Analyzing the graphs below, it can be concluded that breakthrough for each individual well occurs mainly in the middle-time region (MTR) and late-time region (LTR). When tracer breakthrough happens in the MTR, good or fair conductivity between injector-producer pairs can be observed, but when tracer breakthrough happens in the LTR, mostly bad conductive can be observed.

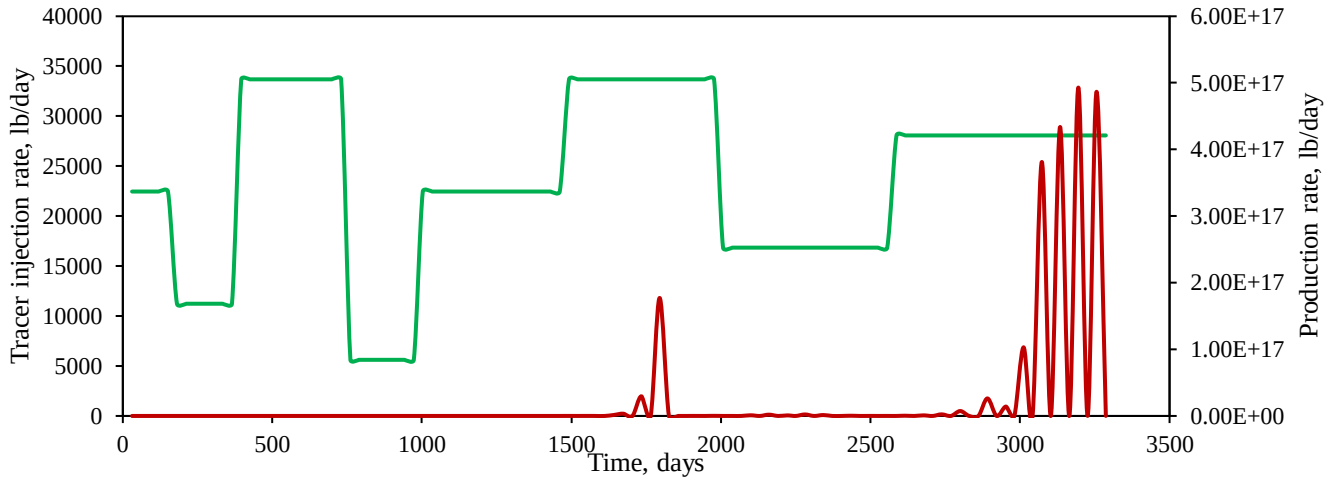

Figure 14. Tracer response in the producers 1 due to the injection from injector 1: the green line shows the production rate and the red line shows the tracer injection

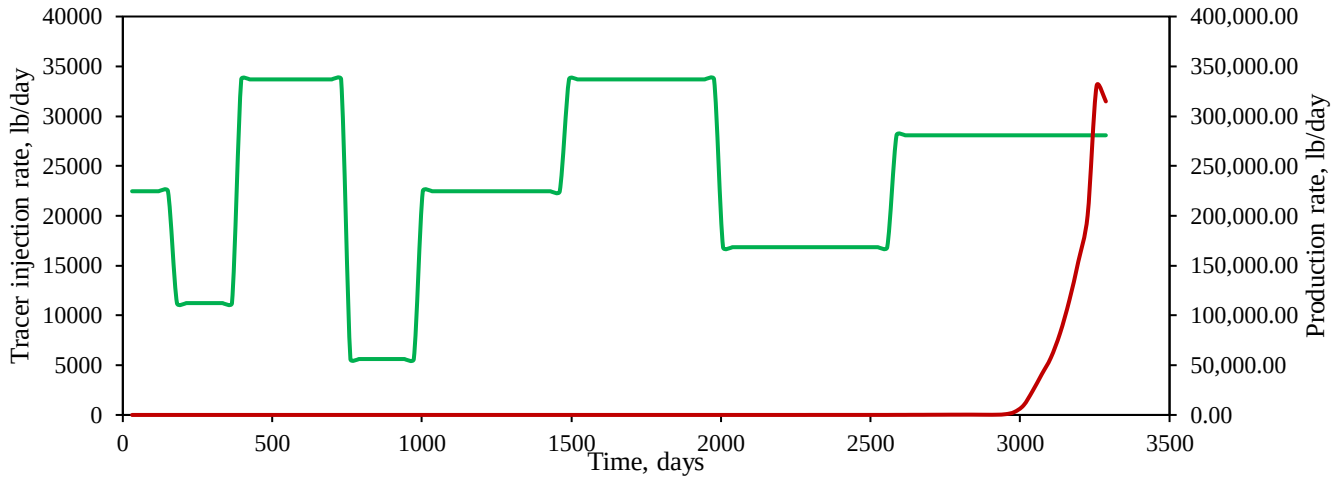

Figure 15. Tracer response in the producers 2 due to the injection from injector 1: the green line shows the production rate and the red line shows the tracer injection

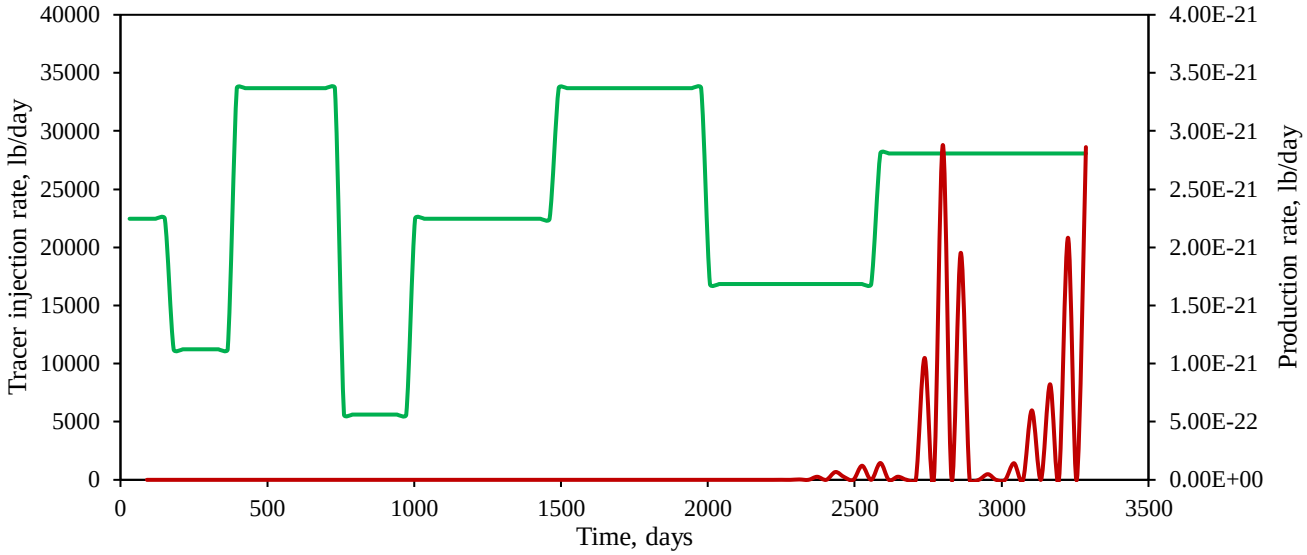

Figure 16. Tracer response in the producers 5 due to the injection from injector 1: the green line shows the production rate and the red line shows the tracer injection

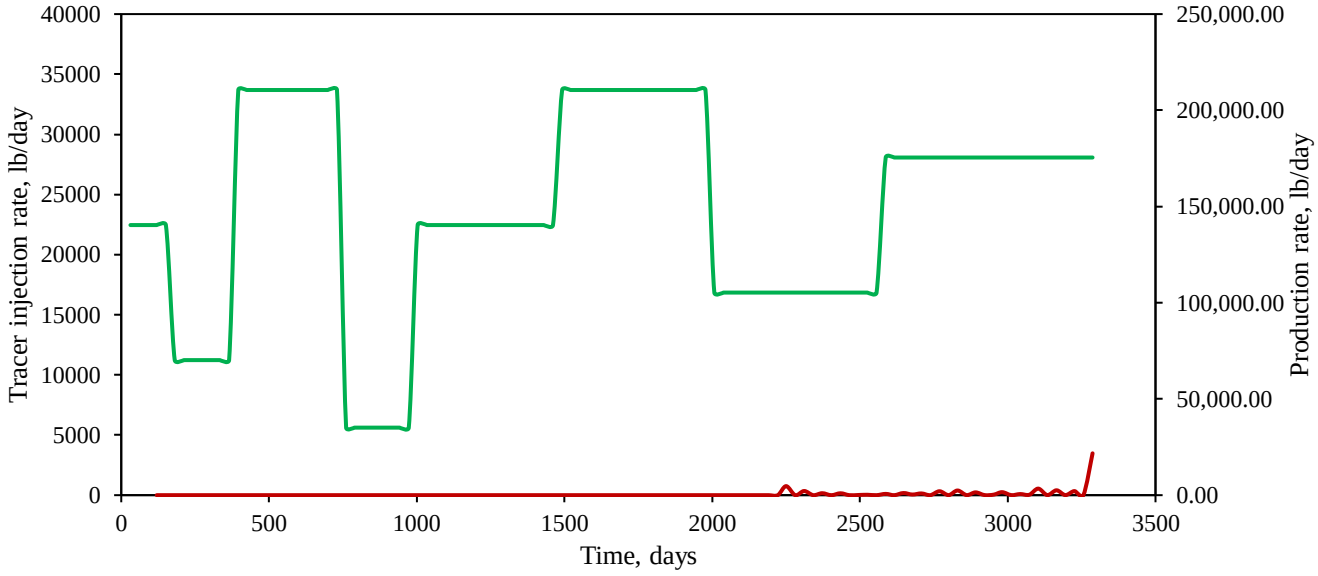

Figure 17. Tracer response in the producers 8 due to the injection from injector 1: the green line shows the production rate and the red line shows the tracer injection

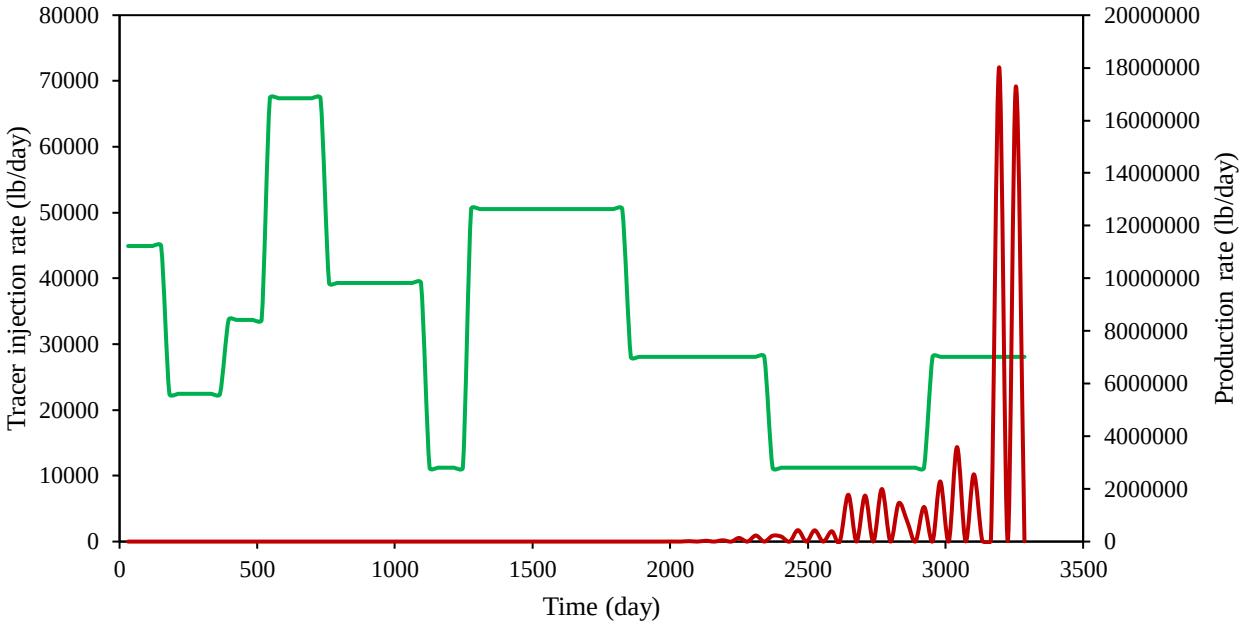

Figure 18. Tracer response in the producers 1 due to the injection from injector 2: the green line shows the production rate and the red line shows the tracer injection

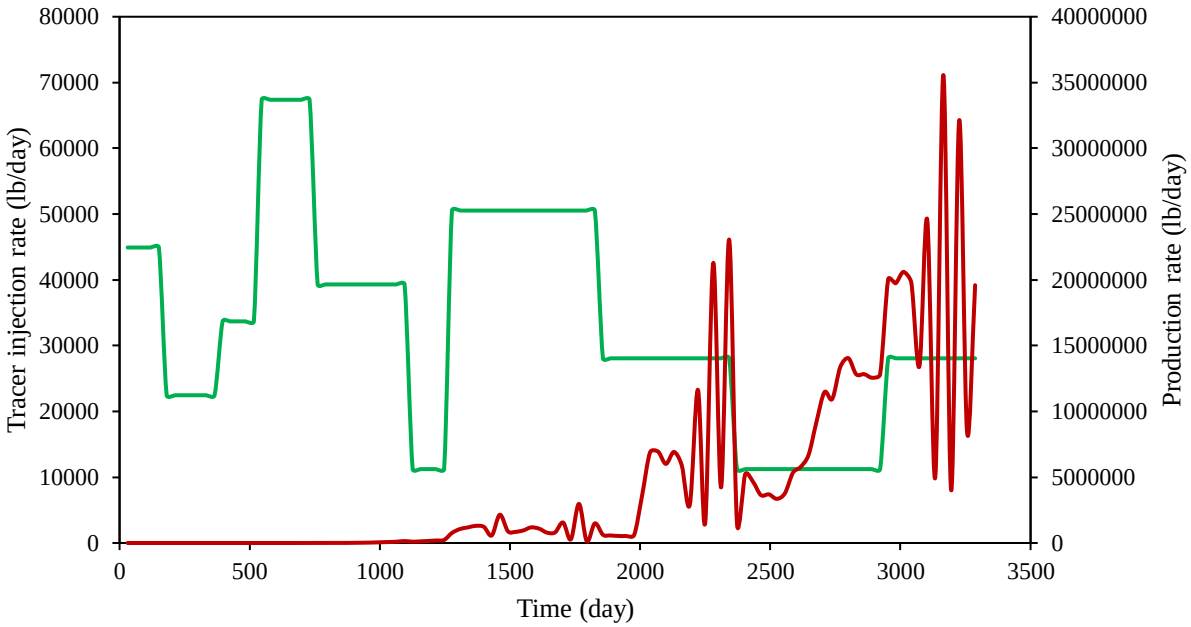

Figure 19. Tracer response in the producers 2 due to the injection from injector 2: the green line shows the production rate and the red line shows the tracer injection

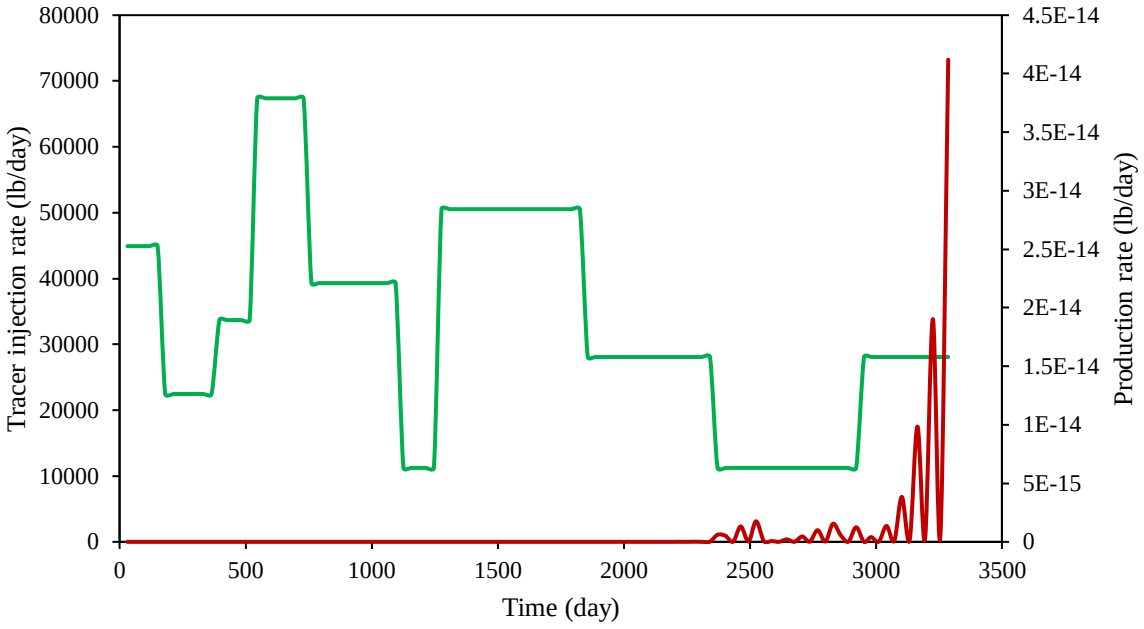

Figure 20. Tracer response in the producers 3 due to the injection from injector 2: the green line shows the production rate and the red line shows the tracer injection

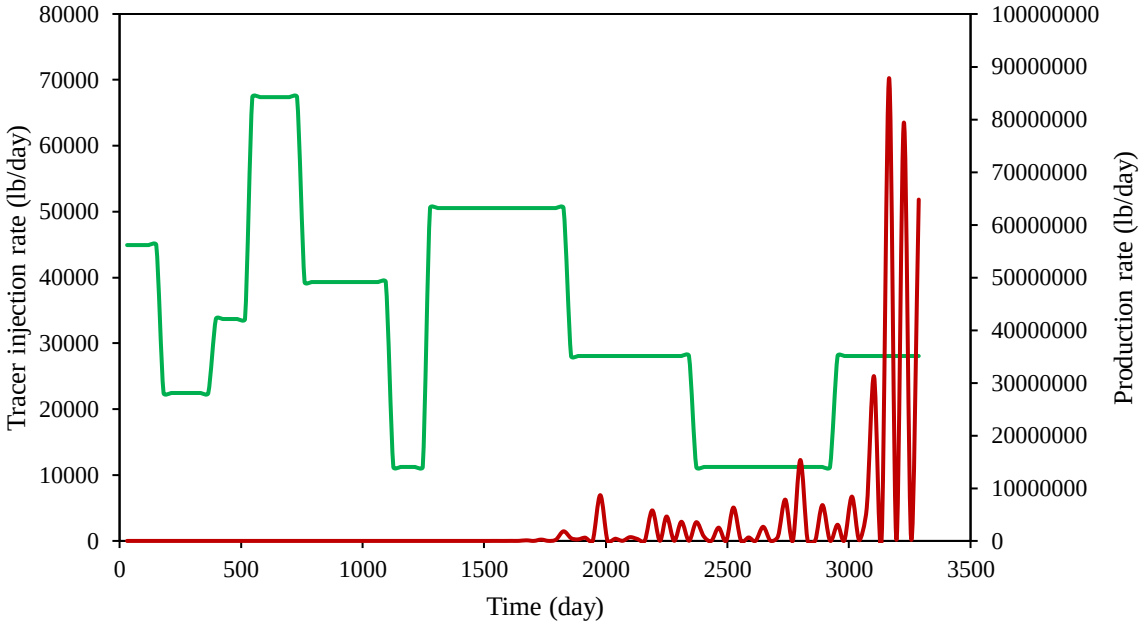

Figure 21. Tracer response in the producers 4 due to the injection from injector 2: the green line shows the production rate and the red line shows the tracer injection

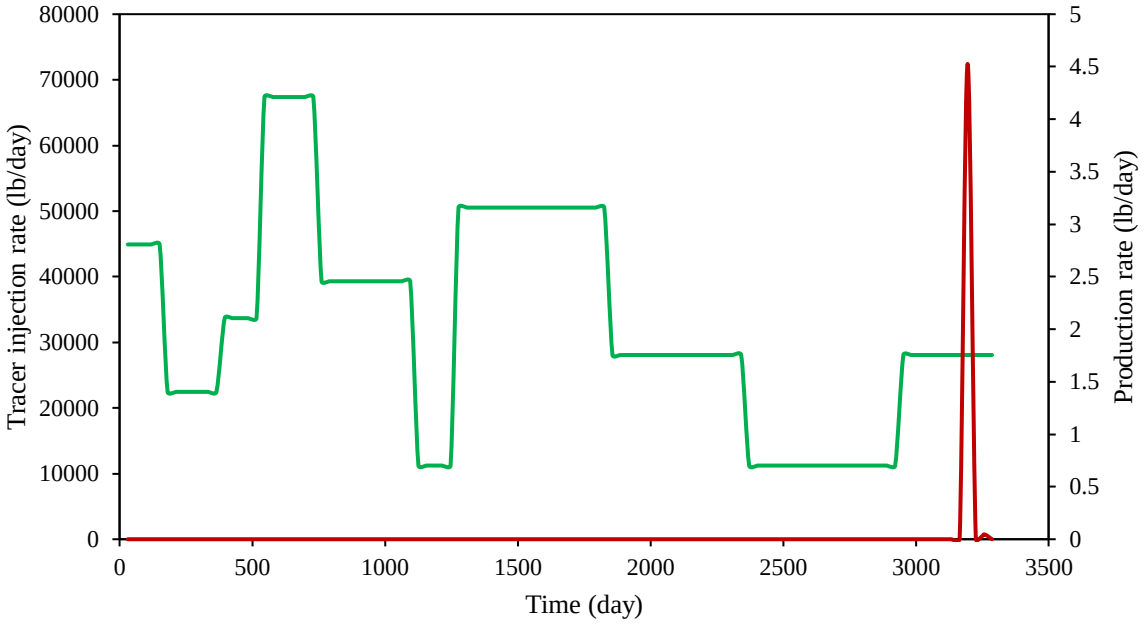

Figure 22. Tracer response in the producers 5 due to the injection from injector 2: the green line shows the production rate and the red line shows the tracer injection

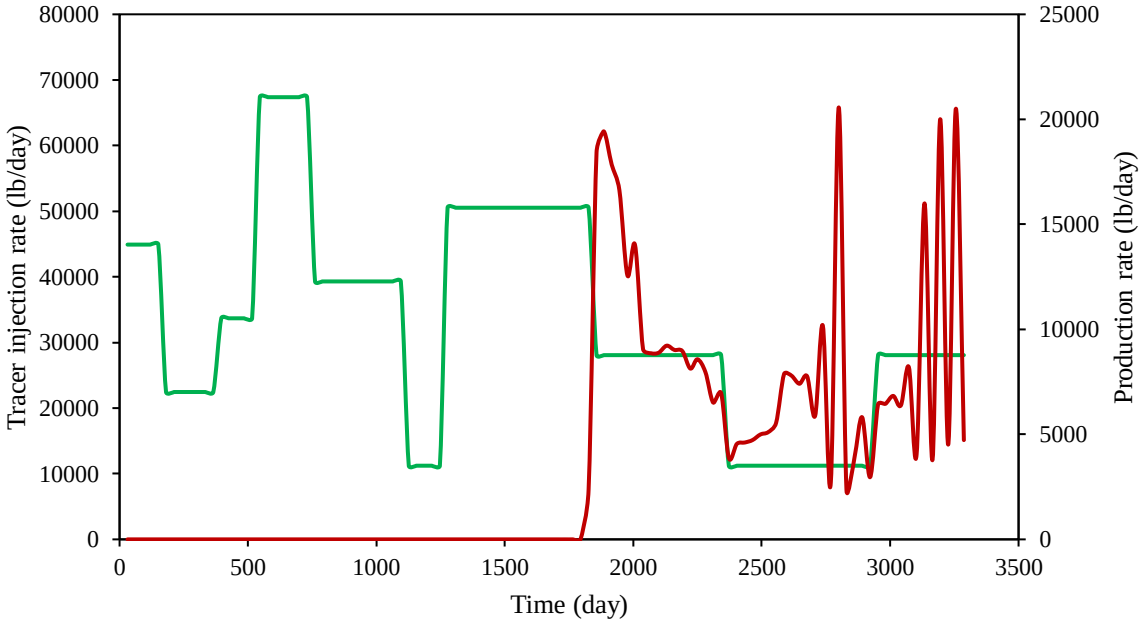

Figure 23. Tracer response in the producers 6 due to the injection from injector 2: the green line shows the production rate and the red line shows the tracer injection

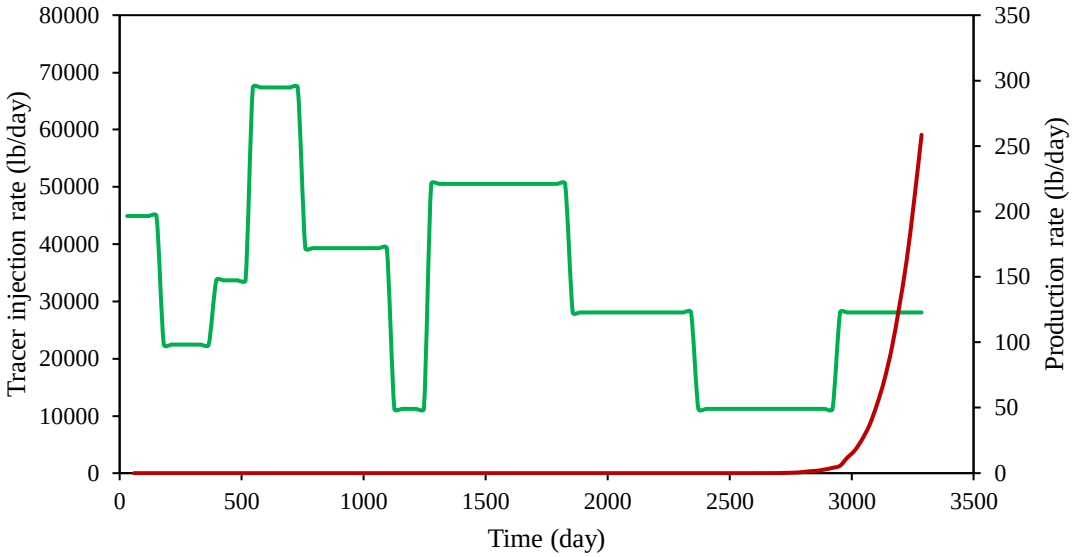

Figure 24. Tracer response in the producers 7 due to the injection from injector 2: the green line shows the production rate and the red line shows the tracer injection

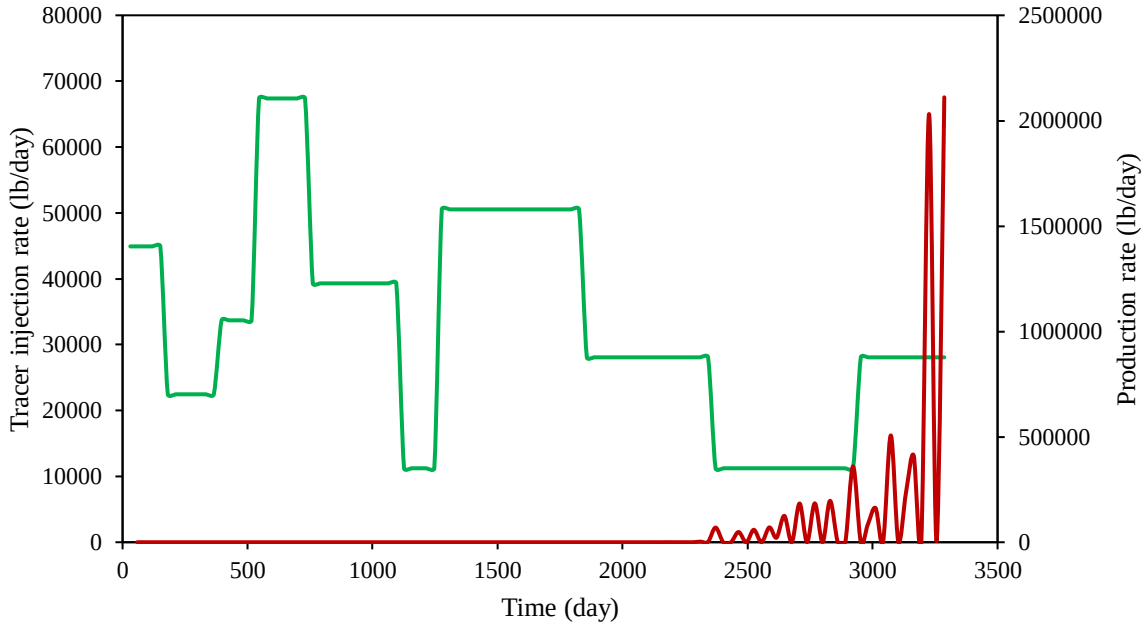

Figure 25. Tracer response in the producers 8 due to the injection from injector 2: the green line shows the production rate and the red line shows the tracer injection

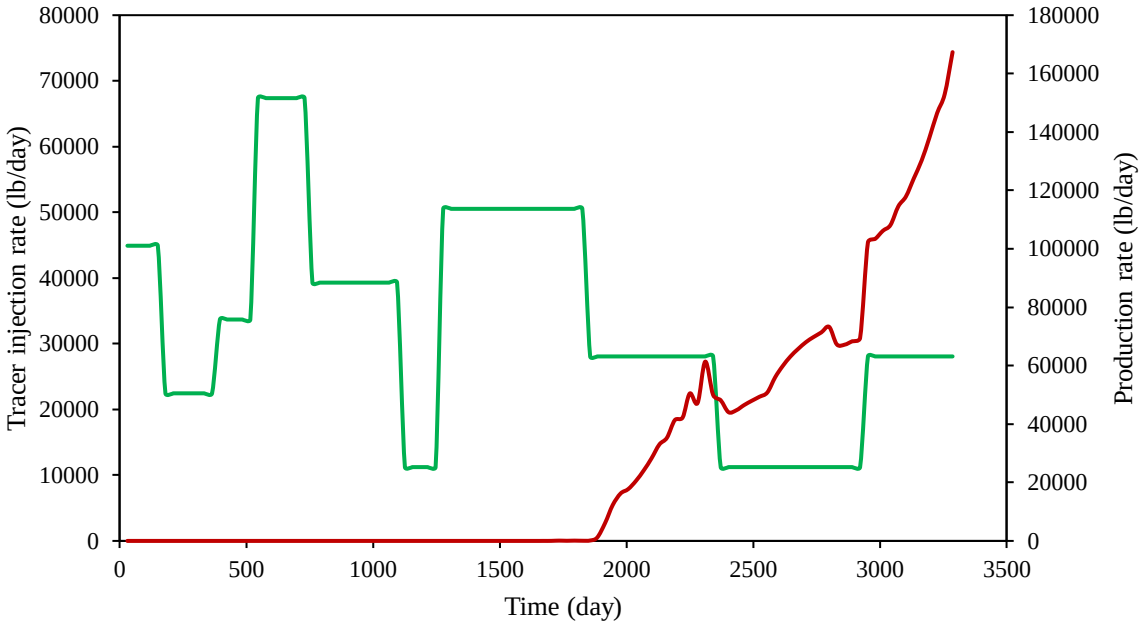

Figure 26. Tracer response in the producers 9 due to the injection from injector 2: the green line shows the production rate and the red line shows the tracer injection

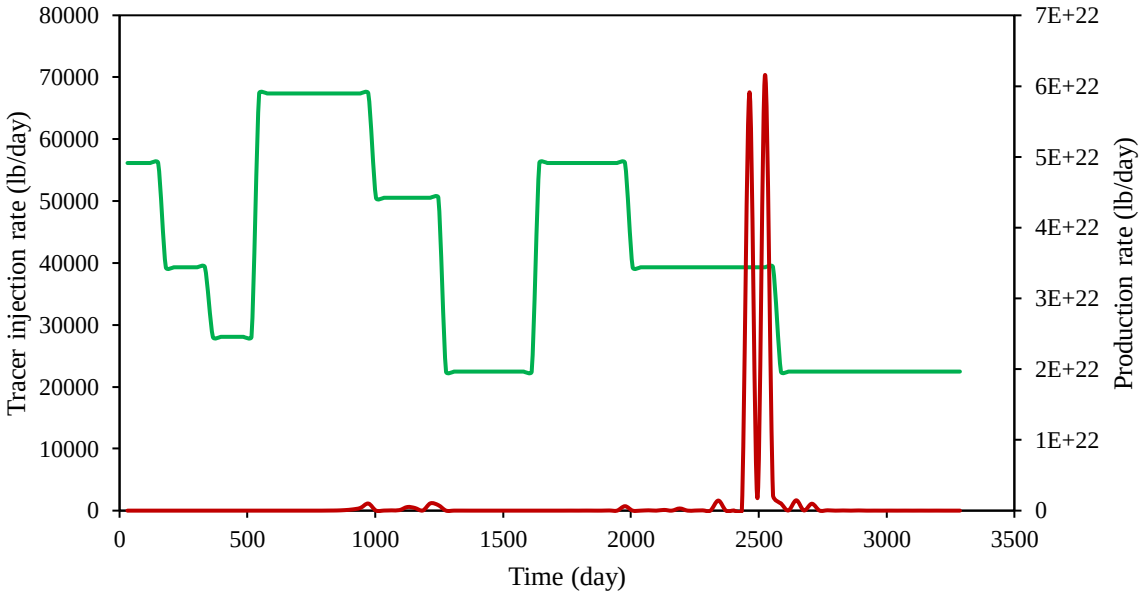

Figure 27. Tracer response in the producers 3 due to the injection from injector 3: the green line shows the production rate and the red line shows the tracer injection

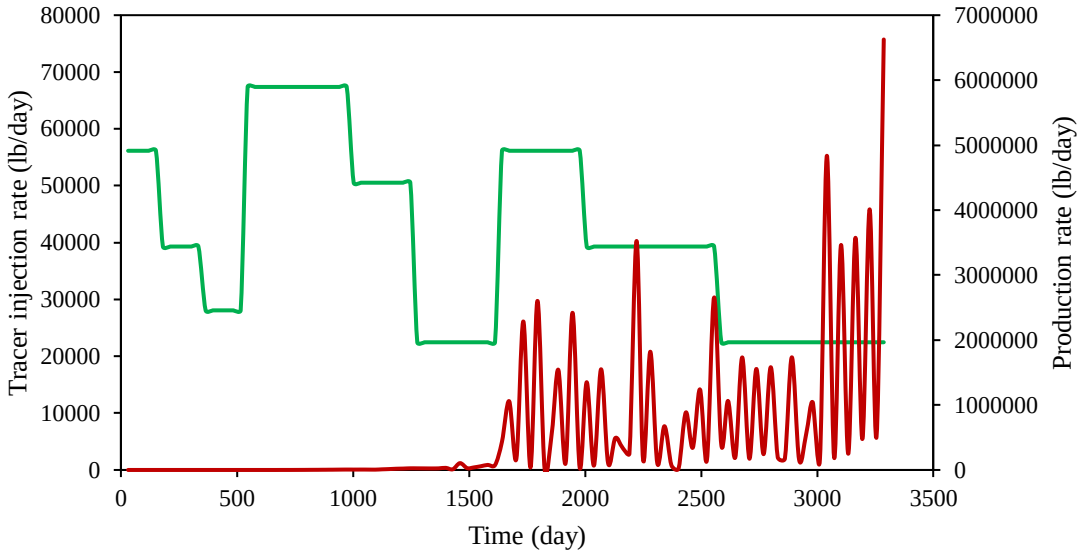

Figure 28. Tracer response in the producers 4 due to the injection from injector 3: the green line shows the production rate and the red line shows the tracer injection

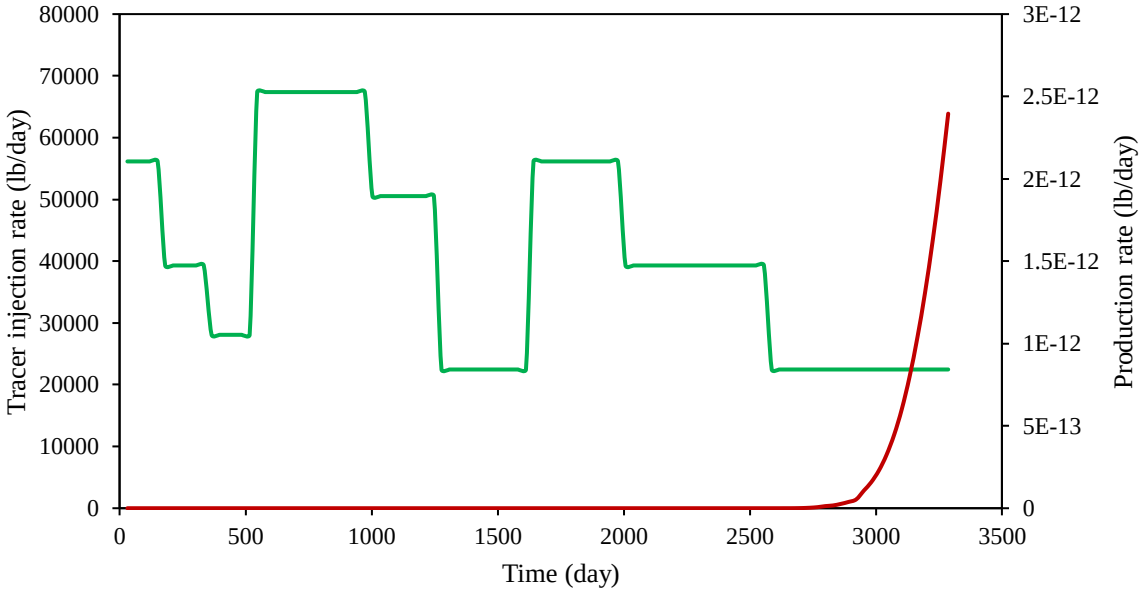

Figure 29. Tracer response in the producers 7 due to the injection from injector 3: the green line shows the production rate and the red line shows the tracer injection

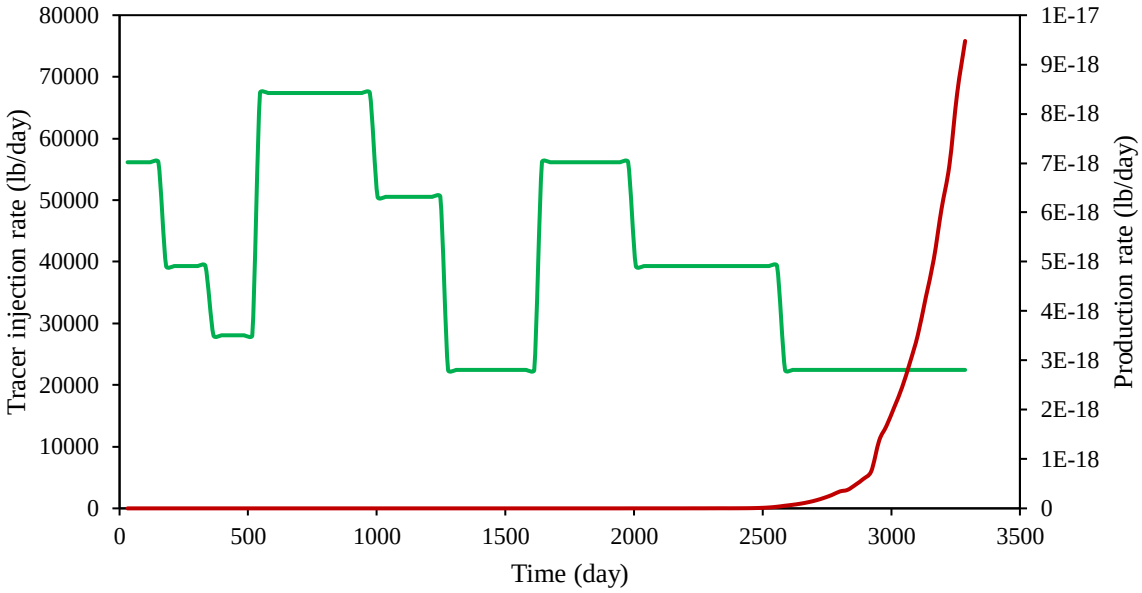

Figure 30. Tracer response in the producers 9 due to the injection from injector 3: the green line shows the production rate and the red line shows the tracer injection

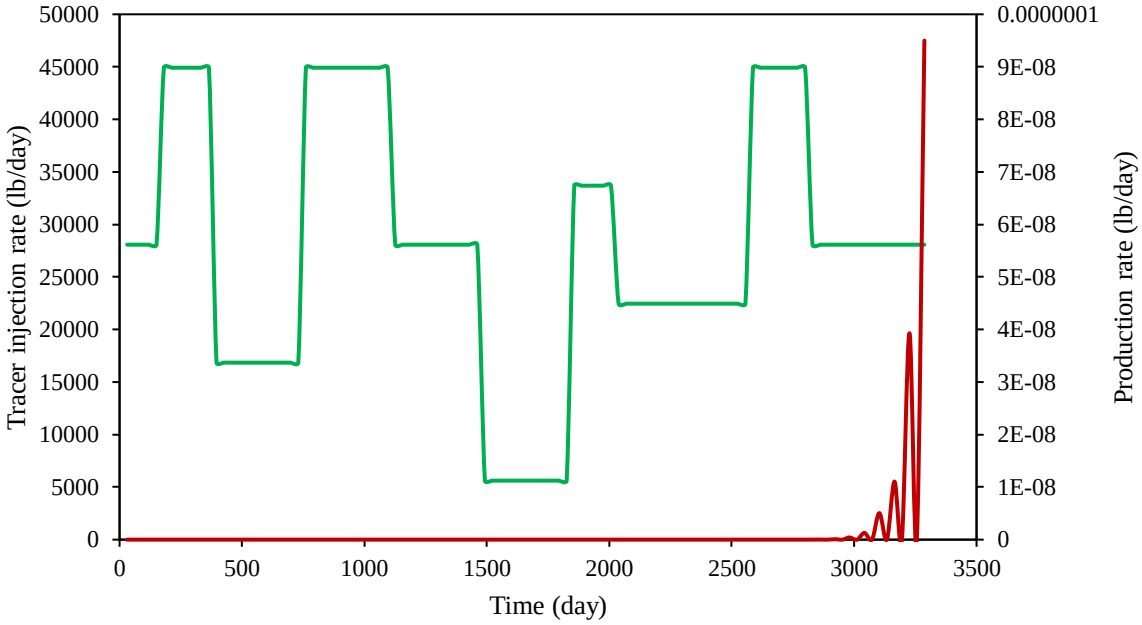

Figure 31. Tracer response in the producers 1 due to the injection from injector 4: the green line shows the production rate and the red line shows the tracer injection

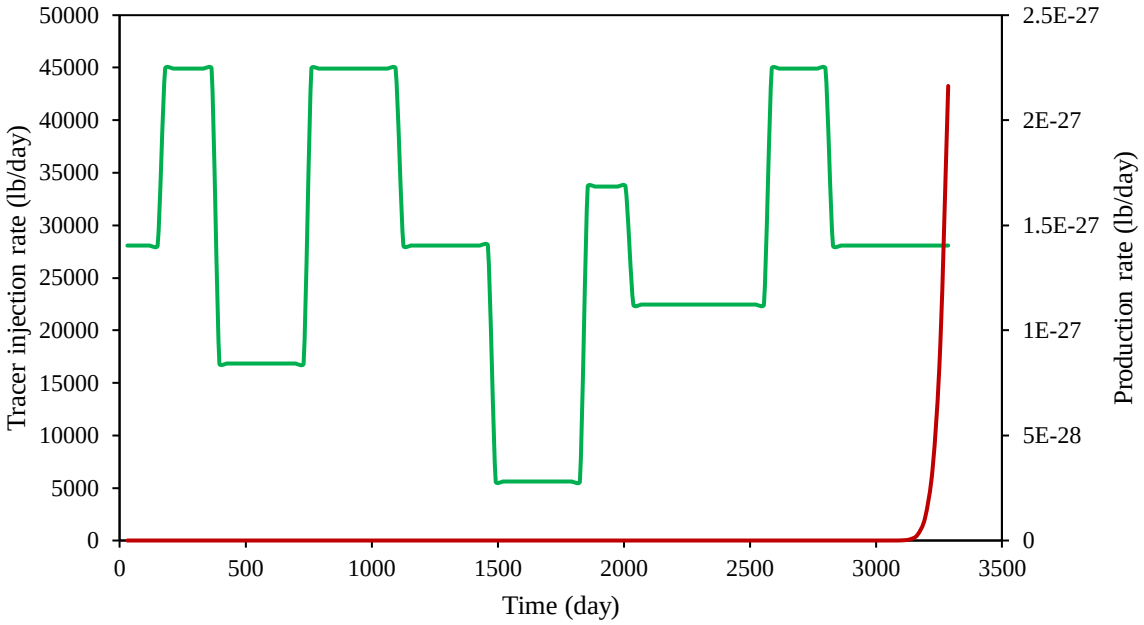

Figure 32. Tracer response in the producers 2 due to the injection from injector 4: the green line shows the production rate and the red line shows the tracer injection

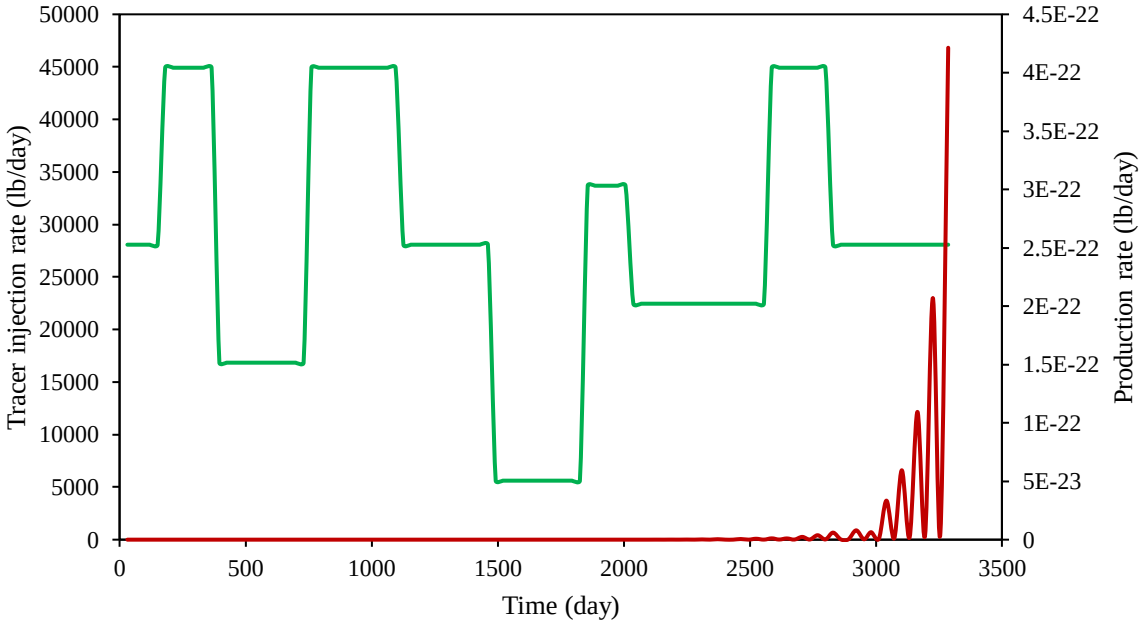

Figure 33. Tracer response in the producers 4 due to the injection from injector 4: the green line shows the production rate and the red line shows the tracer injection

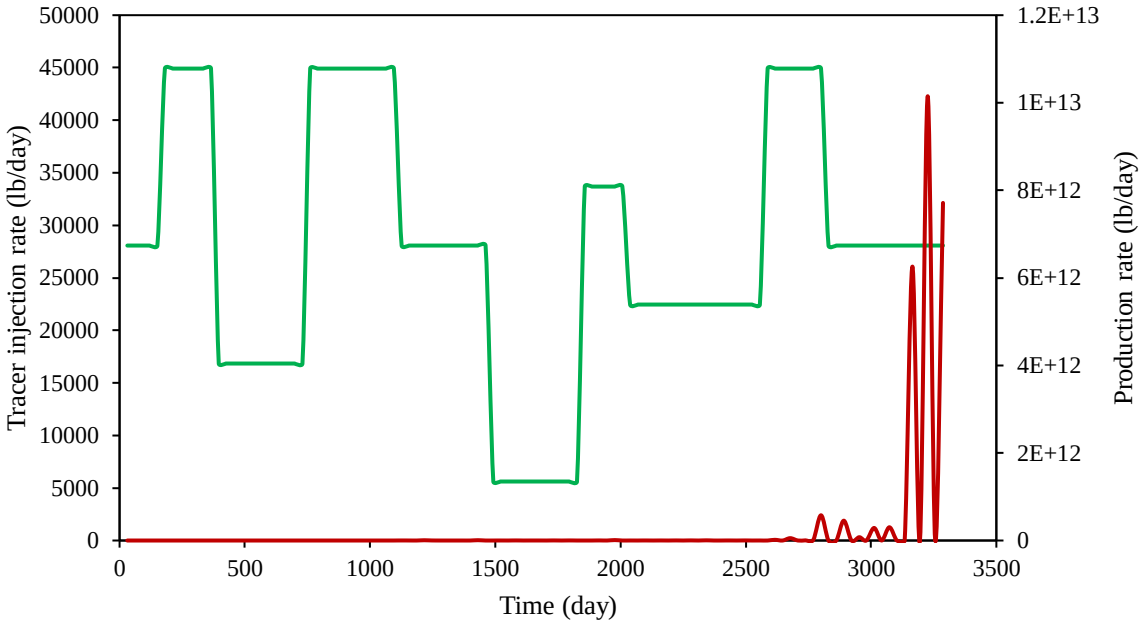

Figure 34. Tracer response in the producers 5 due to the injection from injector 4: the green line shows the production rate and the red line shows the tracer injection

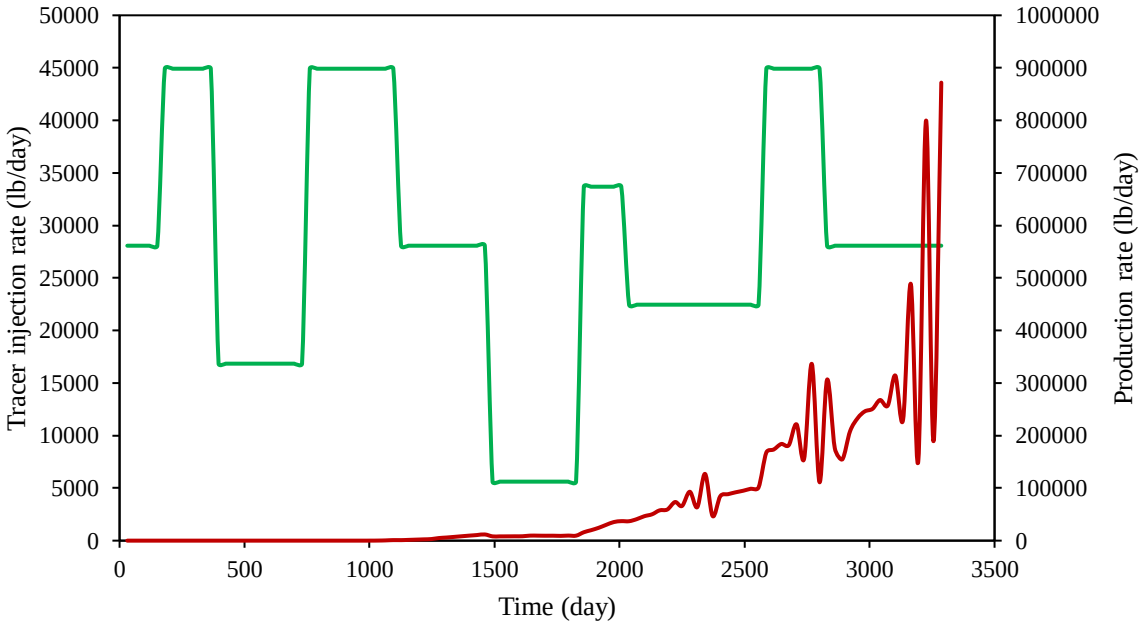

Figure 35. Tracer response in the producers 6 due to the injection from injector 4: the green line shows the production rate and the red line shows the tracer injection

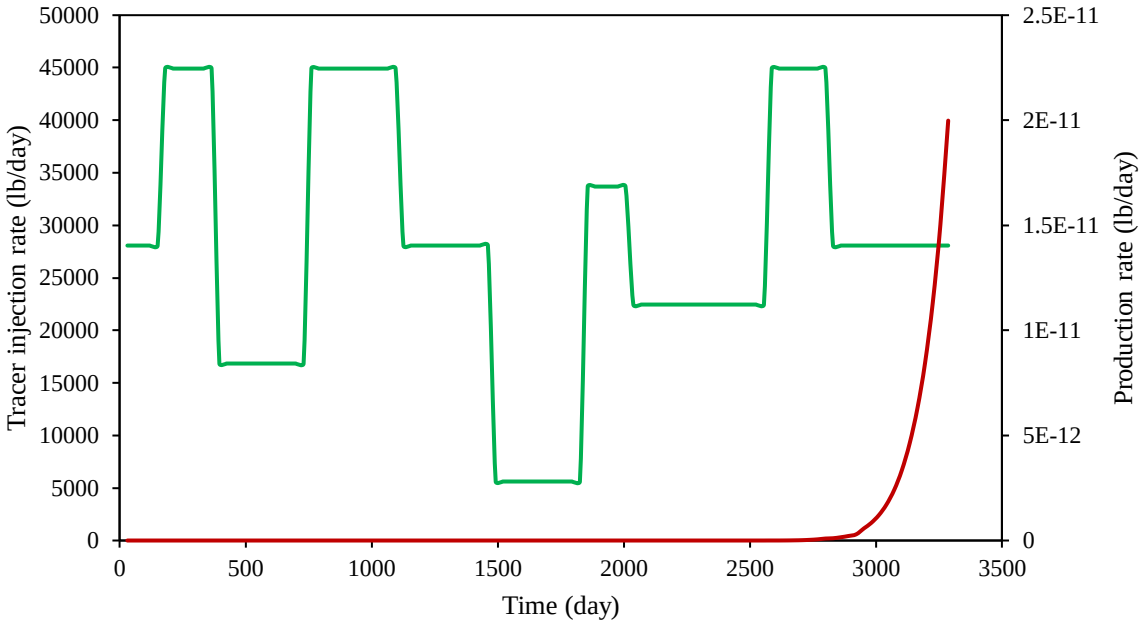

Figure 36. Tracer response in the producers 7 due to the injection from injector 4: the green line shows the production rate and the red line shows the tracer injection

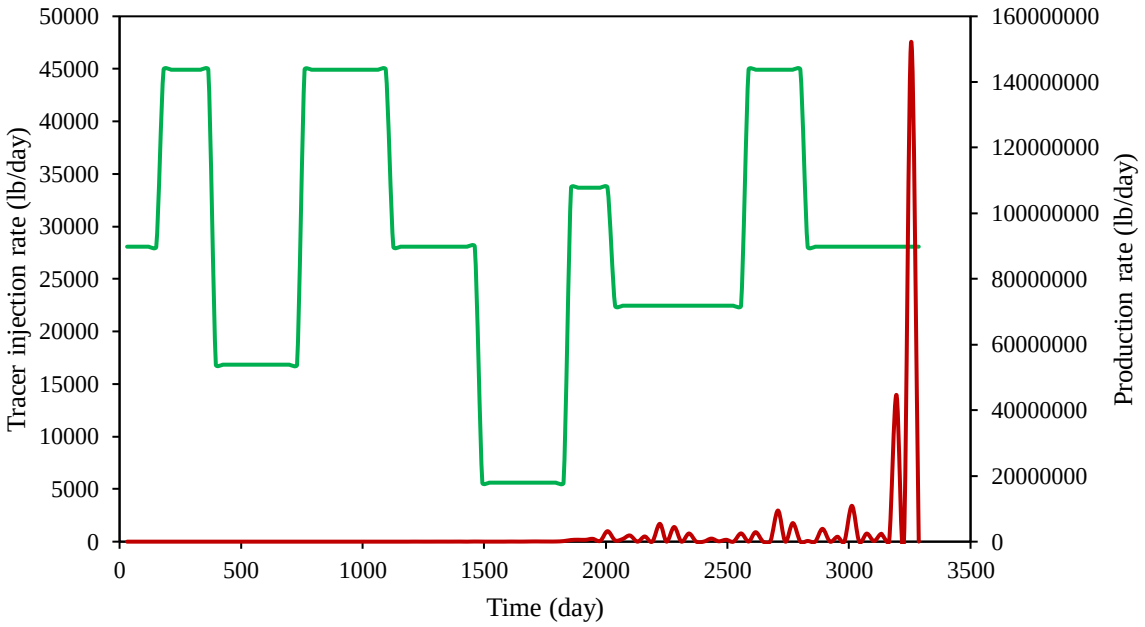

Figure 37. Tracer response in the producers 8 due to the injection from injector 4: the green line shows the production rate and the red line shows the tracer injection

3.1 Synthetic field

Different scenarios have been done to investigate the effect of well spacing in order to model CRM. Figure 38 shows different well spacing scenarios for each injector. $f_{ij} = 0$ for the producers that are out of the well spacing area. Two conditions were tested: the condition when there is no fluid loss ($\Sigma f_{ij} = 1$) and condition with fluid loss ($\Sigma f_{ij} \leq 1$). Hence, different modeling cases are:

- Case 1 – $f_{ij} \neq 0$ and $\Sigma f_{ij} = 1$ for the wells that are only in Area 1;
- Case 2 – $f_{ij} \neq 0$ and $\Sigma f_{ij} = 1$ for the wells that are only in Area 1 and Area 2 together;
- Case 3 – $f_{ij} \neq 0$ and $\Sigma f_{ij} = 1$ for all wells in whole reservoir;
- Case 4 – $f_{ij} \neq 0$ and $\Sigma f_{ij} \leq 1$ for all wells in whole reservoir.

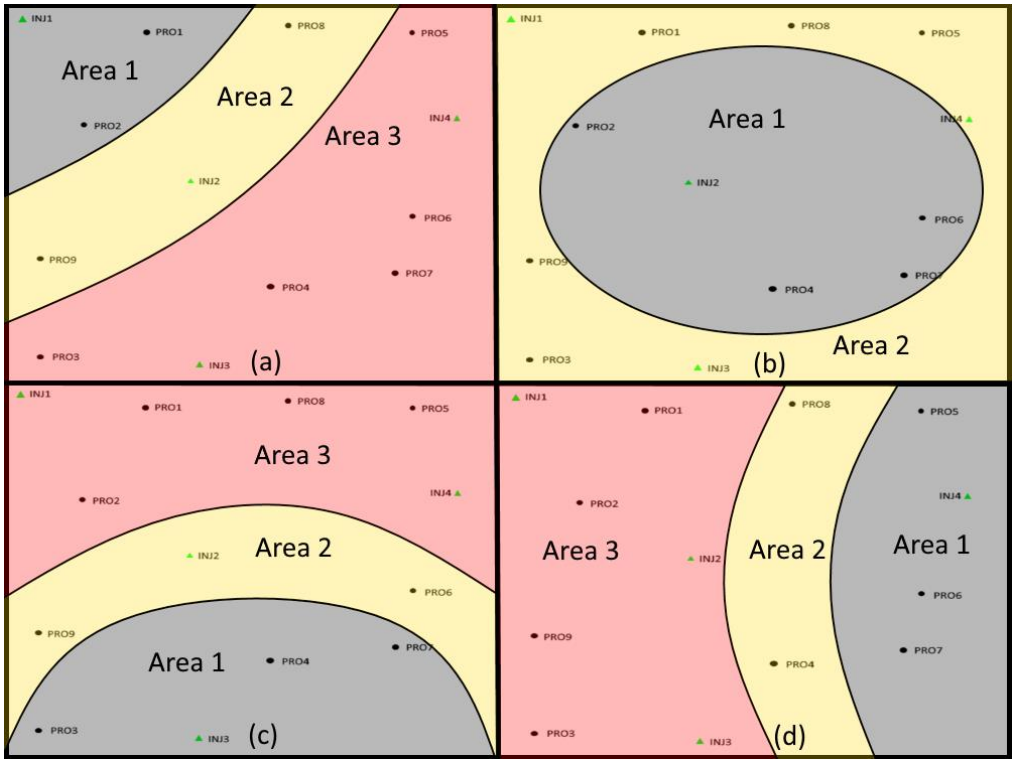

Figure 38. Well spacing for the synthetic field: (a) well spacing for INJ1; (b) wells spacing for INJ2; (c) well spacing for INJ3; (d) well spacing for INJ4

Case 1

$\Sigma f = 1$ and $f_{ij} \neq 0$ for the wells that are inside area 1. Figure 39 – 45 show examples of the CRM modeling of the production of each well. It is clearly seen that producers 1 and 3 are highly affected by its nearby injector and estimated production rates are close to the actual while others have some matchings at different time periods and mimic the overall trend of up

and downs during production. The average simulation error is about 31%, which is almost high due to the neglect of connectivity between some wells.

Comparing Figure 39 – 45 with Figure 14 – 37, it can be noted such a tendency that upon reaching the breakthrough and peak concentration, the calculated production according to the CRM begins to coincide with the actual production. As it can be seen from the example of well producer 1, the breakthrough occurred at about 1640 days and, if we compare this with the CRM, it can be noted the fact that it is in this period of time that there is a good agreement between the calculated and actual production. Then, in a later period of time, the breakthrough of the tracer agent reaches its peak, which is also clearly visible on the CRM. It should be noted that according to the well spacing effect in case 1, producer 1 is affected only by the injection well INJ1. Additionally, paying attention to the producer 2 production well, which is located in the immediate vicinity of injector 1 and injector 2. Despite the fact that the CRM shows a zero value for interwell connectivity between producer 2 and producer 1, the tracer study notes the fact that the breakthrough of the bulk of the tracer agent occurs at a later time. Producer 2 has the predominant influence. It can be seen from tracer response curves that breakthrough occurs in the initial period of time and reaches its peak in the later period. The same trend can be seen for producer 2.

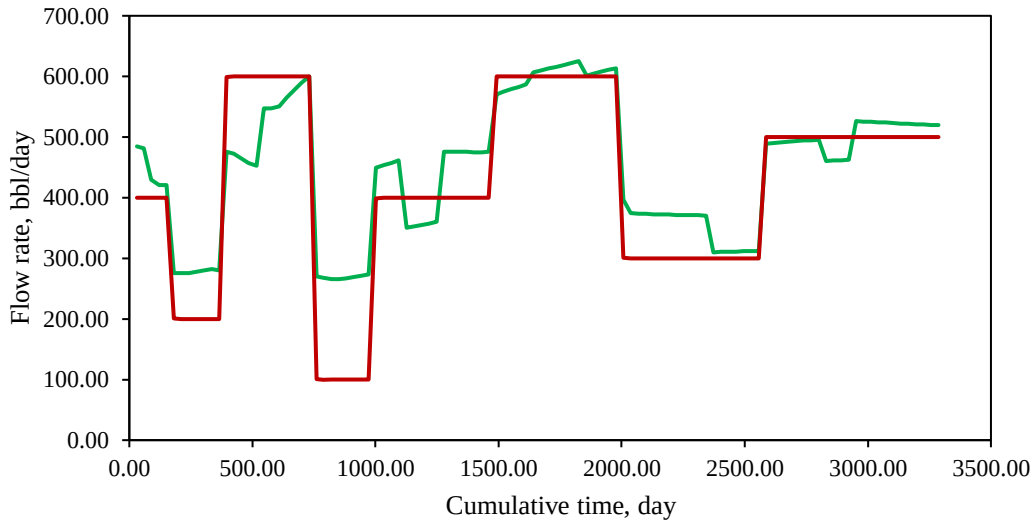

Figure 39. Actual production rate vs estimated production rate for producer 1: the green line shows the actual production and the red line shows the production profile modeled by CRM for Case 1

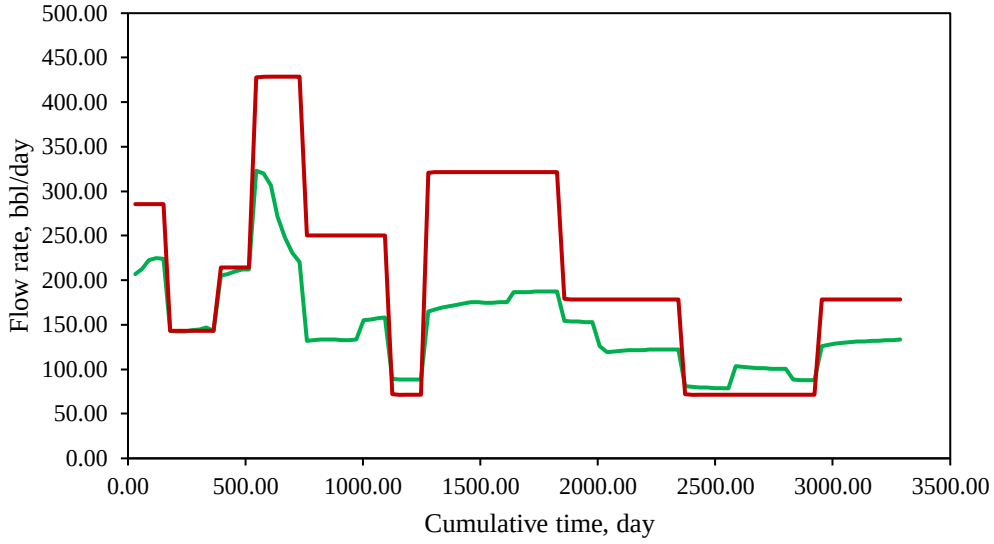

Figure 40. Actual production rate vs estimated production rate for producer 2: the green line shows the actual production and the red line shows the production profile modeled by CRM for Case 1

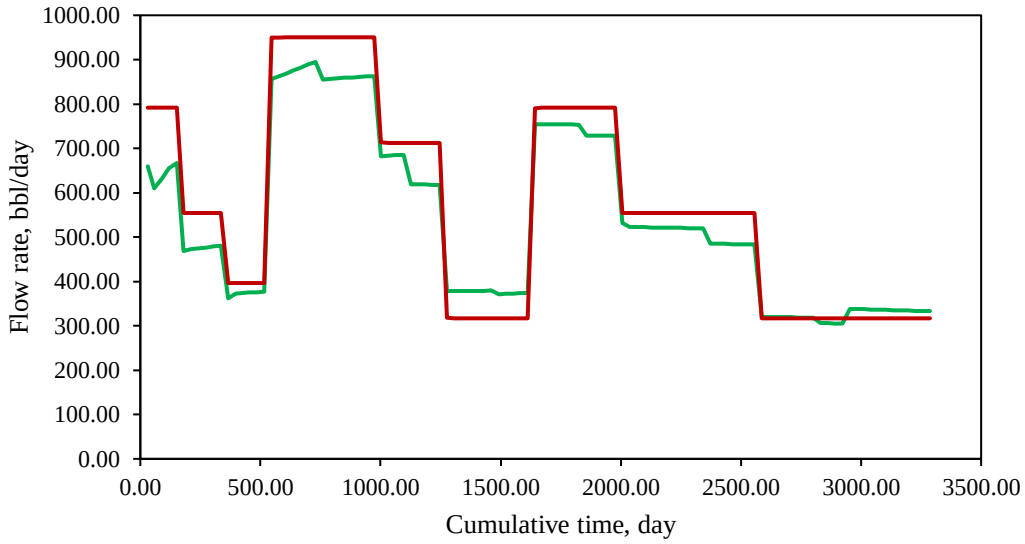

Figure 41. Actual production rate vs estimated production rate for producer 3: the green line shows the actual production and the red line shows the production profile modeled by CRM for Case 1

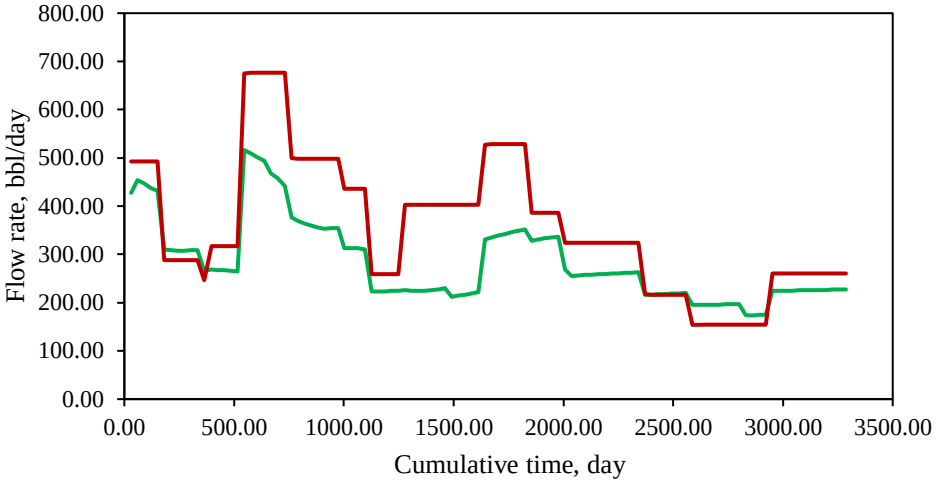

Figure 42. Actual production rate vs estimated production rate for producer 4: the green line shows the actual production and the red line shows the production profile modeled by CRM for Case 1

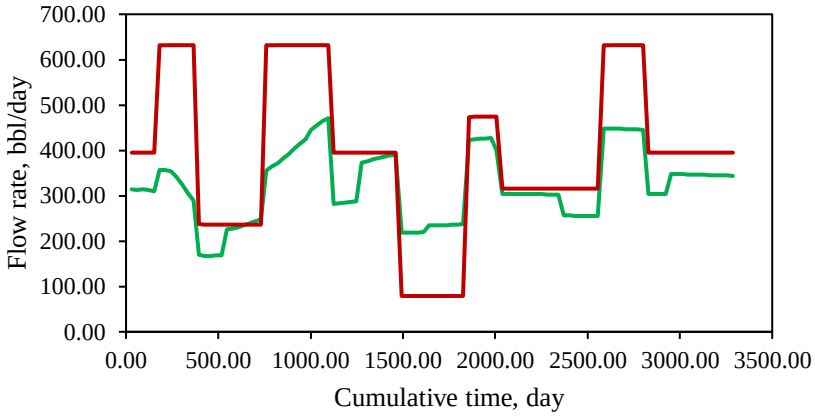

Figure 43. Actual production rate vs estimated production rate for producer 5: the green line shows the actual production and the red line shows the production profile modeled by CRM for Case 1

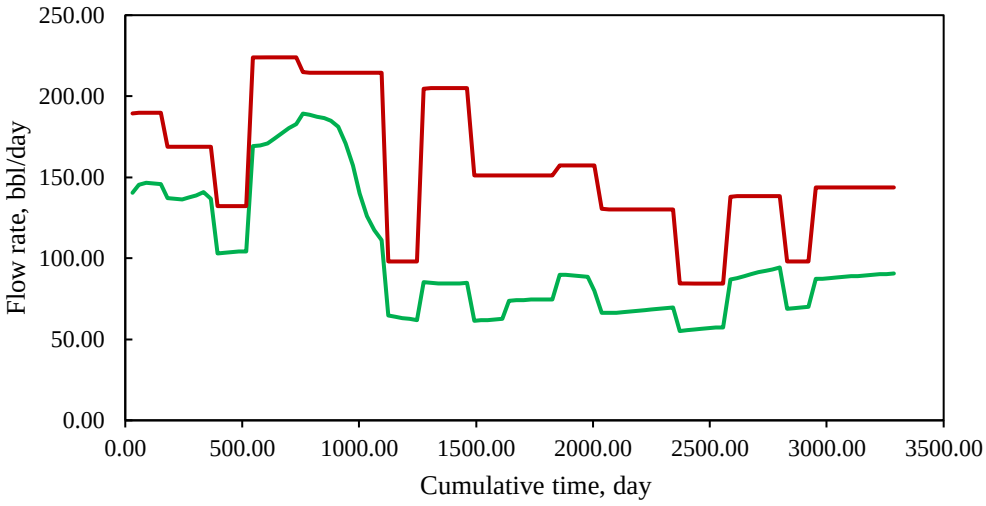

Figure 44. Actual production rate vs estimated production rate for producer 6: the green line shows the actual production and the red line shows the production profile modeled by CRM for Case 1

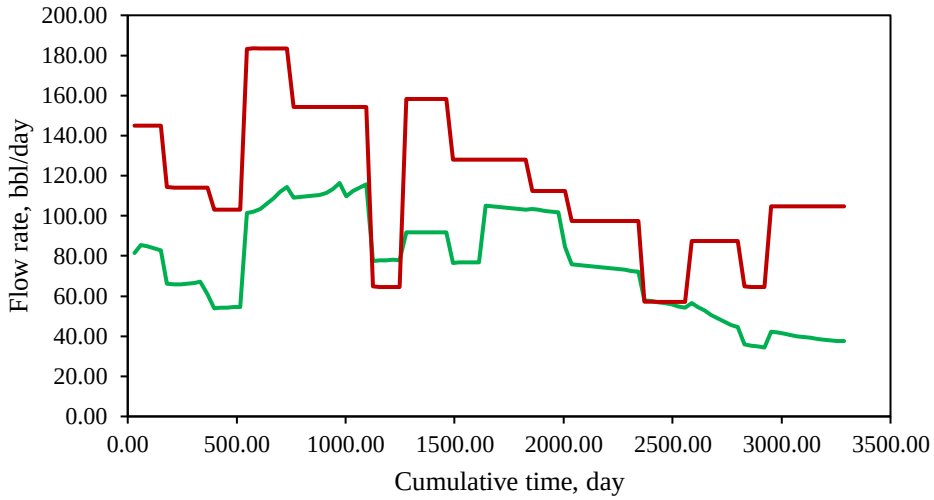

Figure 45. Actual production rate vs estimated production rate for producer 7: the green line shows the actual production and the red line shows the production profile modeled by CRM for Case 1

f_{ij} values are estimated by CRM and shown in Table 2. Close look at the table below and compare the obtained values with wells location shown in Figure 38 gives the justification that closer production wells to injectors, the better connection between them. However, in some situations, for example the area 1 for injector 4, the nearby producers have lesser connectivity, but at the same producer 5 which is located far has better connection which may mean that there is a high permeability path between these wells.

Table 2. Interwell connectivity for Case 1

	INJ1	INJ2	INJ3	INJ4
PRO1	1,00			
PRO2		0,36		
PRO3			0,79	
PRO4		0,36	0,21	
PRO5				0,79
PRO6		0,15		0,13
PRO7		0,13		0,08
PRO8				
PRO9				

Analyzing tracer response curves for each injector, breakthrough time at each producer is estimated. For each injector, the breakthrough dimensionless number was introduced as

$$BDN = \frac{1/t_i}{\sum 1/t_i} \quad \text{Eq. 42}$$

where t_i shows the injected tracer breakthrough time for producer i.

Hence, connectivity values were estimated by CRM and tracer tests. These values are compared as shown in Figure 46. Figure 14 – 37 justify the trend that earlier water breakthrough leads to higher interwell connectivity. The outliers that are presented in these graphs happened because of the high average simulation error for this case.

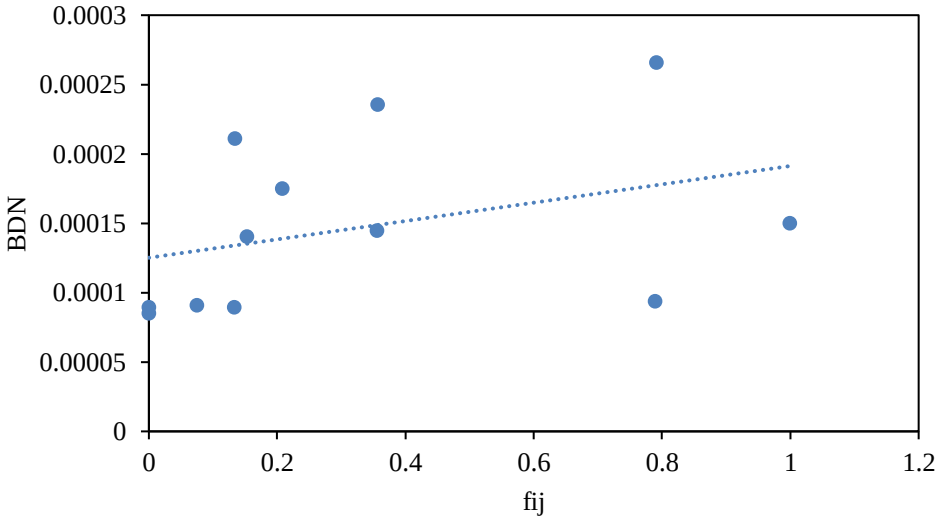

Figure 46. Comparison of connectivity estimated by CRM and by tracer tests for Case 1

Case 2

In this case, it was assumed that $\Sigma f = 1$ and $f_{ij} \neq 0$ for the wells that are inside areas 1 and 2. Taking into account the well spacing, it can be noticed from Figure 47 – 55 that the CRM modeling is more accurate and the average simulation error reduced to about 12%.

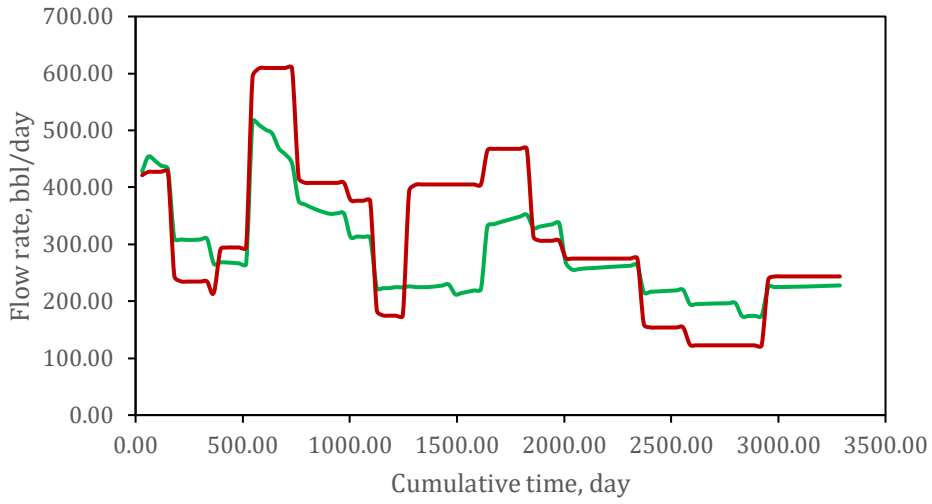

Figure 47. Actual production rate vs estimated production rate for producer 1: the green line shows the actual production and the red line shows the production profile modeled by CRM for Case 2

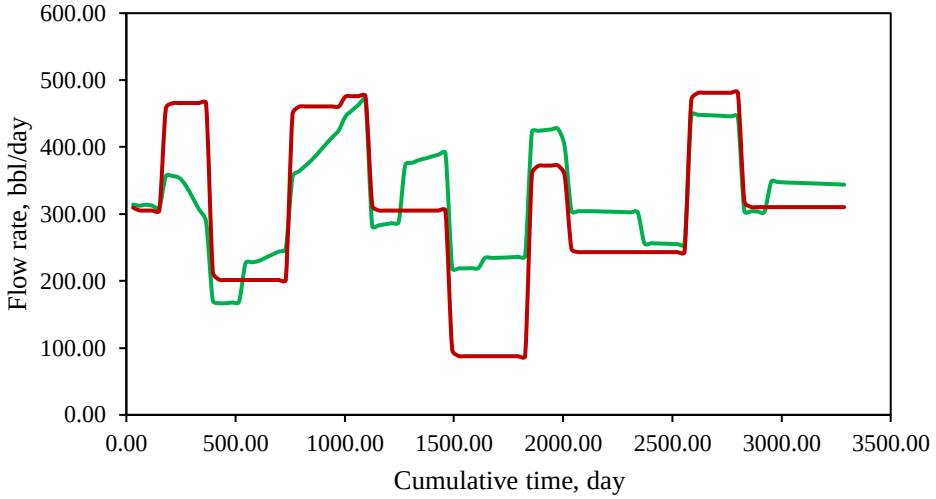

Figure 48. Actual production rate vs estimated production rate for producer 2: the green line shows the actual production and the red line shows the production profile modeled by CRM for Case 2

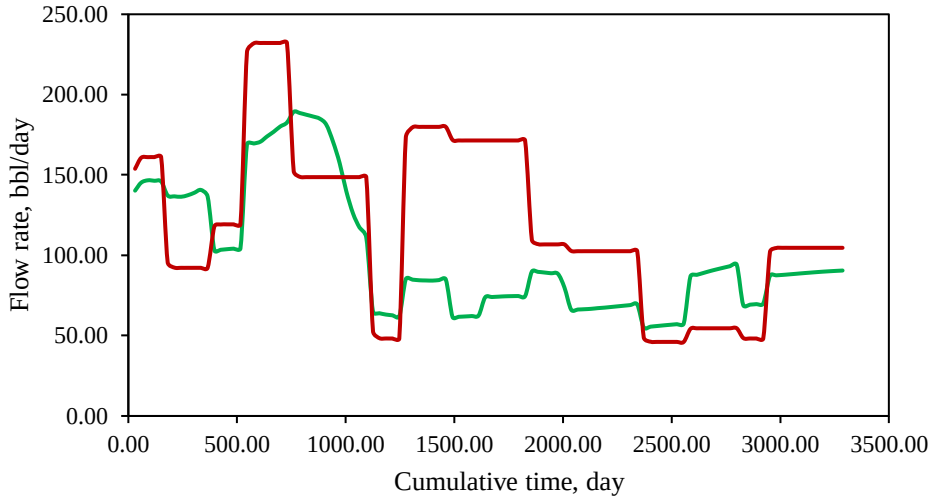

Figure 49. Actual production rate vs estimated production rate for producer 3: the green line shows the actual production and the red line shows the production profile modeled by CRM for Case 2

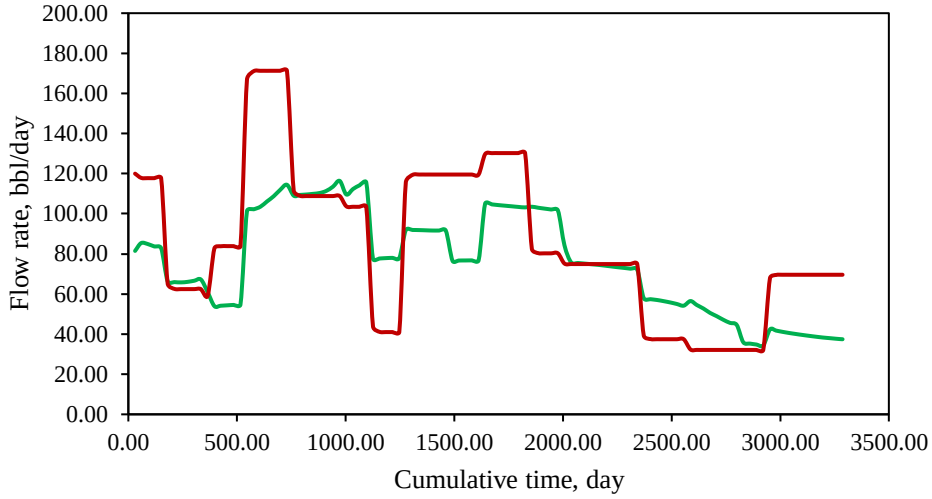

Figure 50. Actual production rate vs estimated production rate for producer 4: the green line shows the actual production and the red line shows the production profile modeled by CRM for Case 2

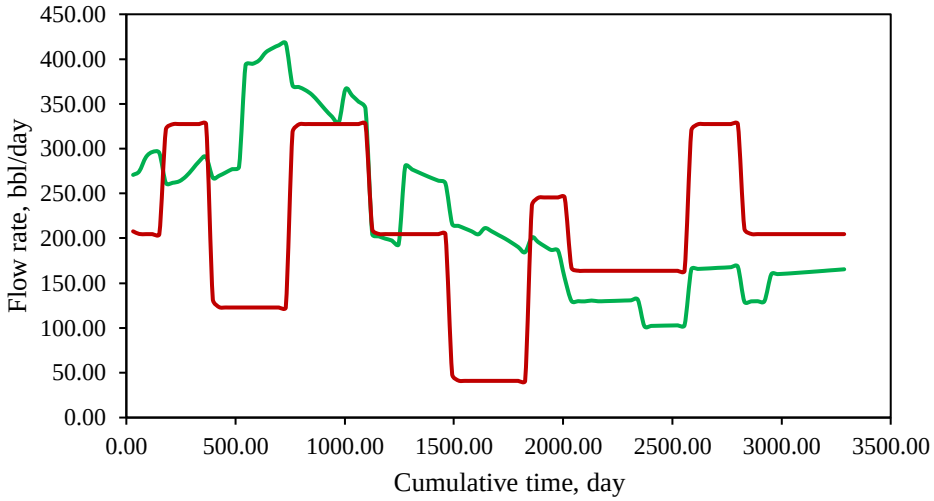

Figure 51. Actual production rate vs estimated production rate for producer 5: the green line shows the actual production and the red line shows the production profile modeled by CRM for Case 2

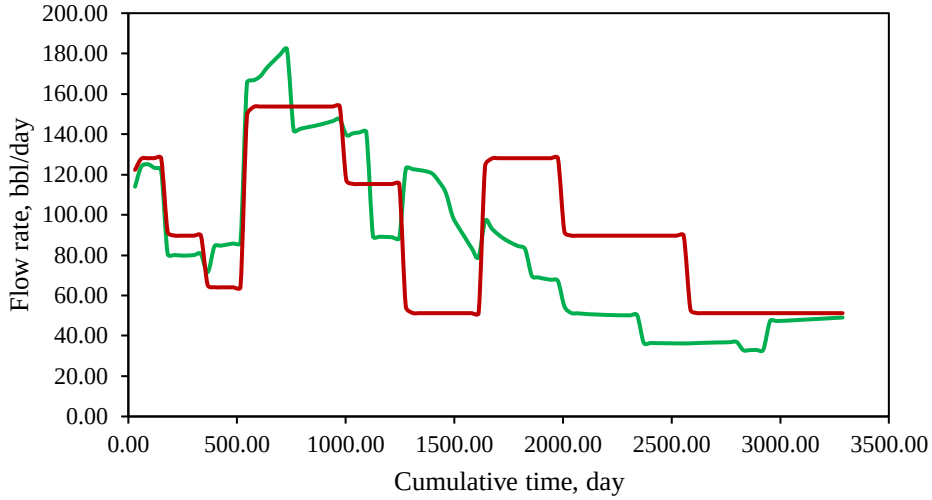

Figure 52. Actual production rate vs estimated production rate for producer 6: the green line shows the actual production and the red line shows the production profile modeled by CRM for Case 2

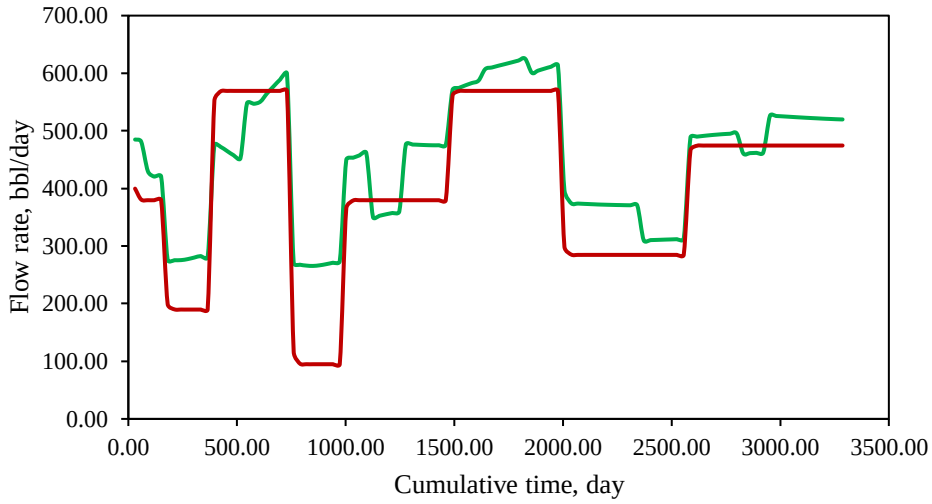

Figure 53. Actual production rate vs estimated production rate for producer 7: the green line shows the actual production and the red line shows the production profile modeled by CRM for Case 2

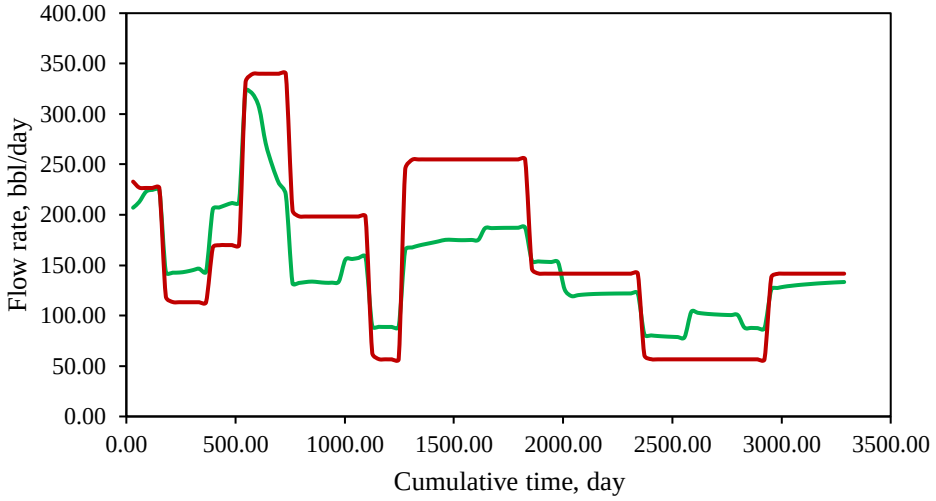

Figure 54. Actual production rate vs estimated production rate for producer 8: the green line shows the actual production and the red line shows the production profile modeled by CRM for Case 2

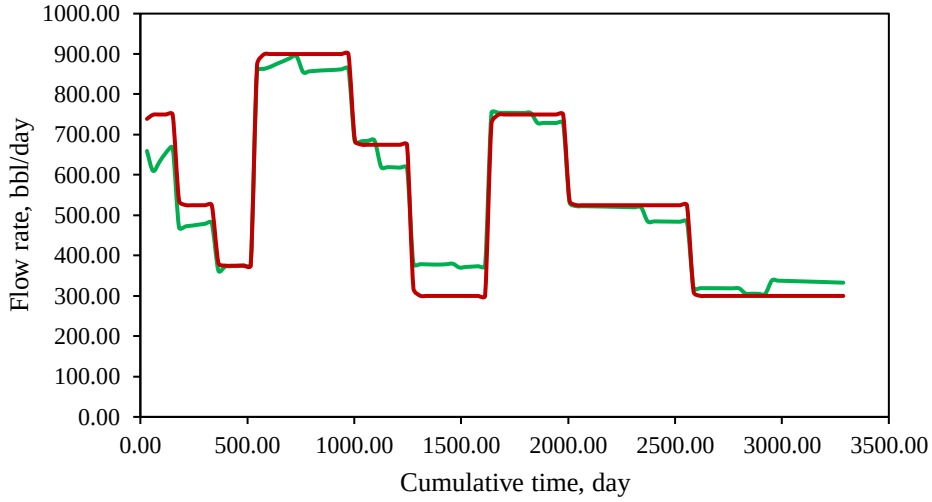

Figure 55. Actual production rate vs estimated production rate for producer 9: the green line shows the actual production and the red line shows the production profile modeled by CRM for Case 2

f_{ij} values are estimated by CRM and shown in Table 3.

Table 3. Interwell connectivity for Case 2

	INJ1	INJ2	INJ3	INJ4
PRO1	0,95			
PRO2		0,28		
PRO3			0,75	
PRO4		0,40	0,10	

PRO5	0,05			0,57
PRO6		0,19		0,02
PRO7		0,12	0,02	
PRO8				0,41
PRO9			0,13	

Figure 56 shows the connectivity estimated by CRM and tracer for case 2. The higher BDN, the more connected wells are to each other, which can be observed by the trend of the line. Still, there is a noticeable error in the modeling and the application of CRM is not very accurate.

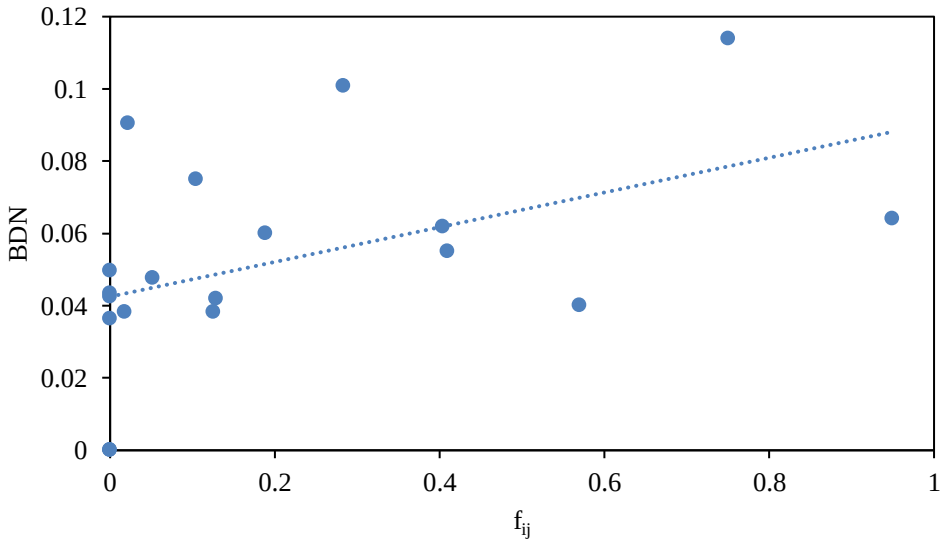

Figure 56. Comparison of connectivity estimated by CRM and by tracer tests for Case 2

Case 3

The same restrictions were applied to Case 3, but for the whole field. The error of the simulation by CRM is low and about 4% in this case, as all well pair connections were considered in the model, as shown in Figure 57 - 65.

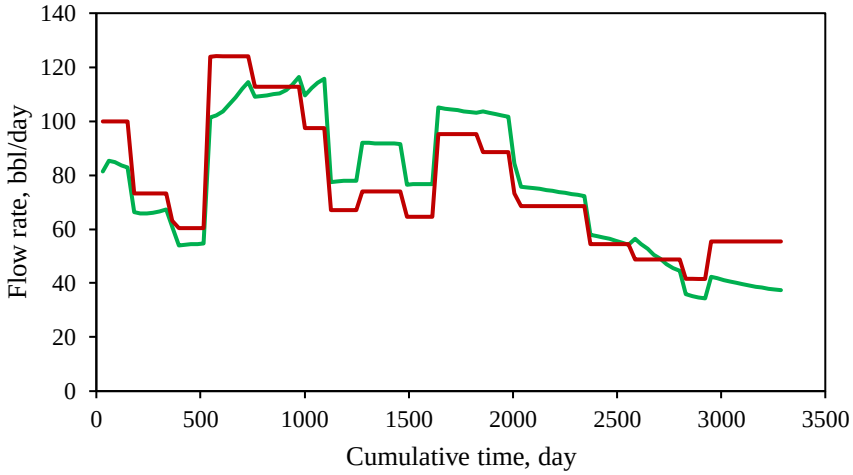

Figure 57. Actual production rate vs estimated production rate for producer 1: the green line shows the actual production and the red line shows the production profile modeled by CRM for Case 3

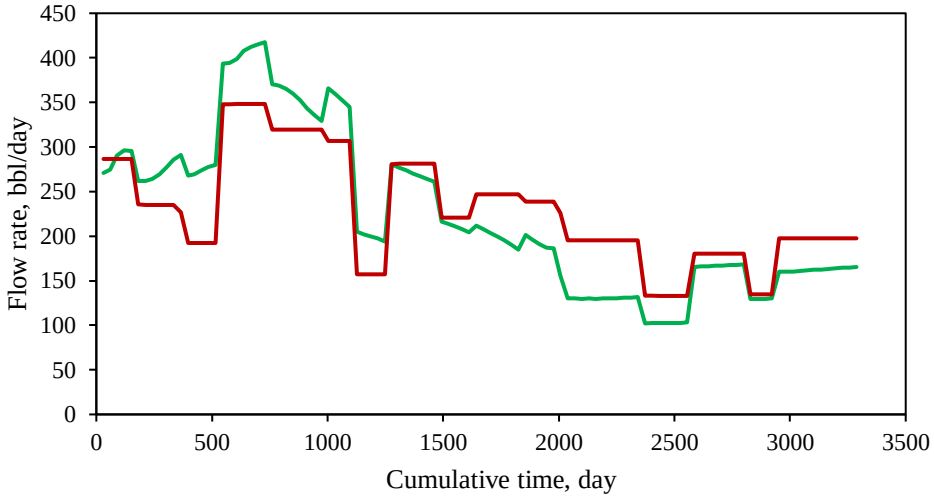

Figure 58. Actual production rate vs estimated production rate for producer 2: the green line shows the actual production and the red line shows the production profile modeled by CRM for Case 3

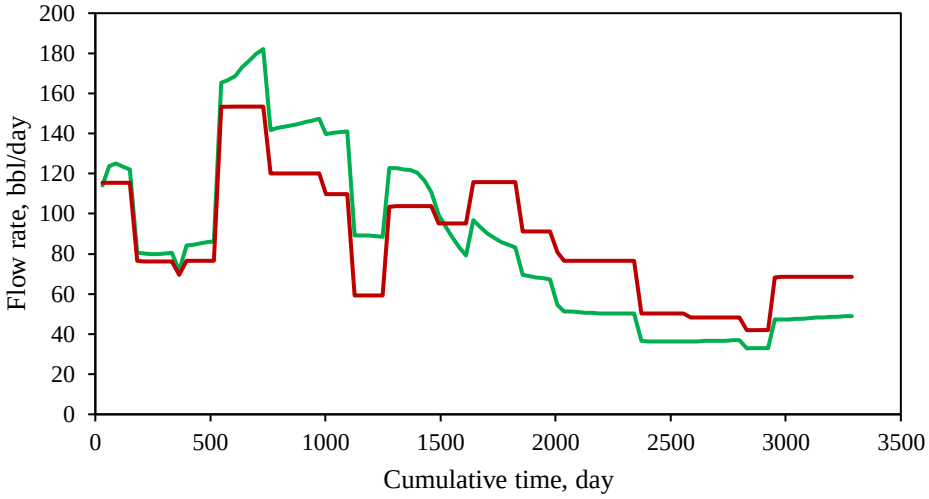

Figure 59. Actual production rate vs estimated production rate for producer 3: the green line shows the actual production and the red line shows the production profile modeled by CRM for Case 3

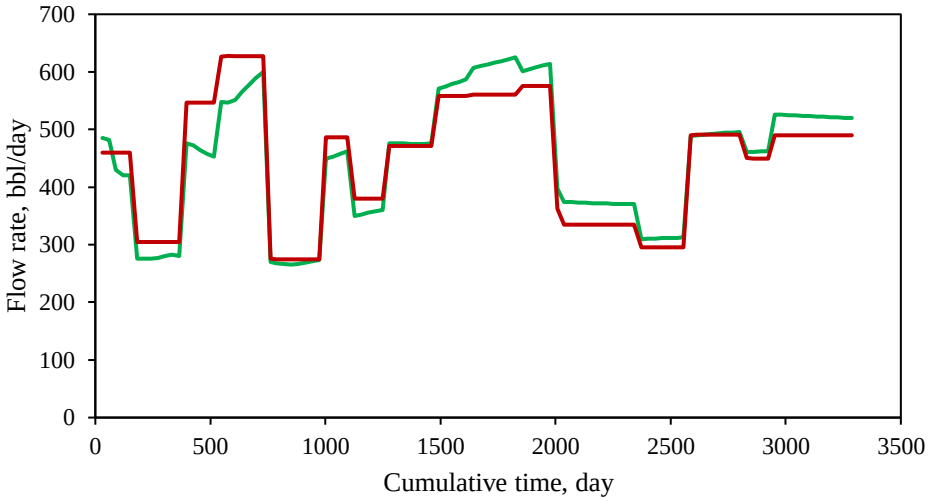

Figure 60. Actual production rate vs estimated production rate for producer 4: the green line shows the actual production and the red line shows the production profile modeled by CRM for Case 3

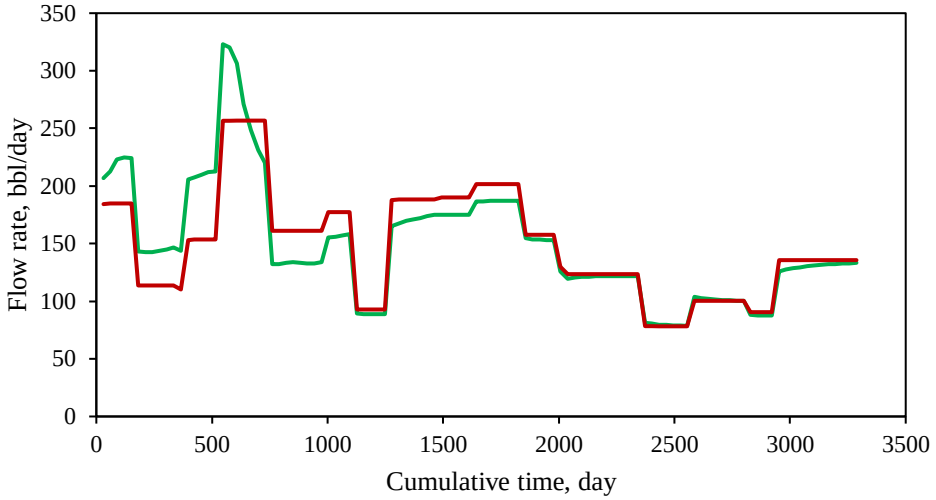

Figure 61. Actual production rate vs estimated production rate for producer 5: the green line shows the actual production and the red line shows the production profile modeled by CRM for Case 3

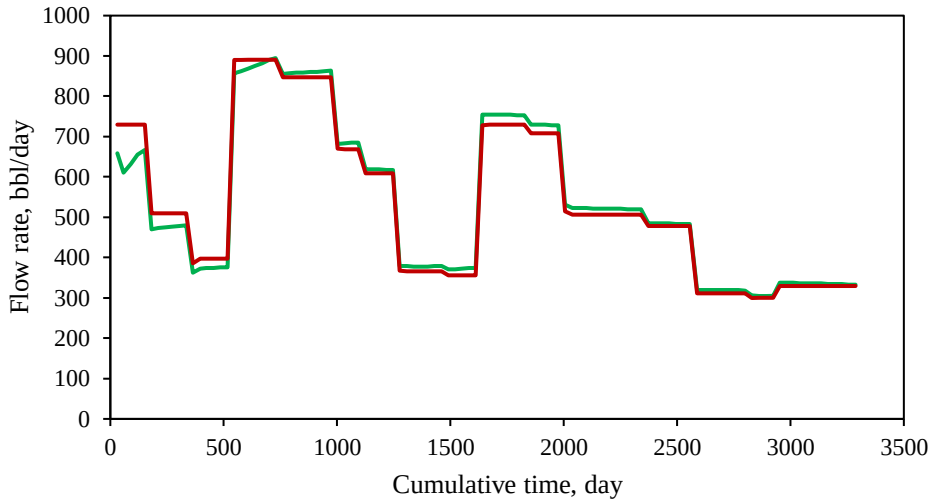

Figure 62. Actual production rate vs estimated production rate for producer 6: the green line shows the actual production and the red line shows the production profile modeled by CRM for Case 3

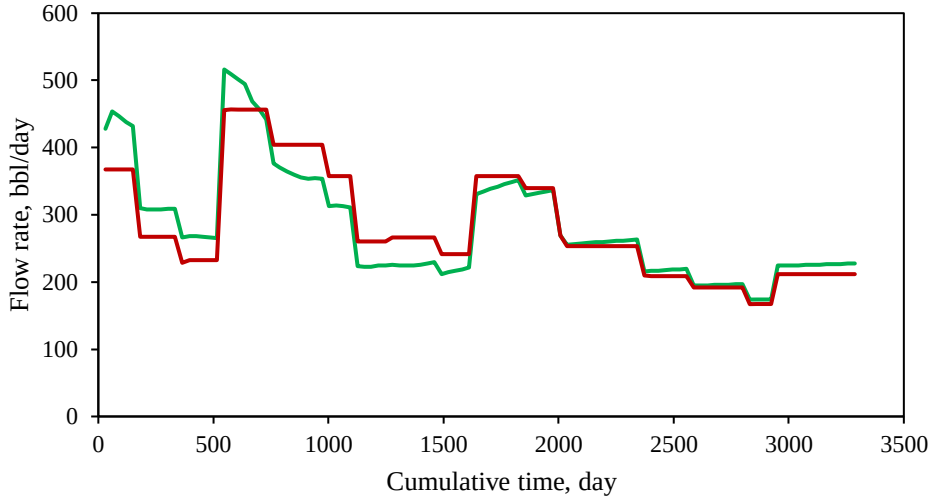

Figure 63. Actual production rate vs estimated production rate for producer 7: the green line shows the actual production and the red line shows the production profile modeled by CRM for Case 3

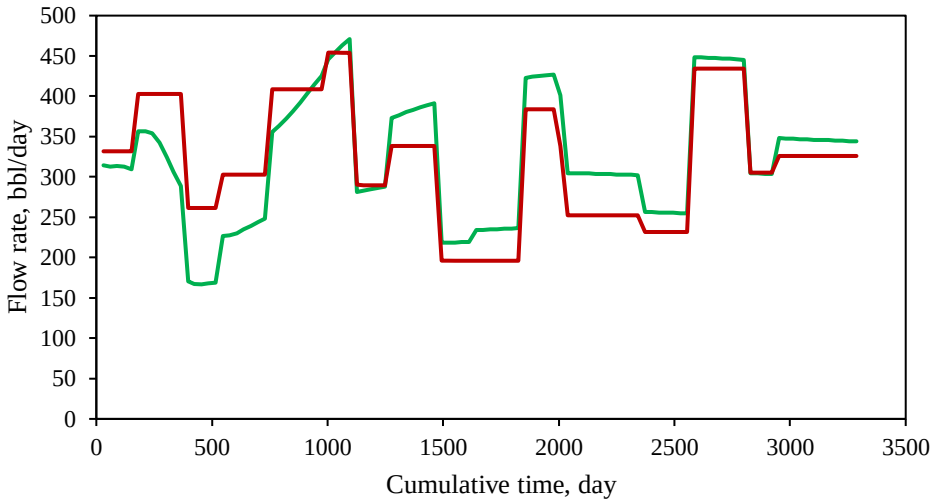

Figure 64. Actual production rate vs estimated production rate for producer 8: the green line shows the actual production and the red line shows the production profile modeled by CRM for Case 3

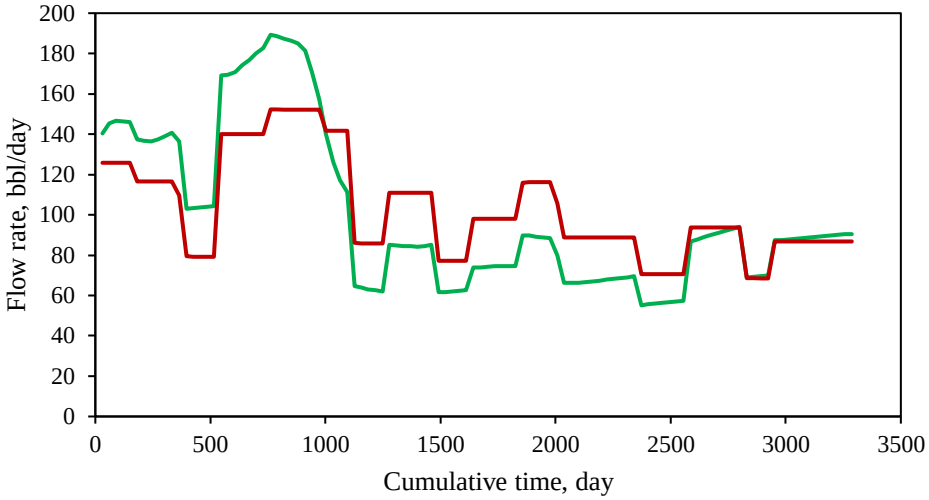

Figure 65. Actual production rate vs estimated production rate for producer 9: the green line shows the actual production and the red line shows the production profile modeled by CRM for Case 3

f_{ij} values are estimated by CRM and shown in Table 4.

Table 4. Interwell connectivity for Case 3

	INJ1	INJ2	INJ3	INJ4
PRO1	0,71	0,13	0,00	0,14
PRO2	0,07	0,15	0,02	0,03
PRO3	0,03	0,10	0,62	0,04
PRO4	0,04	0,15	0,19	0,08
PRO5	0,15	0,07	0,00	0,43
PRO6	0,00	0,06	0,03	0,08
PRO7	0,00	0,05	0,05	0,02
PRO8	0,00	0,21	0,04	0,15
PRO9	0,00	0,09	0,03	0,02

Figure 66 shows the comparison between two methods for this case. This CRM estimates is in better agreement with the connectivity results obtained by tracer test analysis due to considering all wells. However, this case still has problems. So, CRM can just provide

a general picture of the connectivity in the field and estimates the injector/producer wells with very high and very low connectivity.

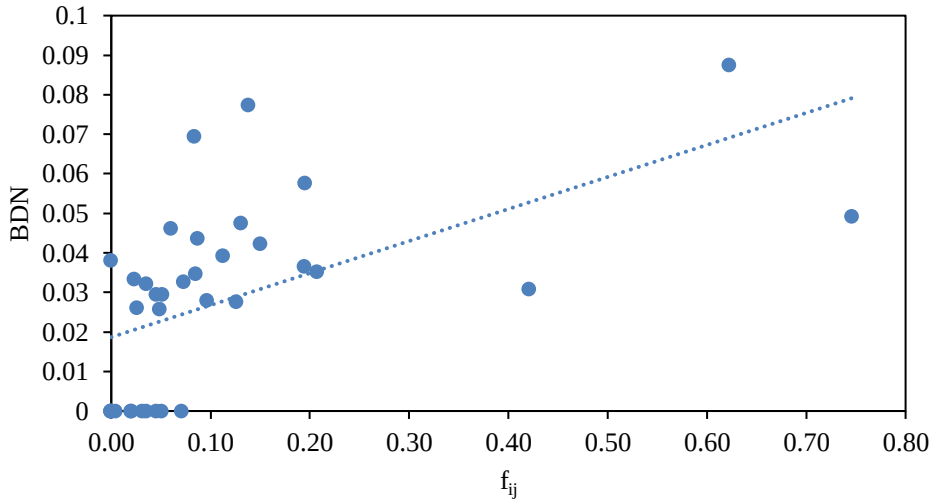

Figure 66. Comparison of connectivity estimated by CRM and by tracer tests for Case 3

Case 4

In this case, it was assumed that $\Sigma f \leq 1.25\ 1$ and $f_{ij} \neq 0$ for the whole reservoir. Taking into account these restrictions, it can be noticed from Figure 67 – 75 that the CRM modeling is more accurate and the average simulation error reduced to about 4% similarly as in Case 3.

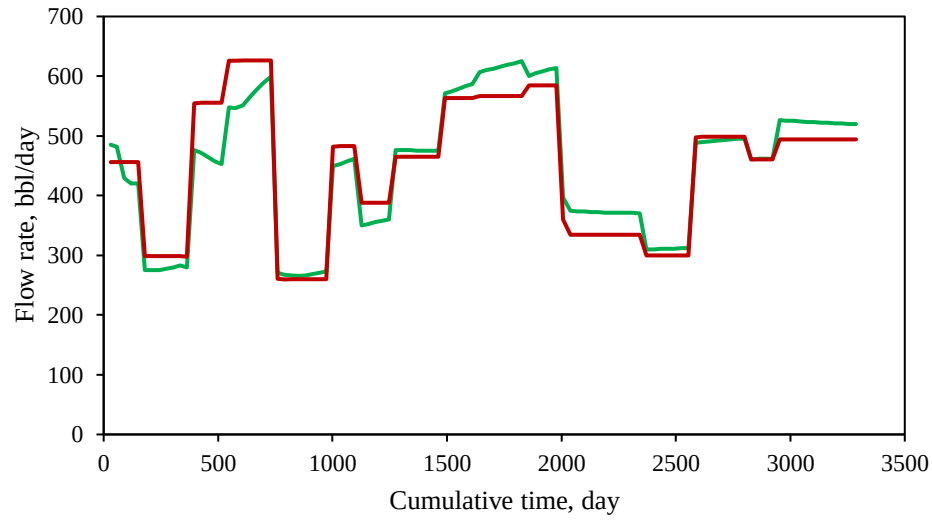

Figure 67. Actual production rate vs estimated production rate for producer 1: the green line shows the actual production and the red line shows the production profile modeled by CRM for Case 4

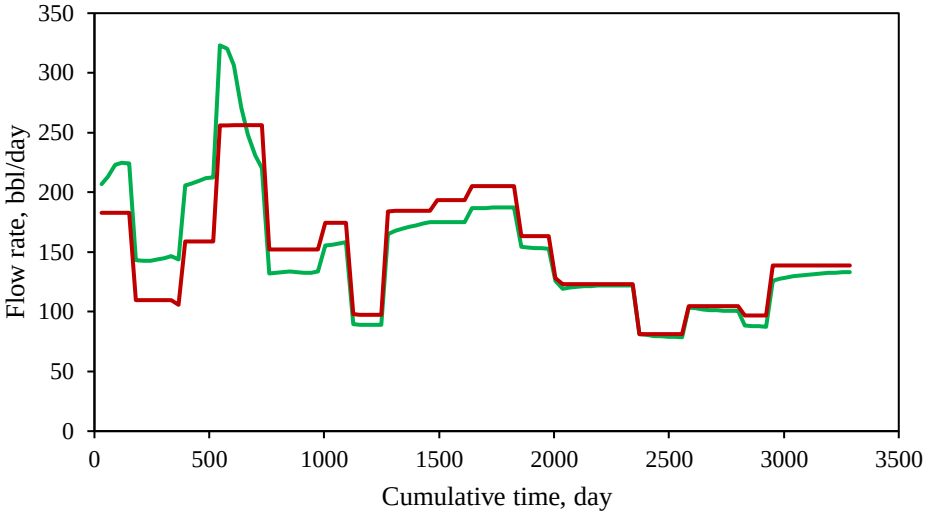

Figure 68. Actual production rate vs estimated production rate for producer 2: the green line shows the actual production and the red line shows the production profile modeled by CRM for Case 4

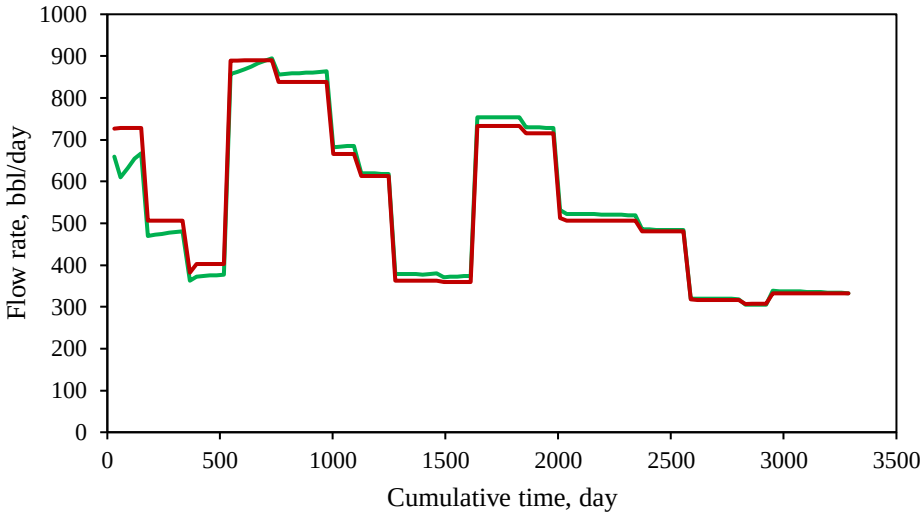

Figure 69. Actual production rate vs estimated production rate for producer 3: the green line shows the actual production and the red line shows the production profile modeled by CRM for Case 4

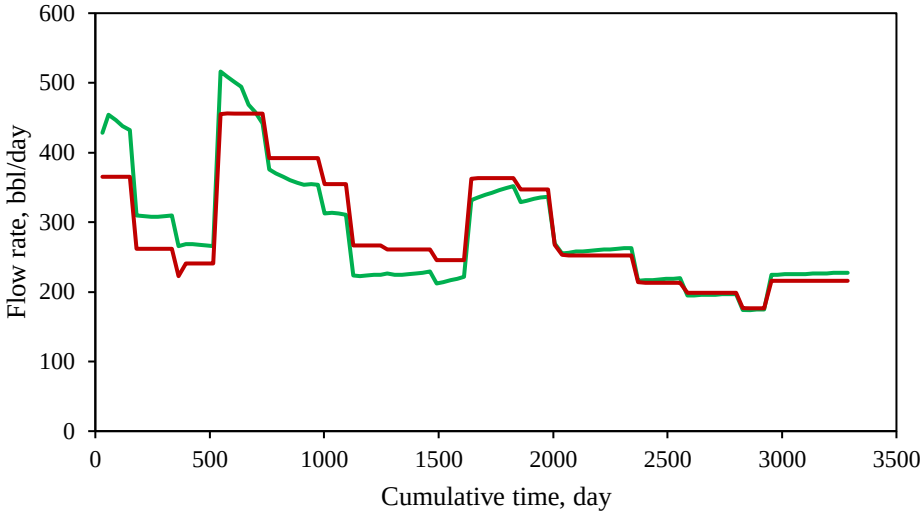

Figure 70. Actual production rate vs estimated production rate for producer 4: the green line shows the actual production and the red line shows the production profile modeled by CRM for Case 4

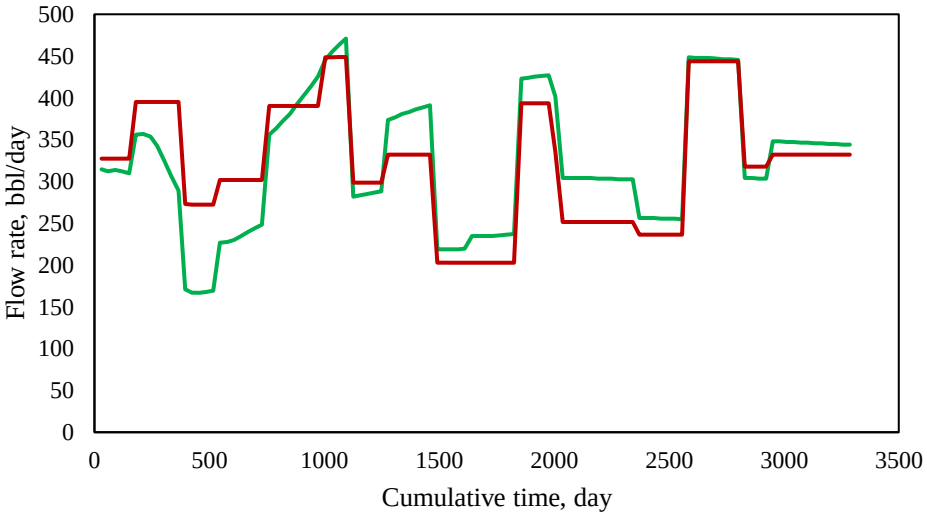

Figure 71. Actual production rate vs estimated production rate for producer 5: the green line shows the actual production and the red line shows the production profile modeled by CRM for Case 4

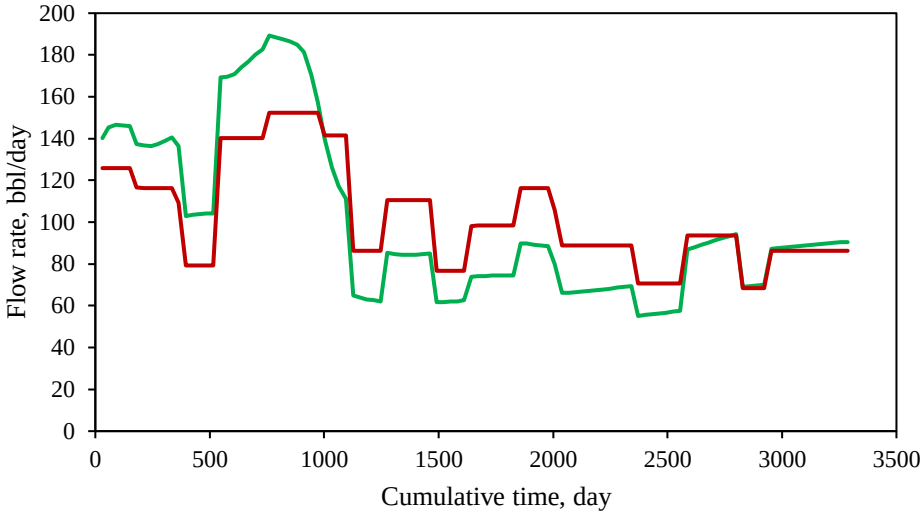

Figure 72. Actual production rate vs estimated production rate for producer 6: the green line shows the actual production and the red line shows the production profile modeled by CRM for Case 4

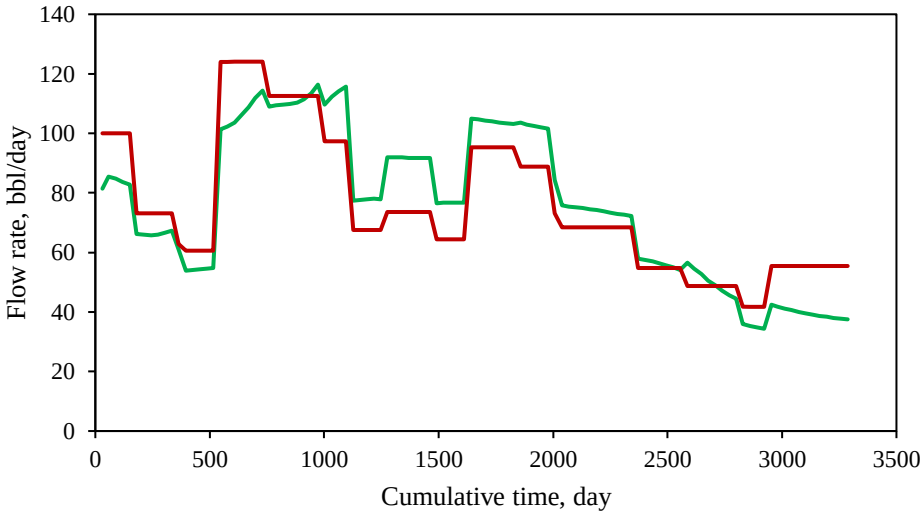

Figure 73. Actual production rate vs estimated production rate for producer 7: the green line shows the actual production and the red line shows the production profile modeled by CRM for Case 4

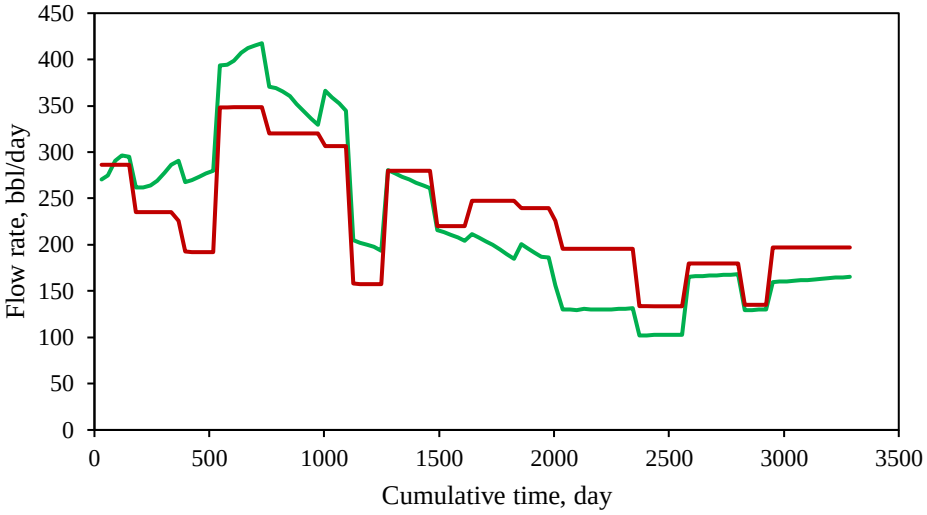

Figure 74. Actual production rate vs estimated production rate for producer 8: the green line shows the actual production and the red line shows the production profile modeled by CRM for Case 4

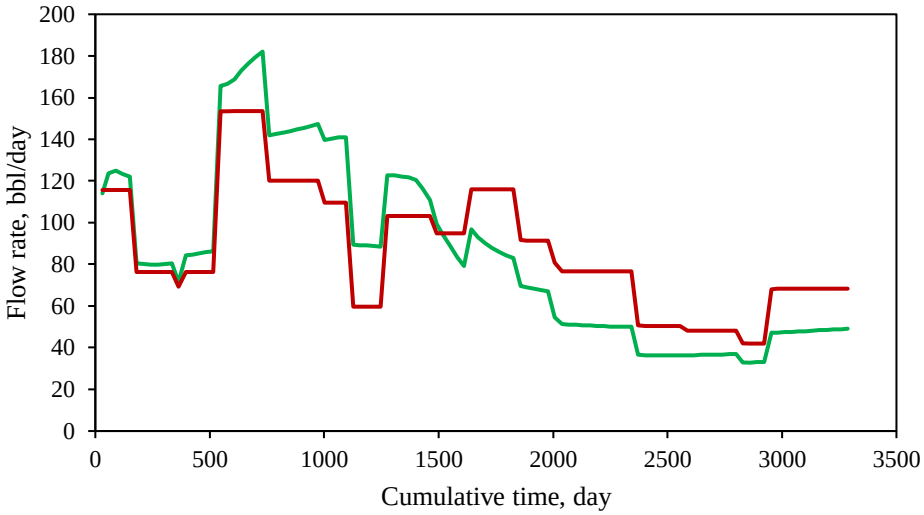

Figure 75. Actual production rate vs estimated production rate for producer 9: the green line shows the actual production and the red line shows the production profile modeled by CRM for Case 4

f_{ij} values are estimated by CRM and shown in Table 5. There is no big difference between Cases 3 and 4 regarding the interwell connectivity values. $\Sigma f \leq 1.25$ gives better history matching. Figure 76 looks similar as in Case 3.

Table 5. Interwell connectivity for Case 4

	INJ1	INJ2	INJ3	INJ4
PRO1	0,75	0,11	0,00	0,13
PRO2	0,10	0,14	0,02	0,03

PRO3	0,05	0,09	0,62	0,03
PRO4	0,07	0,13	0,20	0,07
PRO5	0,19	0,05	0,00	0,42
PRO6	0,00	0,06	0,04	0,08
PRO7	0,00	0,05	0,05	0,02
PRO8	0,00	0,21	0,05	0,15
PRO9	0,00	0,09	0,04	0,02
Σf	1,16	0,92	1,01	0,96

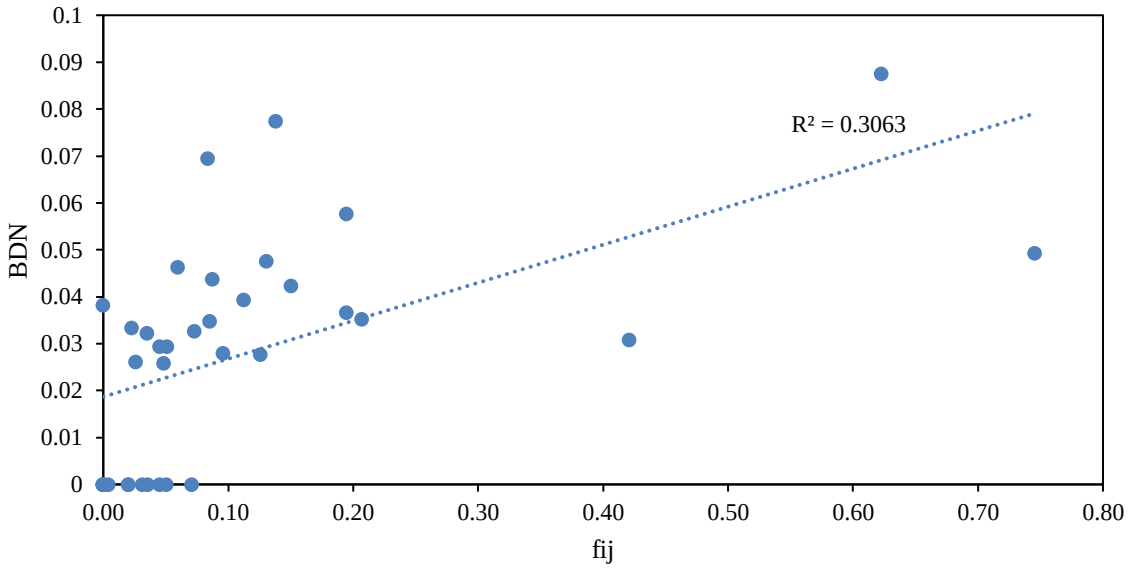

Figure 76. Comparison of connectivity estimated by CRM and by tracer tests for Case 4

3.2 Real field

A robust interwell communication system was discovered to be in place between injection well #22 and its related production wells, with tracer agent removal happening on a consistent basis. It was discovered that injection well #11 had an interwell connection that ran in the southwesterly direction of the area. An increase in tracer agent mass transfer of 115.7-704.9 mD was discovered in the permeability filtering systems, depending on the amount of taken-out indication that was present. Additionally, tracer agent concentrations in unplanned

wells have been discovered, providing evidence of a hydrodynamic connection between injection wells and all production wells.

In order to determine the interwell connectivity between injectors and producers, different scenarios were modeled by CRM. The well spacing was changed for the injectors and different possibilities of $\sum f_{ij}$ were also considered. By analyzing all cases, it was found that due to the presence of an active aquifer, $\sum f$ should be greater than one. Also, well spacing should be assigned to each well. As the best scenario, $\sum f = 1.25$ and well spacing were set as 1300 m for I11 and 950 m for I22 to contain all observation wells as shown in Figure 13.

History for 25 production and 6 injection wells in the period from 01/01/2008 to 06/01/2017 was available. The period from 01/01/2008 to 11/01/2014 was selected as input data since there is more complete information on production and injection rates in this interval. After pre-processing of the data, the CRM was applied to model the history, as shown in Figure 77 – 92. Good agreement of the calculated production with the history was observed. The average simulation error for control wells is 15%.

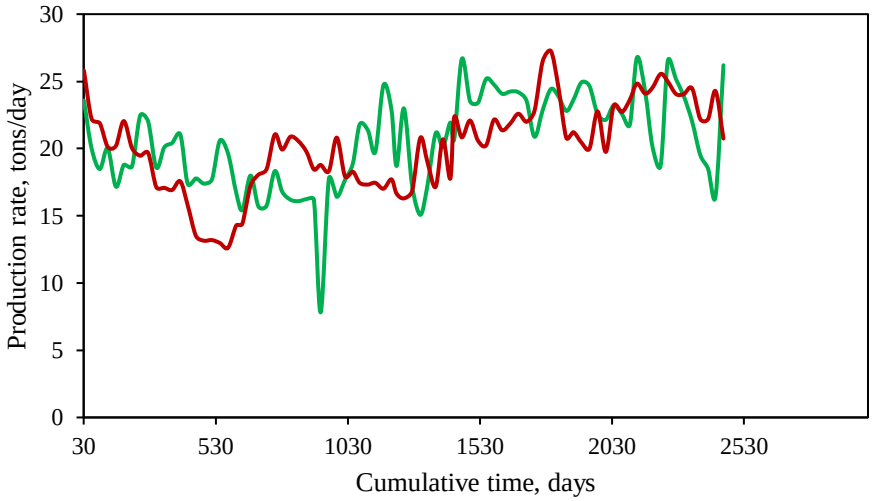

Figure 77. Total production matching by CRM for the real field for producer 1 (Well #13); green – actual production, red – estimated production

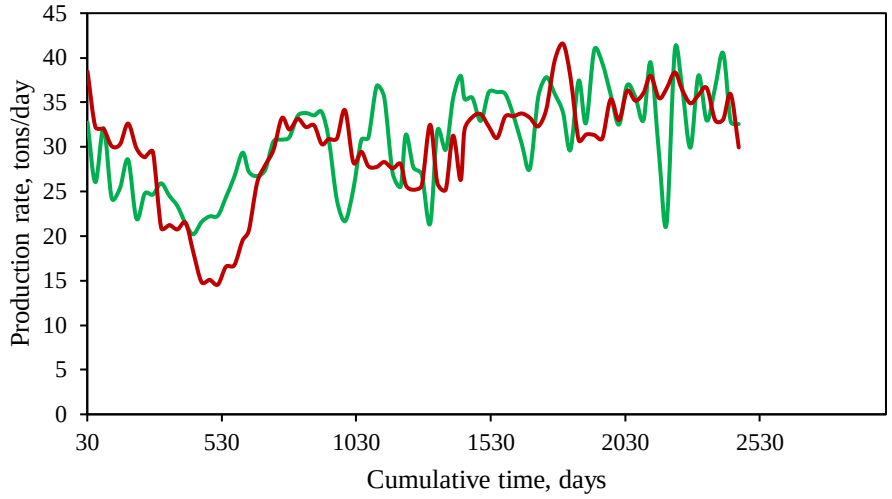

Figure 78. Total production matching by CRM for the real field for producer 2 (Well #14); green – actual production, red – estimated production

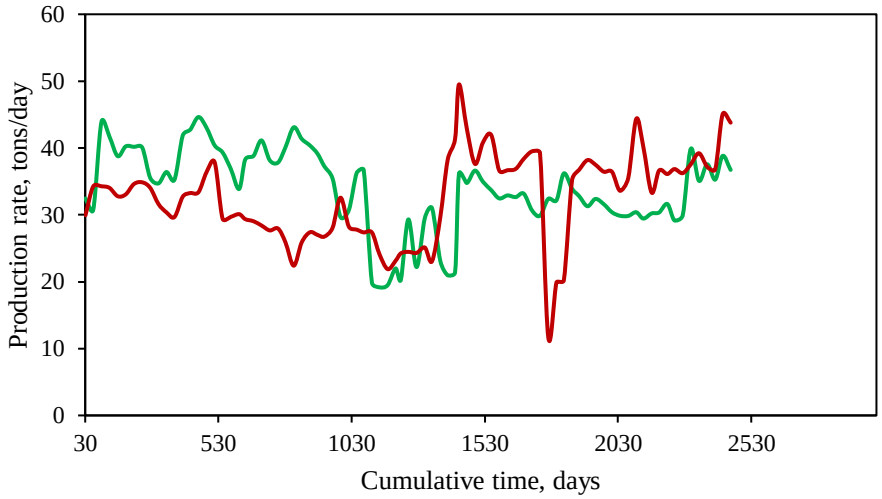

Figure 79. Total production matching by CRM for the real field for producer 3 (Well #19); green – actual production, red – estimated production

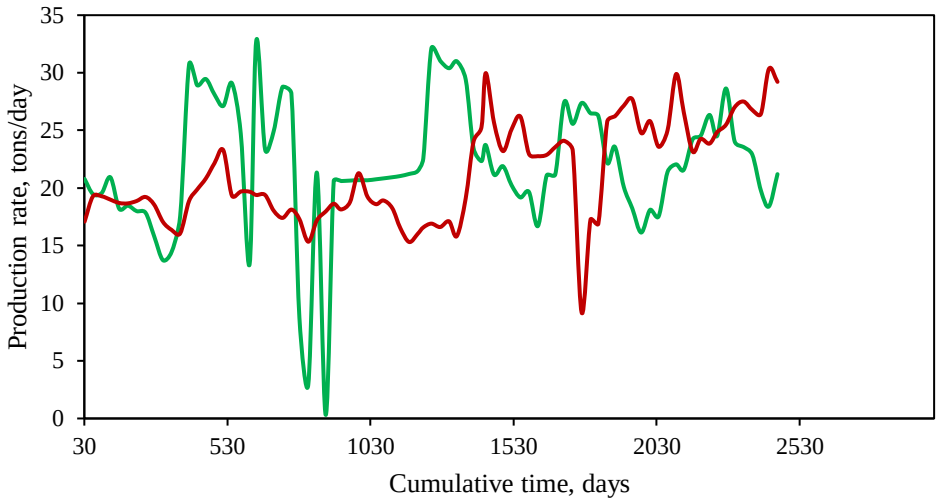

Figure 80. Total production matching by CRM for the real field for producer 4 (Well #30); green – actual production, red – estimated production

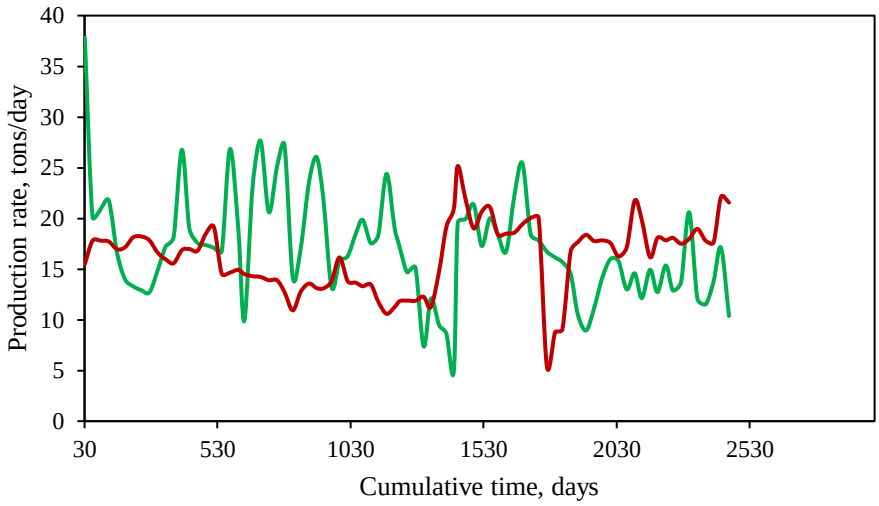

Figure 81. Total production matching by CRM for the real field for producer 5 (Well #32); green – actual production, red – estimated production

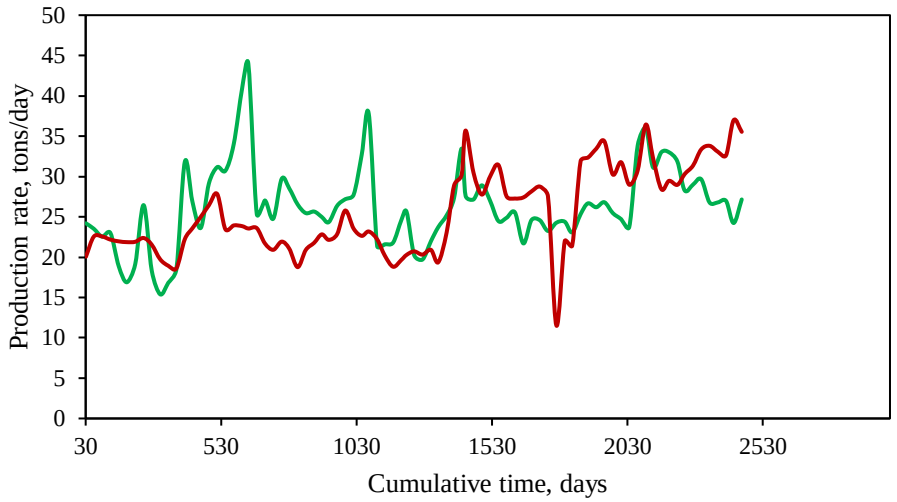

Figure 82. Total production matching by CRM for the real field for producer 6 (Well #34); green – actual production, red – estimated production

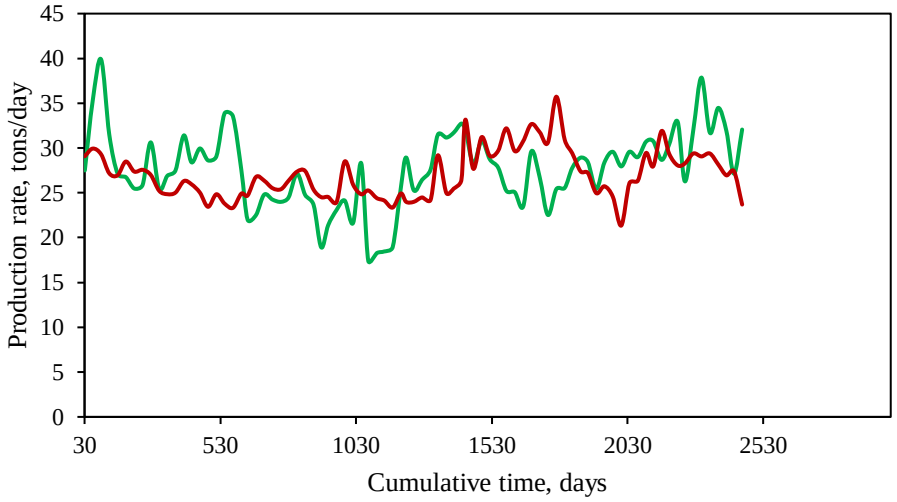

Figure 83. Total production matching by CRM for the real field for producer 7 (Well #37); green – actual production, red – estimated production

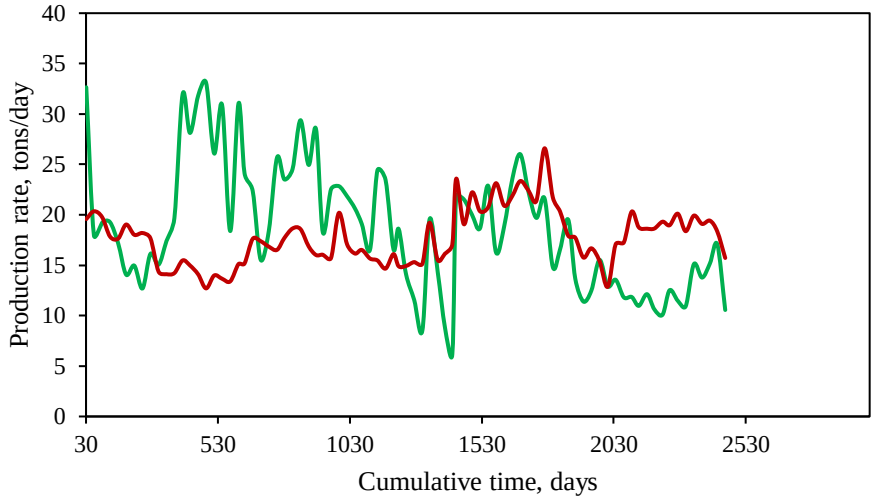

Figure 84. Total production matching by CRM for the real field for producer 8 (Well #46); green – actual production, red – estimated production

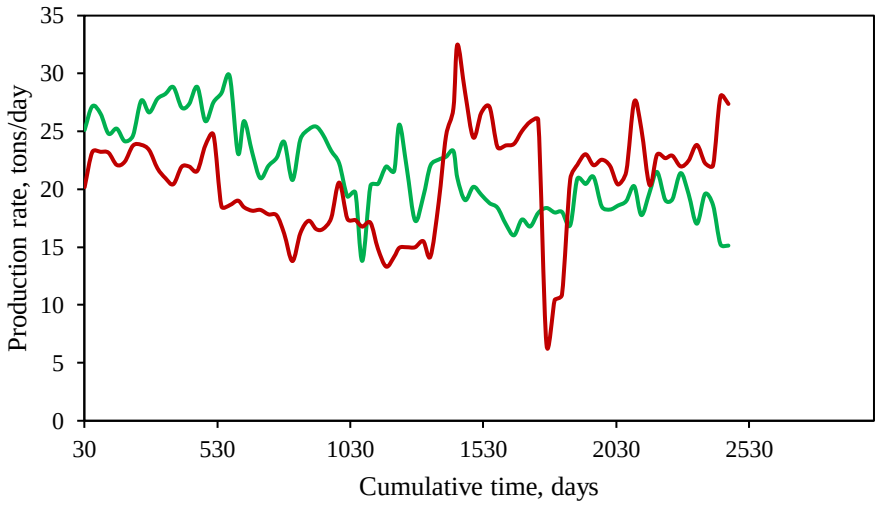

Figure 85. Total production matching by CRM for the real field for producer 9 (Well #57); green – actual production, red – estimated production

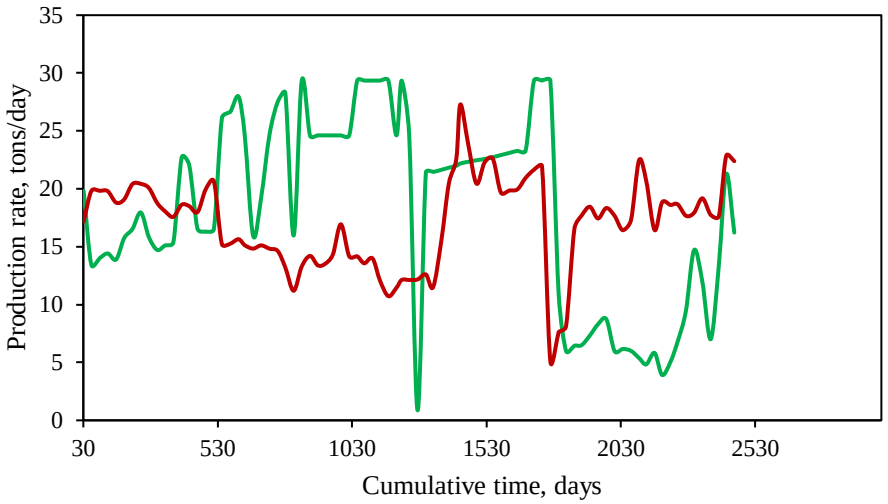

Figure 86. Total production matching by CRM for the real field for producer 10 (Well #61); green – actual production, red – estimated production

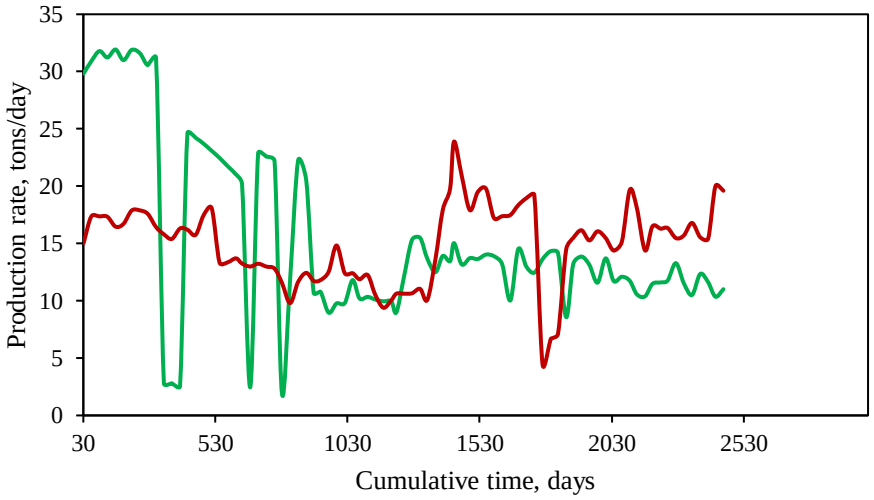

Figure 87. Total production matching by CRM for the real field for producer 11 (Well #71); green – actual production, red – estimated production

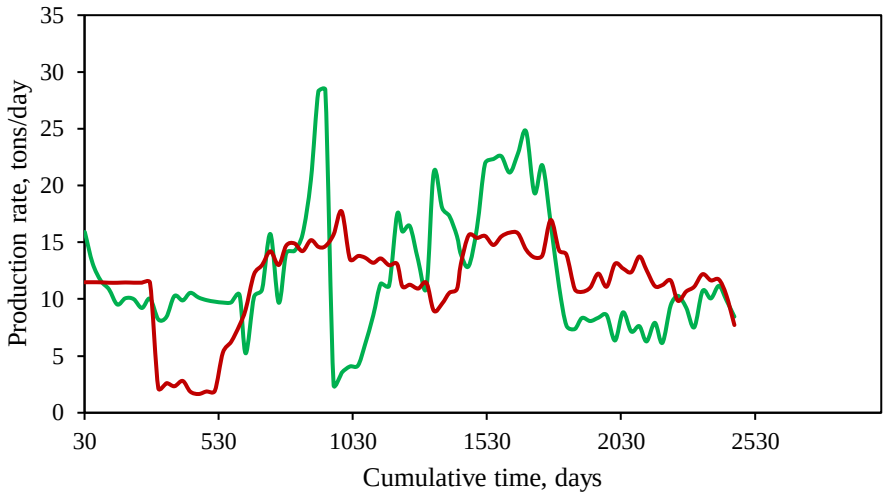

Figure 88. Total production matching by CRM for the real field for producer 12 (Well #72); green – actual production, red – estimated production

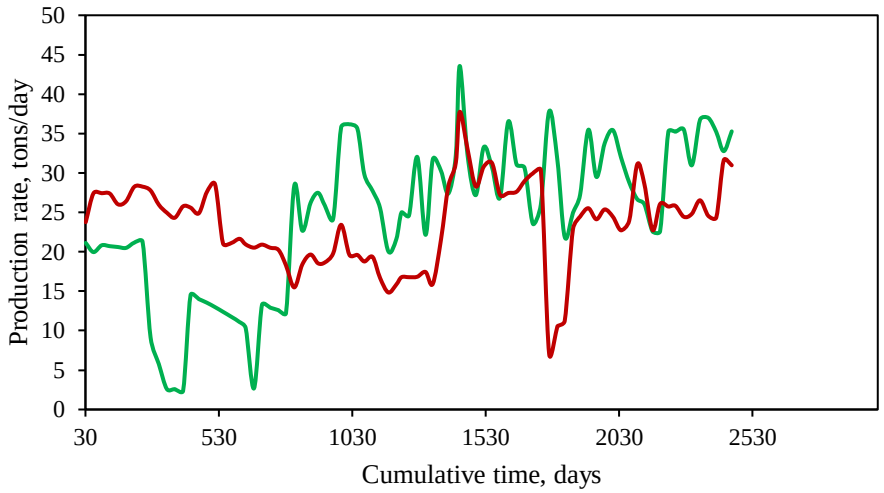

Figure 89. Total production matching by CRM for the real field for producer 13 (Well #73); green – actual production, red – estimated production

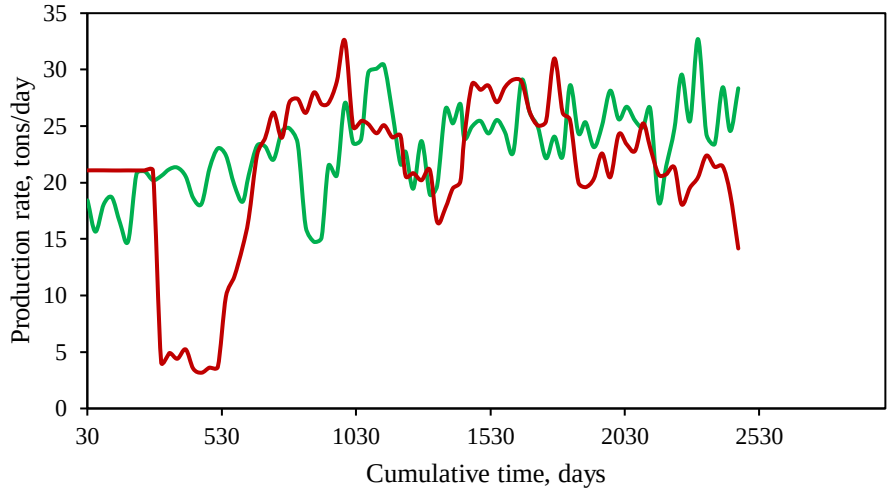

Figure 90. Total production matching by CRM for the real field for producer 14 (Well #75); green – actual production, red – estimated production

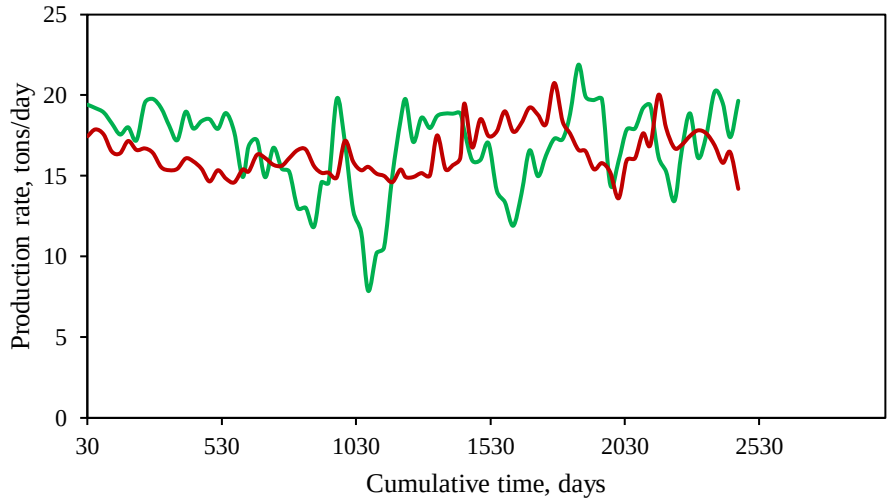

Figure 91. Total production matching by CRM for the real field for producer 20 (Well #81); green – actual production, red – estimated production

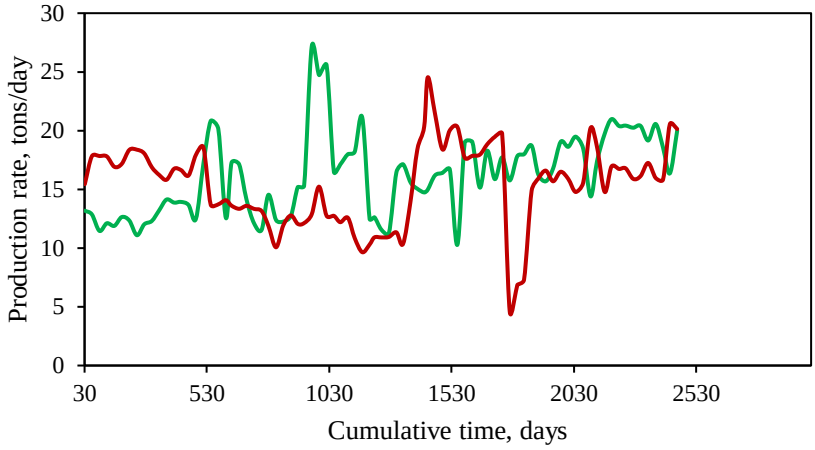

Figure 92. Total production matching by CRM for the real field for producer 22 (Well #84); green – actual production, red – estimated production

f_{ij} values are estimated by CRM and shown in Table 6.

Table 6. Interwell connectivity for the real case

	I12	I22	I5	I45	I11	I10
Well 13 - P1	0,11	0,00	0,00	0,02	0,04	0,08
Well 14 - P2	0,08	0,00	0,00	0,00	0,15	0,13
Well 19 - P3	0,00	0,20	0,04	0,00	0,00	0,00
Well 30 - P4	0,00	0,10	0,07	0,00	0,00	0,00
Well 32 - P5	0,00	0,10	0,01	0,00	0,00	0,00
Well 34 - P6	0,00	0,11	0,09	0,00	0,00	0,00
Well 37 - P7	0,21	0,00	0,00	0,27	0,00	0,00
Well 46 - P8	0,19	0,00	0,00	0,00	0,03	0,00
Well 57 - P9	0,00	0,14	0,01	0,00	0,00	0,00
Well 61 - P10	0,00	0,12	0,00	0,00	0,00	0,00
Well 71 - P11	0,00	0,11	0,00	0,00	0,00	0,00
Well 72 - P12	0,00	0,00	0,00	0,01	0,15	0,00
Well 73 - P13	0,00	0,17	0,00	0,00	0,00	0,00
Well 74 - P14	0,06	0,00	0,03	0,00	0,00	0,00

Well 75 - P15	0,00	0,00	0,00	0,04	0,27	0,00
Well 76 - P16	0,04	0,00	0,06	0,00	0,00	0,00
Well 77 - P17	0,00	0,00	0,11	0,00	0,00	0,00
Well 78 - P18	0,00	0,04	0,10	0,00	0,00	0,00
Well 80 - P19	0,00	0,00	0,21	0,00	0,00	0,00
Well 81 - P20	0,11	0,00	0,00	0,21	0,00	0,00
Well 82 - P21	0,22	0,00	0,02	0,00	0,00	0,00
Well 84 - P22	0,00	0,11	0,00	0,00	0,00	0,00
Well 016A - P23	0,00	0,00	0,00	0,69	0,00	0,00
Well 018 A - P24	0,22	0,00	0,00	0,00	0,00	0,00
Well 083A - P25	0,00	0,00	0,08	0,00	0,00	0,00
Σf	1,25	1,19	0,83	1,25	0,64	0,21

A set of situations are described in this situation, one in which there are difficulties between wells in one zone and the other in which there are no such problems in the second zone. These two figures give a general insight into connectivities obtained from both the CRM and tracer tests. Figure 92 shows that six wells have mostly similar interwell connectivities obtained from the CRM and tracer test and one well shows the higher value. According to Figure 93, the interwell connectivities for the wells adjacent to the injection well I11 still have problems and are very different from the data obtained by the service company. It was estimated that I11 has a serious loss of fluid in this zone. This fact may be the key factor in which there is such a large difference between the data. An overall picture of fluid behavior in porous media may still be obtained from the CRM even when it seems that particular wells are not connected when they are in reality connected. This is because the CRM indicates the lack of connections between certain wells when they are in fact connected. Furthermore, according to the field's service company, there are difficulties with the filtration system in the northeast direction from the injection well №11, and CRM revealed somewhat abnormally high values in the same zone as the problems with the filtration system. This may imply that CRM may also describe challenges that are comparable to these. Such an approach may serve as a good

precursor for actual tracer test analysis on the field and be a help for creating the tracer flooding strategies giving the initial idea of the fluid behavior in porous media.

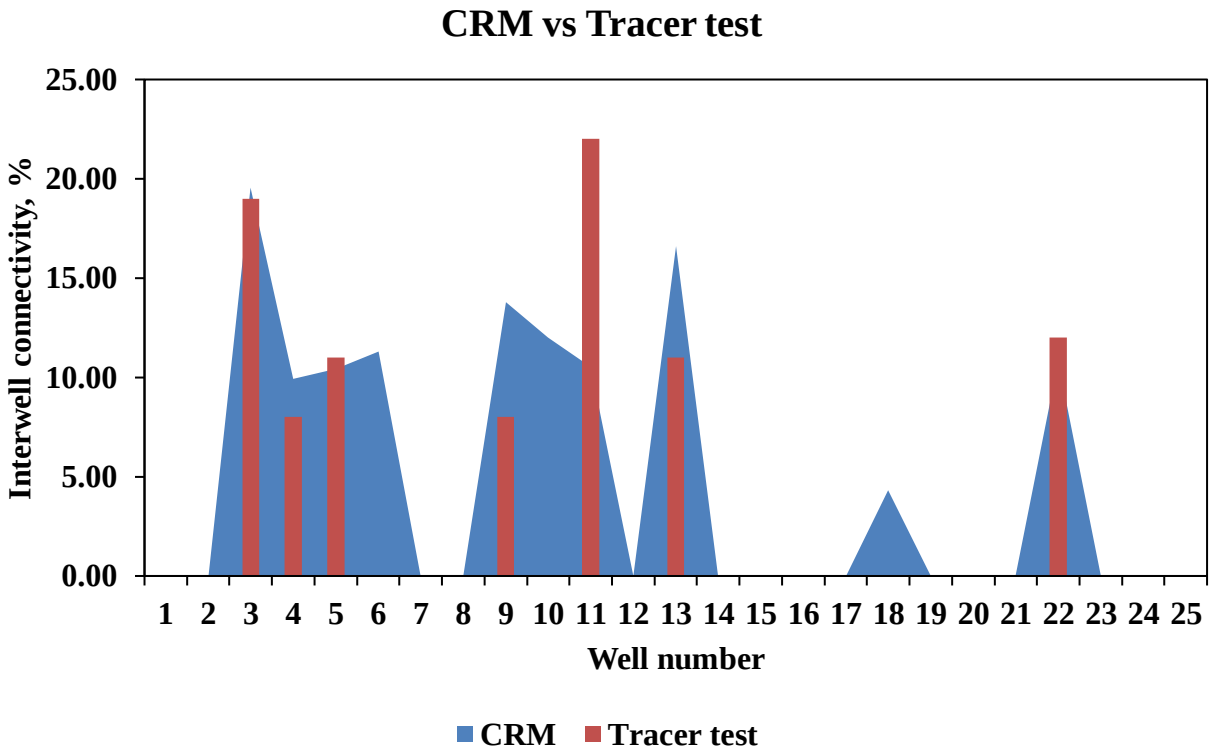

Figure 93. CRM vs Tracer test interwell connectivities comparison for I22

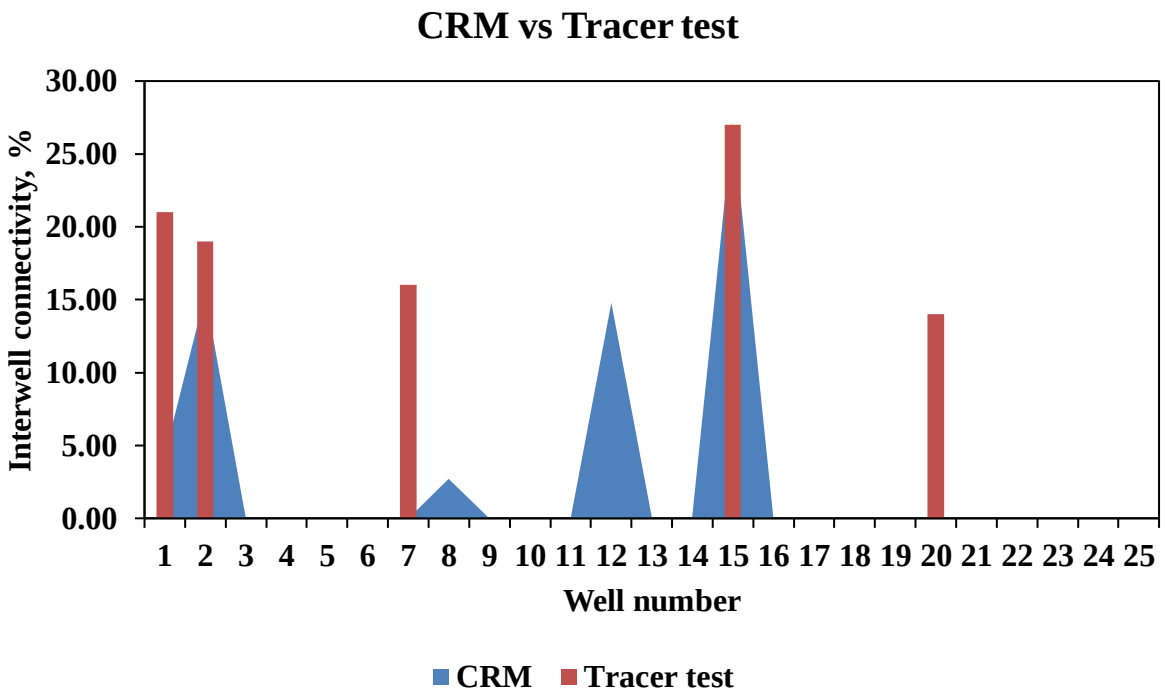

Figure 94. CRM vs Tracer test interwell connectivities comparison for I11

CHAPTER 4. CONCLUSION AND RECOMMENDATIONS

Two fields were used in this work: the synthetic field and the real field. The Capacitance – Resistance Model: Producer-based Representation (CRMP) was used in both fields. Different cases were explored in order to see which one could best represent the physical meaning of the interwell connection under particular assumptions. The results of the experiment were used to determine which case was the most accurate. While simulating the tracer field analysis, factors such as fluid loss and well spacing were taken into consideration. Based on these assumptions, various restrictions were applied in an attempt to determine the most likely path that fluids may take between wells.

Summing everything up, the following conclusion can be made:

1. Well spacing is an important constraint that replicates the tracer flow test, which also helps to isolate unwanted wells which leads to reducing the number of unknowns;
2. Fluid loss is another critical parameter which should be taken into account while isolating certain wells from others in order to check for fluid cross-flow between wells;
3. It is justified that earlier breakthrough results in better interwell connectivity values;
4. Despite the fact that the CRM can match overall output more accurately in certain circumstances, interwell connectivities deviate from real tracer data and cannot accurately represent the physical behavior of the injected fluid.

To summarize, it should be highlighted that the introduction of well spacing and fluid loss criteria to estimate interwell connection is both necessary and important to achieve. A key benefit of this strategy is that it replicates tracer analysis, during which only certain wells are picked for testing. It also has the physical meaning of the fact that the sooner breakthrough happens, the greater is the interwell connectivity. Based on the above, it may be stated that, in some scenarios with well set restrictions, the CRM can be considered as a viable alternative to tracer testing for quick field analysis, but not fully replace tracer test.

For further study, it would be recommended to investigate different CRM approaches with similar restrictions in order to identify at which cases which approach could represent the tracer analysis better. Data imputation techniques can also be additional improvement for CRM. Different machine learning – based algorithms may increase the quality of data and accurately impute missing values which may increase the overall CRM solutions. Finally,

machine and deep learning – based optimization algorithms may be recommended in order to improve the optimization steps.

REFERENCES

Abadie J., C. J. (1969). Generalization of the Wolfe Reduced Gradient Method to the Case of Nonlinear Constraints. *Optimization*, 37-47.

Akin, S. (2014). Optimization of Reinjection Allocation in Geothermal Fields Using Capacitance-Resistance Models.

Aziz, & Settari. (1979). *Petroleum Reservoir Simulation.* APPLIED SCIENCE PUBLISHERS LTD.

Davood Zivar, A. I. (2022). Insights into wettability alteration during low-salinity water flooding by capacitance-resistance model. *Petroleum Research*.

Duribe, V. (2016). Capacitance Resistance Modeling for Improved Characterization inWaterflooding and Thermal Recovery Projects.

Eshraghi, S., Rasaei, M., & Zendehboudi, S. (2016). Optimization of miscible CO2 EOR and storage using heuristic methods combined with capacitance/resistance and Gentil fractional flow models. *J. Natl. Gas Sci. Eng.*

Fox, M., Chedburn, A., & Stewart, G. (1988). Simple Characterization of Communication Between Reservoir Regions. *Paper presented at the European Petroleum Conference, London, United Kingdom, October 1988.* London, United Kingdom.

Gildin, E., & King, M. (2013). Robust Reduced Complexity Modeling (R2CM) in Reservoir Engineering.

Holanda, R. d., Gildin, E., Jensen, J. L., Lake, L. W., & Kabir, C. S. (2018). A State-of-the-Art Literature Review on Capacitance Resistance Models for Reservoir Characterization and Performance Forecasting.

Izgec, O. (2012). Understanding waterflood performance with modern analytical techniques. *J. Pet. Sci. Eng.*, 100-111.

Izgec, O., & Kabir, C. (2012). Quantifying reservoir connectivity, in-place volumes, and drainage-area pressures during primary depletion. *J. Pet. Sci. Eng.*

Kaviani. (2014). How accurate are Capacitance Model connectivity estimates?

Koval, E. (1963). A method for predicting the performance of unstable miscible displacement in heterogeneous media.

Lake, L. (2014). *Fundamental of Enhanced Oil Recovery.*

Lake, L. W. (2017). Extension of Capacitance-Resistance Model to Tracer Flow for Determining Reservoir Properties.

Laochamroonvorapongse, R. (2013). Advances in the Development and Application of a Capacitance-Resistance Model.

Laochamroonvorapongse, R., Kabir, C., & Lake, L. (2014). Performance assessment of miscible and immiscible water-alternating gas floods with simple tools. *J. Pet. Sci. Eng.*

Leverett, M., & Buckley, S. (1942). Mechanism of fluid displacement in sands.

Li, Y., Júlíusson, E., Pálsson, H., Stefánsson, H., & Valfells, A. (2017). Machine learning for creation of generalized lumped parameter tank models of low temperature geothermal reservoir systems.

Liang, X., Weber, D., Edgar, T., Lake, L., Sayarpour, M., & Al-Yousef, A. (2007). Optimization Of Oil Production Based on A Capacitance Model of Production and Injection Rates.

Marguerite Frank, P. W. (1956). An algorithm for quadratic programming.

Mollaei, A., & Delshad, M. (2011). General Isothermal Enhanced Oil Recovery and Waterflood Forecasting Model.

Nguyen, A. (2012). Capacitance Resistance Modeling for Primary Recovery, Waterflood and Water-CO2 Flood.

Nguyen, A., Kim, J., Lake, L., Edgar, T., & Haynes, B. (2011). Integrated Capacitance Resistive Model for Reservoir Characterization in Primary and Secondary Recovery.

Salazar, M., Gonzalez, H., Matringe, S., & Castiñeira, D. (2012). Combining Decline-Curve Analysis and Capacitance-Resistance Models To Understand and Predict the Behavior of a Mature Naturally Fractured Carbonate Reservoir Under Gas Injection.

Sayarpour, M. (2008). *Development and Application of Capacitance-Resistive Models to Water/CO2 Floods. Ph.D. Dissertation.*

Sayarpour, M. (2009). The use of capacitance–resistance models for rapid estimation of waterflood performance and optimization. *Journal of Petroleum Science and Engineering*.

Sayarpour, M., Zuluaga, E., Kabir, C. S., Lake, L. W., & Haynes, B. (2011). *Integrated Capacitance Resistive Model for Reservoir Characterization in Primary and Secondary Recovery.*

Sayarpour, M., Zuluaga, E., Kabir, C., & Lake, L. (2009). The use of capacitance-resistance models for rapid estimation of waterflood performance and optimization.

Tao, Q. (2012). Modeling CO2 Leakage from Geological Storage Formation and Reducing the Associated Risk.

Tao, Q., & Bryant, S. (2013). Optimizing CO2 storage in a deep saline aquifer with the capacitance-resistance model.

Tao, Q., & Bryant, S. (2015). Optimizing carbon sequestration with the capacitance/resistance model.

Weber, D. B. (2009). *The use of capacitance-resistance models to optimize injection allocation and well location in water floods.* Texas, Austin, TX, USA: Ph.D. Dissertation, University of Texas, Austin, TX, USA.

Yousef, A., Gentil, P., Jensen, J., & Lake, L. (2006). A Capacitance Model to Infer Interwell Connectivity from Production and Injection Rate Fluctuations. *SPE Reserv. Eval. Eng*.

Yousef, A., Gentil, P., Jensen, J., & Lake, L. (2007). A Capacitance Model to Infer Interwell Connectivity from Production and Injection Rate Fluctuations. *SPE Reserv. Eval. Eng. 2006*, 630–646.

Yousef, A., Jensen, J., & Lake, L. (2009). Integrated interpretation of interwell connectivity using injection and production fluctuations. *Math. Geosci*, 81-102.